University of Alberta
Printing Department

THE UNIVERSITY OF ALBERTA

INSTRUMENTATION FOR FLUID DEVICE TESTS

by

E.A. MIROSH BSC. (MANITOBA)

A THESIS

SUBMITTED TO THE FACULTY OF GRADUATE STUDIES

IN PARTIAL FULFILLMENT OF THE REQUIREMENTS FOR THE DEGREE OF

MASTER OF SCIENCE

DEPARTMENT OF ELECTRICAL ENGINEERING

EDMONTON, ALBERTA

JULY, 1966

UNIVERSITY OF ALBERTA

FACULTY OF GRADUATE STUDIES

The undersigned certify that they have read and recommended to the Faculty of Graduate Studies for acceptance, a thesis entitled Instrumentation For Fluid Device Tests submitted by E.A. Mirosh in partial fulfillment of the requirements for the degree of Master of Science.

TO DIANNE

ABSTRACT

This thesis describes the design and analysis of air pressure and air flow measuring instrumentation, as well as its use in determining the static and dynamic properties of air operated fluid amplifiers.

The transducers used were a piezoelectric ceramic for the pressure measurement and a heated wire for the flow measurement.

Both the air pressure and the air flow circuitry utilize semiconductors throughout.

Some properties of the proportional, bistable, and turbulence fluid amplifiers are determined with the equipment.

ACKNOWLEDGEMENTS

The author wishes to express his appreciation to the staff members and graduate students of the Department of Electrical Engineering for their co-operation and helpfulness during the course of this work. The author particularly wishes to acknowledge Professor Y.J. Kingma for his supervision of this project.

The financial assistance provided the by National Research Council is gratefully acknowledged by the author.

TABLE OF CONTENTS

LIST OF FIGURES

LIST OF SYMBOLS

Hz.	hertz
kHz.	kilohertz
MHz.	megahertz
mV.	millivolt
psi.	pounds per square inch
db.	decibel
SCFH	standard cubic feet per hour
pf.	picofarad
μf	microfarad
f	frequency
$\|M\|$	log magnitude of gain
dec.	decade
C.M.	circular mil
mA.	milliamp
psia.	pounds per square inch absolute
mW.	milliwatt
C.L.	closed loop
O.L.	open loop
r/s	radians per second
psig	pounds per square inch gage
SCFM	standard cubic feet per minute
P.A.	proportional amplifier
ms.	millisecond
cm.	centimeter
B.A.	bistable amplifier

T.A.	turbulence amplifier
I.D.	inner diameter
psid.	pounds per square inch differential
SCIS	standard cubic inches per second

Other symbols as defined in the text.

INTRODUCTION

The field of pneumatic control is a relatively old and proven one, but the principles involved in pneumatic recorders and controllers have remained relatively unaltered for many years. The heart of many of these instruments is the nozzle-baffle assembly used for error sensing. Diaphram actuated ball or pin-type relay valves normally supply the power amplification. In addition, these instruments utilize many other moving parts: pivots and linkages, diaphrams, levers, and springs, all subject to wear and to consequent loss of calibration or failure due to atmospheric aging or corrosion, vibration of mounting, and process noise.

In recent years, much work has been done in the development of so called 'fluid state' or fluidic amplifiers.[1,2] As the name implies, these devices all use a fluid, be it oil, water, hot gas, or air for the transmission medium. Various forms of these devices are able to perform switching, memory and/or amplification of fluid pressure or flow with the benefit of utilizing no moving parts. Other advantages of note are the fluidic device's environmental tolerance, low cost, and high reliability.[1]

The main disadvantage fluidic devices possess is their slow operating speed. Presently available units are claimed to have bandwidths the order of 1kHz, and 20 kHz is being predicted as the uppermost practical bandwidth. Other disadvantages are their high power consumption, their lack of a high degree of linearity, and their low input impedance which presents interconnection problems.[1]

Before utilizing effectively the various types of fluidic devices presently available, an understanding of the device's static and dynamic characteristics must be attained. Presently available manufacturer's data is of a sparse and general nature and, as a result, the design of fluidic control systems is largely a trial and error procedure.

The primary purpose of this thesis report, is to present a solid state air pressure and air flow instrumentation scheme which is employed in determining the static and dynamic properties of various pneumatic fluidic devices.

A fluid flow tube, into which the pressure and flow transducers are placed into contact with the air to be metered, was constructed. The details of the flow tube and the transducer mounting assemblies are given in Appendix A.

The air pressure measuring scheme (Figure 1), employs a piezoelectric ceramic as the pressure transducer.

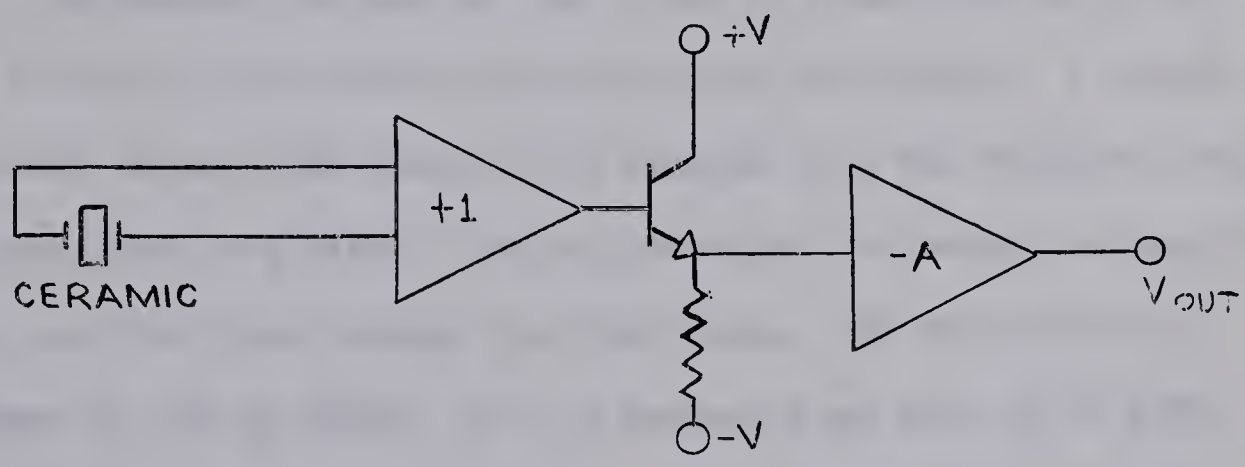

FIGURE 1. AIR PRESSURE MEASURING SCHEMATIC

The transducer signal passes into a bootstrapped field-effect transistor unity gain amplifier and then through an emitter-follower into an operational amplifier of gain A.

The sensitivity of this scheme was found to be linear and was set to 350mV./psi. The maximum measurable pressure is limited by the power supply voltage to a 20 psi. step. The system bandwidth, (-3db. down) is from 0.035 Hz. to 5kHz. and the output noise level is 6mV. peak to peak.

The air flow measuring scheme (Figure 2) employs a heated small diameter platinum wire in one leg of a Wheatstone bridge as the flow transducer.

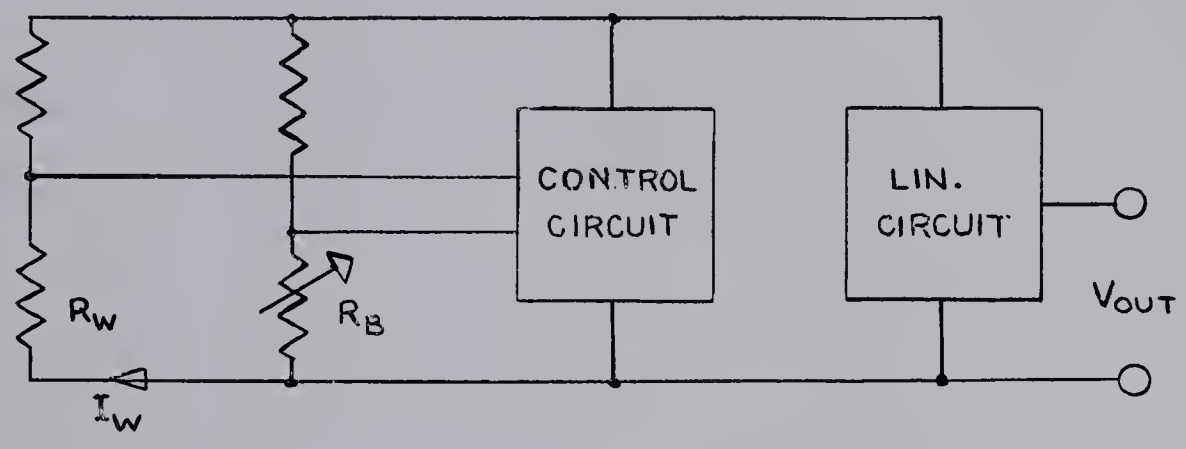

FIGURE 2. AIR FLOW MEASURING SCHEMATIC

Unbalanced voltage at the bridge is transformed, by the control circuit, into current which supplies the bridge. A signal proportional to the wire current, is removed from the feedback loop and is processed by a circuit which linearizes the output voltage to the mass air flow rate through the flow tube. The sensitivity of this scheme is 200 mV./SCFH. up to a maximum flow rate of 10 SCFH. The linearity of the system is determined by the accuracy of reading the calibrating instrument scale and by the flow tube inlet tubing configuration. For a specific inlet tubing configuration, such as a straight inlet tubing section of 15 to 20 inlet tubing diameters in length, the system may be calibrated to a linearity

of 2% of full scale. System bandwidth (-3db down) is from d.c. to 5kHz and the output noise level is 1 mV. peak to peak at zero flow.

Both the pressure and the flow measuring circuitry are contained in one box which is connected to the flow tube by coaxial cable.

Two such complete units were constructed and used to determine fluid amplifier static and dynamic characteristics. These characteristics are discussed in Chapter Six.

CHAPTER ONE

THE PRESSURE MEASUREMENT

1.1 PIEZOELECTRIC CERAMIC DATA

The ceramic chosen for this application was PZT-5H, a lead zironate-lead titanate composition made by Clevite. This material possesses a combination of high piezoelectric (g_{33}) constant and high dielectric constant providing both high signal sensitivity and high internal capacity. The main disadvantage of this ceramic was its low Curie Point and consequent low temperature stability. However, since this application was for laboratory use on compressed air at room temperature, the Curie Point was only of concern when soldering leads to the ceramic's electrodes.

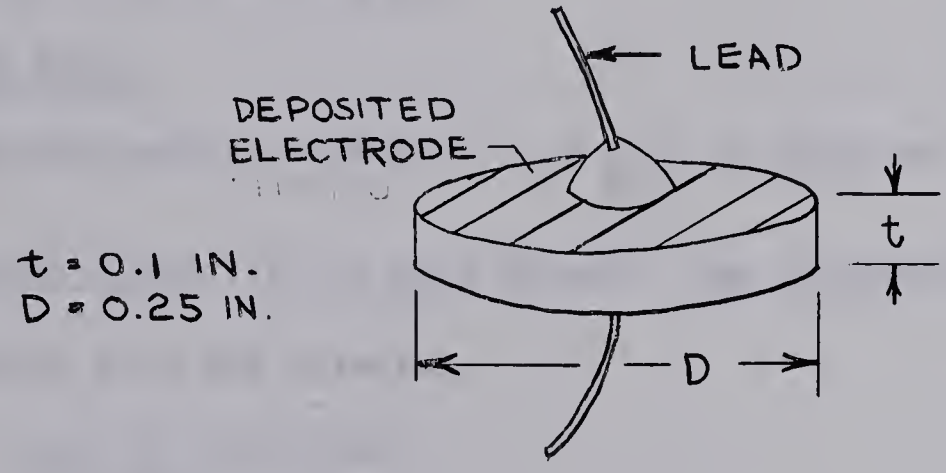

FIGURE 3. PIEZOELECTRIC CERAMIC

In describing piezoelectric properties, superscripts and subscripts are normally used to define the conditions of operation. A subscript t, indicates operation in the thickness mode. The first subscript 3, indicates that the electrodes are perpendicular to the 3 axis whereas the second subscript 3, indicates that the applied stress is in the direction of the 3 axis. For a ceramic

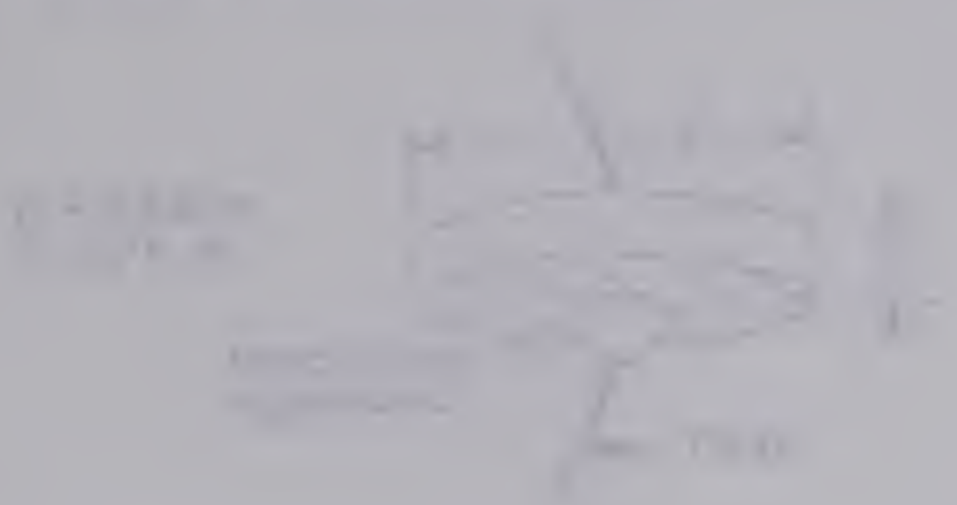

disc, the 3 direction is the axial-direction.

INTERNAL CAPACITY

From the data sheets, the relative dielectric constant, K=3400. The ceramic capacitance is given by

$$C_c = 0.2244 \frac{KA}{t} \text{ pf.} \qquad (1.1)$$

where the electrode area, A= 0.049 square inches, and the ceramic thickness, t= 0.1 inch. By equation 1.1, C_c= 370 pf.

RESONANT FREQUENCY

From the data sheets, the frequency constant, N_{3t}, is given as 7.9×10^4 cycle-inches/sec.

The resonant frequency, f_R, for operation in the thickness mode, is given by

$$f_R = \frac{N_{3t}}{t} \text{ Hz.} \qquad (1.2)$$

and f_R was found to be 790 kHz.

TRANSDUCER RATIO

The piezoelectric constant, $g_{33} = \frac{V/t}{F/A}$, is given as 3.45 volts/inch/psi. in the data sheets. The transducer ratio, N_{33}, is found from the relation

$$N_{33} = \frac{V}{F/A} \text{ volts/psi.} \qquad (1.3)$$

where V is the generated voltage

and F is the force on the ceramic electrode area.

N_{33} was calculated to be 345 mV./psi.

LEAKAGE RESISTANCE

From the data sheets, the volume resistivity, ρ_c, is given as 4×10^{12} ohm-inches at 25°C. The leakage resistance, R_L, is given by the relation

$$R_L = \rho_c \frac{t}{A} \text{ ohms} \qquad (1.4)$$

and was found to be 8×10^{12} ohms.

CURIE POINT

The Curie Point, the temperature beyond which the ceramic may be permanently and completely damaged is given as 193°C.

TEMPERATURE EFFECT ON CAPACITY

The effect of temperature on the relative dielectric constant is given as $\frac{\Delta K}{\Delta \text{temp}} = \frac{30}{^\circ C}$ between 0 and 100°C. This corresponds to an 11°C variation in temperature for a 10% change in capacity, and as such produced negligible effect in this application.

1.2 INPUT CIRCUIT CONSIDERATIONS

In non-resonant, mechanically driven operation of the ceramic, the device may be simply represented by a voltage source e, a capacitor C_c, and a resistor, R_L [3]. This is shown in Figure 4, where, in addition, C_i and R_i are the amplifier input capacitance and resistance.

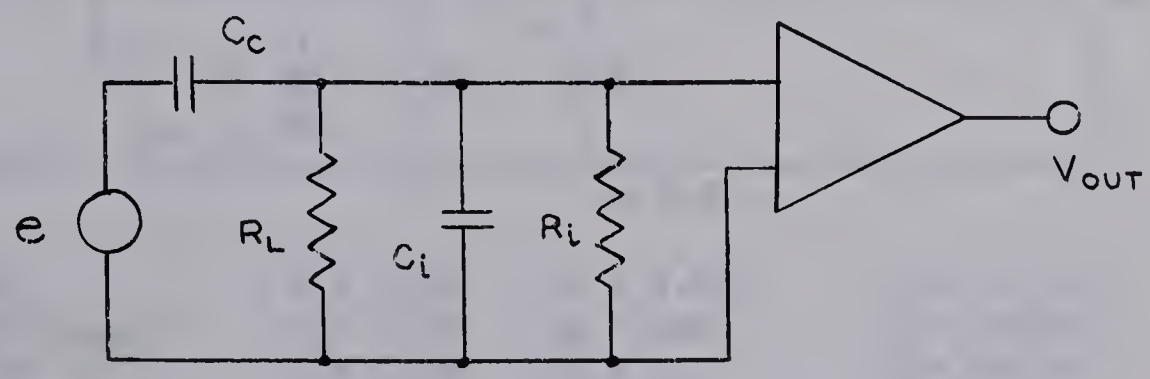

FIGURE 4. SIMPLIFIED INPUT CIRCUIT

In high frequency operation, the capacitances C_c and C_i

will have reactances lower in value than the circuit resistances. The input circuit then reduces to a capacitance divider exhibiting a constant attenuation factor.

In low frequency operation, a lower corner frequency will occur when $\tau = R_i(C_c + C_i)$. The lower corner frequency may be extended with the addition of amplifier input capacitance, but only at the expense of a larger signal attenuation. Following this, the lower corner frequency may be further extended by bootstrapping of the amplifier input bias network.[4] Both of these procedures were used in order to extend the input time constant.

1.3 PIEZOELECTRIC INPUT AMPLIFIER

The complete schematic of the piezoelectric input amplifier is shown in Figure 5.

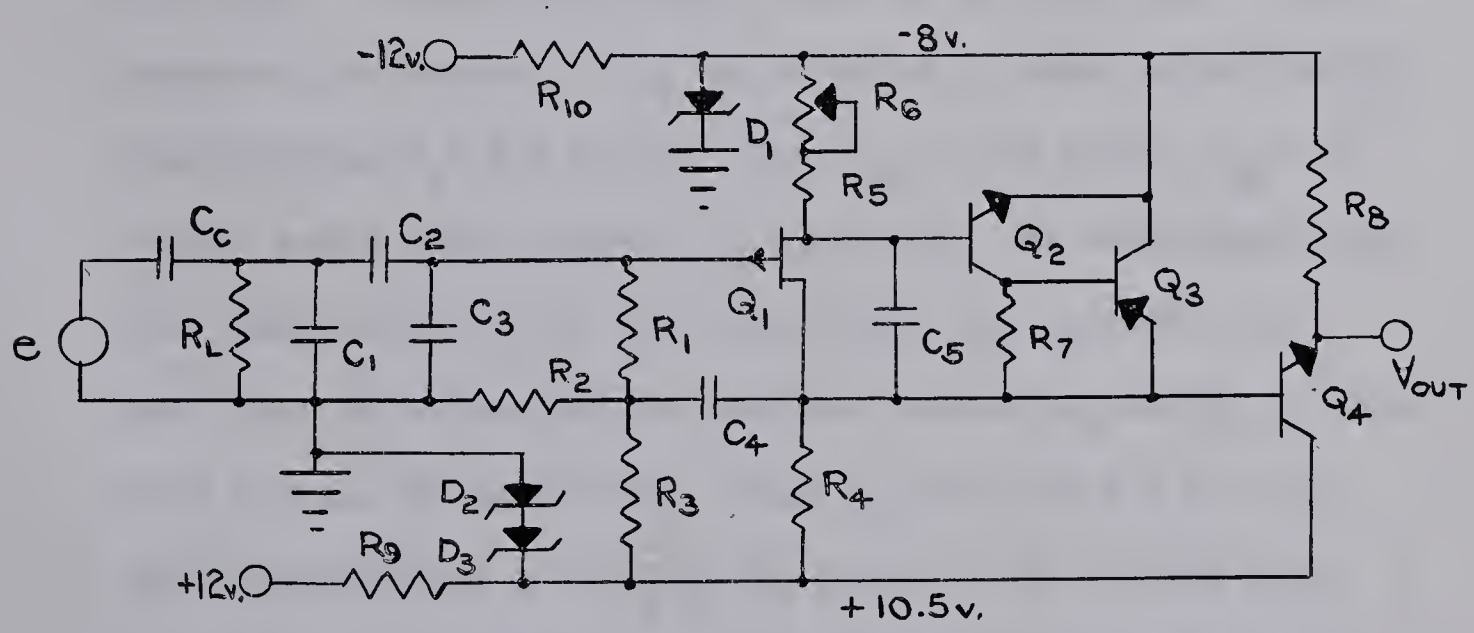

C_c =	370pf	R_1 =	100M	R_7 =	5.6K	D_3 =	IN 752
C_1 =	40 pf (cable)	R_2 =	1.8M	R_8 =	10K	Q_1 =	2N2606
C_2 =	0.68Mf	R_3 =	5.6M	R_9 =	39	Q_2 =	2N3707
C_3 =	0.033Mf	R_4 =	47K	R_{10} =	270	Q_3 =	2N3702
C_4 =	0.51Mf	R_5 =	22K	D_1 =	OAZ 212	Q_4 =	TI412
C_5 =	0.001Mf	R_6 =	10K	D_2 =	IN 751		

FIGURE 5. PIEZOELECTRIC INPUT AMPLIFIER

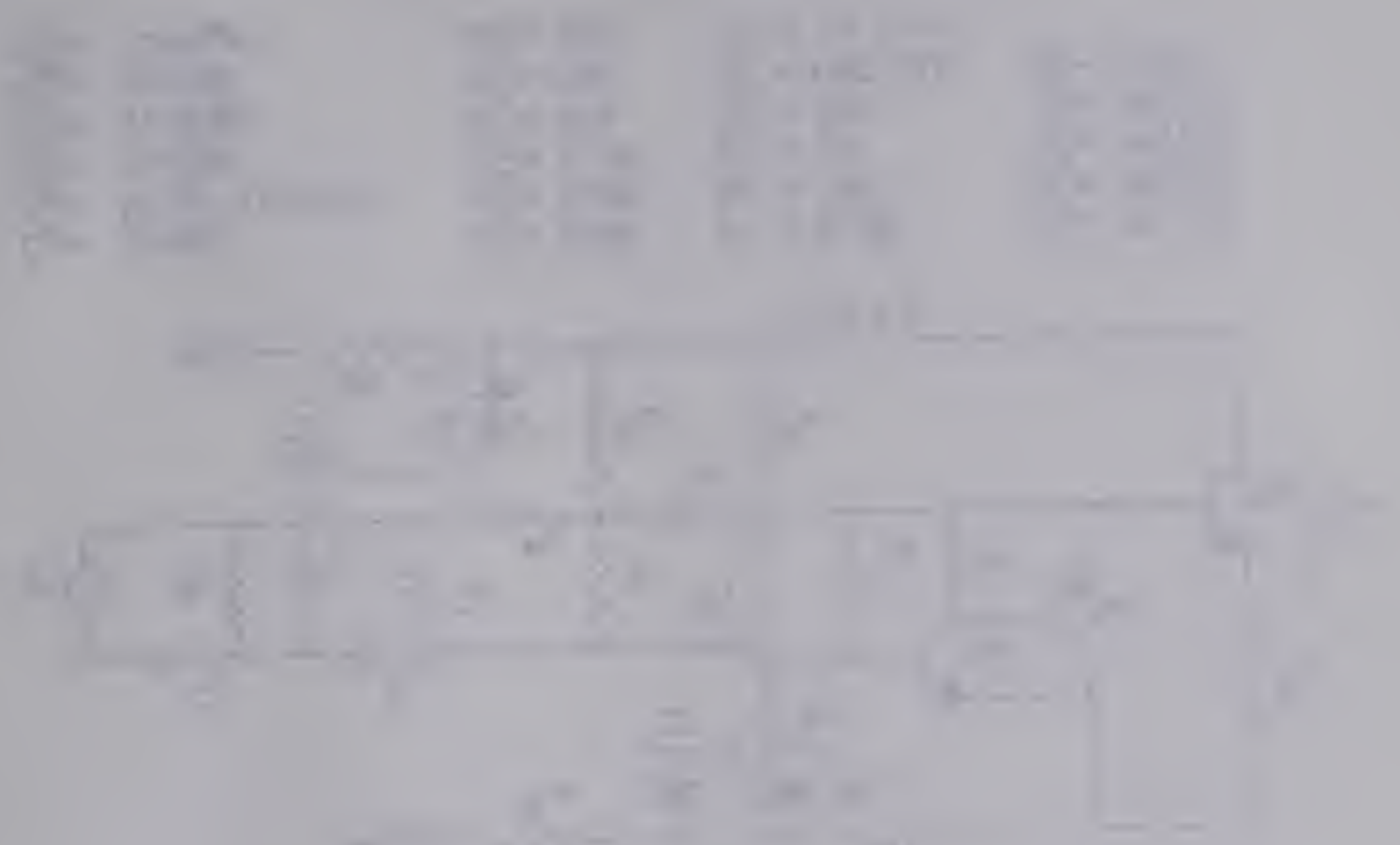

The input capacitive attenuation factor is given approximately by

$$\gamma \doteq \frac{C_c}{C_1+C_3+C_c} \qquad (1.5)$$

The input proportion of the generated signal appearing at the gate is calculated to be, $\gamma = 0.011$. The input time constant without bootstrapping is given approximately by, $R_1C_3 \doteq 3.3$ sec. With bootstrapping, the effective input time constant is extended to 4.3 sec. and the response curve has a calculated low frequency boost of 1.2 db. The bootstrapping calculations are shown in Appendix B.

BIAS CONDITIONS

The gate to source leakage current, I_{gss} for Q_1 is given in the data sheets as about 0.1 nA. at room temperature and for V_{gs}= 5 volts. V_g is then found to be 2.55 volts. In operation, the emitter of Q_4 is adjusted to zero volts with R_6, thus forcing V_s= 0.6 volts. Then V_{gs}= 1.95 volts, V_{ds}= -8 volts, and a drain current, I_d= 0.02 mA., as determined from the characteristics of Q_1, will flow. The current in R_4 must then be maintained at 0.22 mA. forcing Q_2 and Q_3 to provide 0.2 mA. of this total. When Q_2 delivers 0.1 mA., Q_3 must also deliver 0.1 mA. as dictated by the voltage drop across R_7. Q_4 operates at 0.8 mA. under bias conditions.

R_9, R_{10}, and the zero diodes provide additional supply voltage regulation and thus reduce the effect of power supply gain modulation under heavy power supply current demands of the air flow measuring circuit.

CLOSED LOOP GAIN

The transconductance, g_m, of Q_1 about the bias point was measured and found to be 55μ mhos. The measured current gains (β), of Q_2, Q_3, and Q_4 were found to be 310, 115, and 195 respectively, at their bias conditions.

The gate to source gain, A_{gs}, of the circuit of Figure 5, is given by

$$A_{gs} = \frac{g'_m \cdot R'_s}{1+g_m' \cdot R_s'} \tag{1.6}$$

where $$g_m' = g_m \cdot \beta'_2 \cdot \beta'_3 \tag{1.7}$$

$$\beta'_2 = \frac{\beta_2(R_5+R_6)}{R_5+R_6+\beta_2 h_{ib_2}} \tag{1.8}$$

$$\beta'_3 = \frac{\beta_3 R_7}{R_7+\beta_3 h_{ib_3}} \tag{1.8}$$

$$h_{ib} = \left[\frac{26}{I_c(mA.)} + 1.5\right] \text{ohms} \tag{1.9}$$

and $$R'_s = R_s // \left[\beta_4 (R_L // R_8)\right] \tag{1.10}$$

where $R_L = 680$ ohms

and // $\equiv$ in parallel with

Using equations 1.7 to 1.10, β'_2 and β_3' were found to be 86 and 18 respectively, g_m' was found to be 0.085 mhos, and R_s' was found to be 34 K ohms. From equation 1.6, $A_{gs} \doteq 1$.

The gain of the emitter follower stage is given as

$$A_e \doteq \frac{1}{1+\frac{h_{ib_4}}{R_L}} \tag{1.11}$$

From equation 1.11, $A_e \doteq 0.95$.

The gain of the input circuit and amplifier is given by

$$A_{in} = \gamma \cdot A_{gs} \cdot A_e \doteq 0.01 \qquad (1.12)$$

OUTPUT IMPEDANCE

The amplifier output impedance is given by

$$Z_o \doteq h_{ib_4} + \frac{Z_g}{\beta_4} \qquad (1.13)$$

where $$Z_g \doteq \frac{R_s}{1+g'_m R_s} = 12 \text{ ohms} \qquad (1.14)$$

Z_o was calculated and found to be 34 ohms.

CORNER FREQUENCIES

The upper corner frequency is determined by the time constant, $\tau_u = R_{eff} \cdot C_5$.

where $$R_{eff} = r_{ds} // \left\{ \left[(R_s + R_6) // (\beta_2 h_{ib_2}) \right] + R_4 // \left[\beta_4 (R_L // R_8) \right] \right\} \qquad (1.15)$$

and r_{ds}, the drain to source resistance of Q_1, is given in the data sheets as 40 K ohms at $V_{gs} = 1.95$ volts.

From equation 1.15, R_{eff} was found to be 24 K ohm and the upper corner frequency, $f_u \doteq 0.16/\tau_u$ was calculated to be 6.7 kHz. The lower corner frequency, $f_L \doteq 0.16/\tau_{eff}$ was calculated to be 0.037 Hz. τ_{eff} was determined in Appendix B, as were other pertinent points given in the input amplifier response curve of Figure 6.

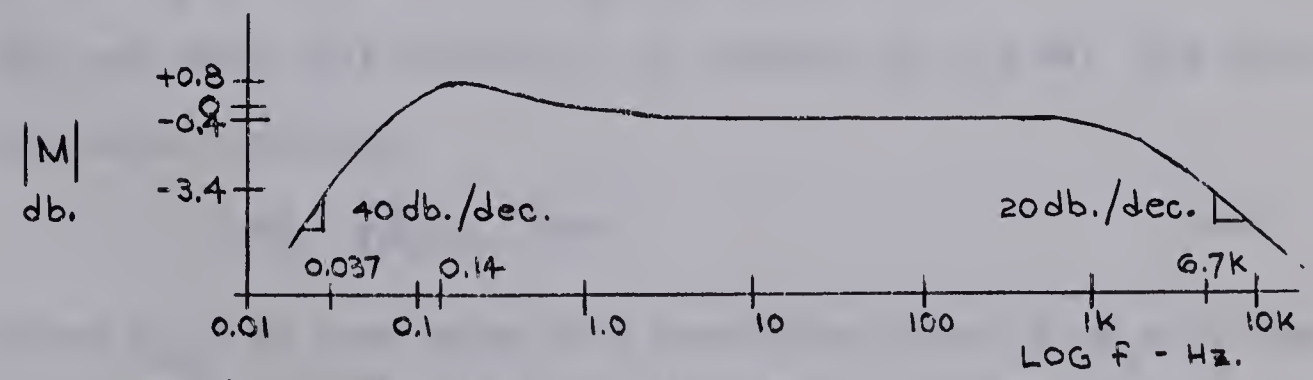

FIGURE 6. INPUT AMPLIFIER CALCULATED RESPONSE CURVE

1.4 PIEZOELECTRIC OUTPUT AMPLIFIER

To recover the loss in signal due to input attenuation by the factor γ of equation 1.5, an operational amplifier (Figure 7) was chosen to follow the input stage.

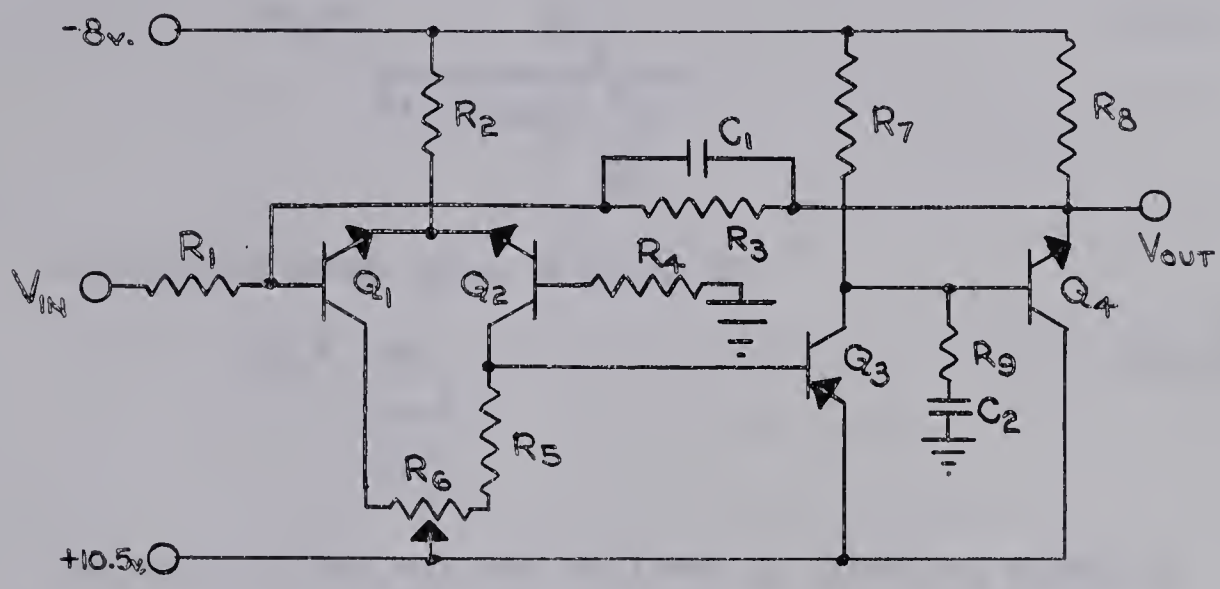

R_1 =	680	R_6 =	1K	C_2 =	0.01 μF
R_2 =	8.2K	R_7 =	8.2K	Q_1 =	TI412
R_3 =	68K	R_8 =	1.5K	Q_2 =	TI412
R_4 =	680	R_8 =	150	Q_3 =	2N3703
R_5 =	1K	C_1 =	300 pf.	Q_4 =	TI 412

FIGURE 7. PIEZOELECTRIC OUTPUT AMPLIFIER

BIAS CONDITIONS

The current gains of transistors Q_1 though Q_4 at their bias conditions are, respectively, 120, 120, 85, and 130. Q_1 and Q_2 together must supply R_2 with 0.9 mA. Assuming that this current is shared equally by Q_1 and Q_2, then each supplies 0.45 mA. to R_2. The emitter of Q_4 is adjusted to zero volts with R_6, and under this condition, Q_4 operates at 0.9 mA. For optimum noise operation,

$$R_1 = R_4 = \sqrt{\beta_1} h_{ib_1} \text{ ohms} \qquad (1.16)$$

Since h_{ib_1} = 60 ohms under bias conditions, then, $R_1 = R_4 = 660$ ohms

was calculated with equation 1.16. As a result, $R_1=R_4=680$ ohms were chosen as the input resistors.

OPEN LOOP GAIN

The differential stage single-ended gain is given by

$$A_{12} \doteq \frac{R_{L_2}}{h_{ib_1}+h_{ib_2}+\frac{R_4}{\beta_4}} \qquad (1.17)$$

The second stage gain is given by

$$A_3 \doteq \frac{-R_{L_3}}{h_{ib_3}} \qquad (1.18)$$

The gain of the emitter follower is given by equation 1.1 and was calculated to be; $A_4 \doteq 1$. Utilizing equations 1.17 and 1.18, the first and second stage gains were calculated to be $A_{12} = 7$ and $A_3 = -295$. The amplifier open loop gain is given as

$$A_{OL} \doteq A_{12} \cdot A_3 \cdot A_4 \qquad (1.19)$$

The open loop gain was calculated to be -2000 or 66 db.

OPEN LOOP CORNER FREQUENCIES

For purposes of determining the open loop amplifier response curve, several simplifying assumptions were made, namely:

(i) C_{ob} for all transistors is 6 pf.

(ii) C_e for all transistors is determined by the formula: $C_e \doteq \frac{.16}{h_{ib} f_t}$ where f_t is the unity gain frequency of the transistor as given in the data sheets.

(iii) The input and output time constants have been neglected due to their small resistive components in the closed loop.

The interstage time constants of importance are given by the following equations as

$$\tau_{13} \doteq R_{L_2}\left[(1-A_3)C_{ob} + C_{e_3}\right] \qquad (1.20)$$

and

$$\tau_{34} \doteq R_{L_3}\left[C_{ob} + (1-A_4)C_{e_4}\right] \qquad (1.21)$$

Using equations 1.20 and 1.21, the time constants τ_{13} and τ_{34} were found to be 1.5×10^{-6} sec. and 0.48×10^{-7} sec. respectively, and their corresponding break frequencies, f_{13} and f_{34}, were found to be 107 kHz and 3.2 MHz respectively. The uncompensated open loop response curve is shown in Figure 8.

In order to re-shape the response curve for stable closed loop operation, capacitor C_2 and resistor R_9 were added to the circuit. The addition of these components modified f_{34} into a lag and a lead corner frequency given by

$$f'_{34} \doteq \frac{0.16}{R_{L_3}C_2} \quad \text{Hz(lag)} \qquad (1.22)$$

and

$$f''_{34} \doteq \frac{0.16}{C_2R_9} \quad \text{Hz(lead)} \qquad (1.23)$$

With the aid of equations 1.22 and 1.23, f'_{34} and f''_{34} were calculated to be 2kHz and 105kHz respectively. The compensated open loop response curve is shown in Figure 8.

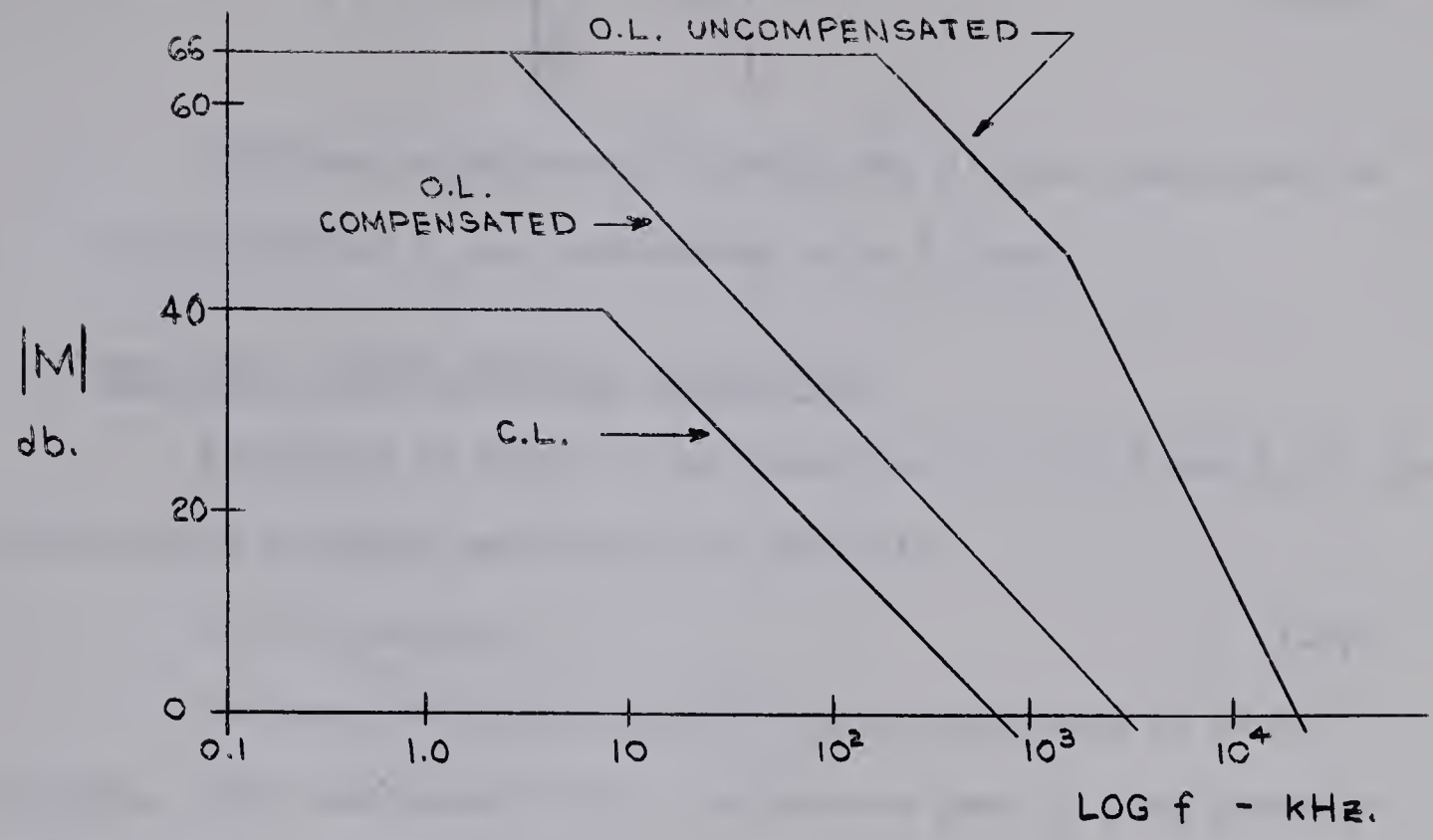

FIGURE 8. OUTPUT AMPLIFIER RESPONSE CURVES

CLOSED LOOP GAIN AND RESPONSE

In the closed loop, the output amplifier gain is determined by the relationship

$$A_{CL} = \frac{-R_3}{R_1} \cdot \frac{1}{1+s\tau_3} \qquad (1.24)$$

where $\tau_3 = R_3C_1$

Referring to the component values given in Figure 7, the closed loop corner frequency was found to be 7.8 KHz and the low frequency closed loop gain was set at -100. The output amplifier closed loop response is also shown in Figure 8.

OUTPUT IMPEDANCE

The output impedance of a closed loop operational amplifier is given as

$$Z_o \doteq R'_o // \left[\frac{R'_o(R_1 + R_2)}{R_1 \cdot A_{OL}} \right] \qquad (1.25)$$

where $$R'_o \doteq R_8 \,//\left[\frac{R_7}{\beta_4} + h_{ib_4}\right] \qquad (1.26)$$

Utilizing equations 1.25 and 1.26, R'_o was calculated to be 75 ohms and Z_o was calculated to be 4 ohms.

1.5 THE TOTAL SYSTEM PRESSURE SENSITIVITY

Referring to Figure 1 and equations 1.3, 1.12 and 1.24, the total system pressure sensitivity is given by

$$S_p = N_{33} \cdot A_{in} \cdot A_{cL} \qquad (1.27)$$

By means of equation 1.27, S_p was calculated to be 364 mV./psi. With this sensitivity, the maximum peak to peak pressure measurable is 40 psi.

1.6 PRESSURE MEASURING SYSTEM TESTS

The capacitance of the ceramic, while mounted in the flow tube, was measured, and found to be 375 pf. Input co-axial cable capacitance was measured and found to be 40 pf.

The system response was tested by replacing the ceramic with a 375 pf. capacitor and applying an electrical sine wave to this capacitor. A low frequency boost of 1.9 db. was noted at 0.14Hz whereas the mid-band gain was measured as 0.6db. Upper and lower corner frequencies were found at 5KHz and 0.035 Hz respectively. The test response curve is shown in Figure 9.

A hold time constant of 4.5 seconds was determined by applying steps of air pressure to the ceramic and observing the output system response.

System sensitivity was found to be linear at 350 mV./psi. by applying steps of known air pressure to the ceramic.

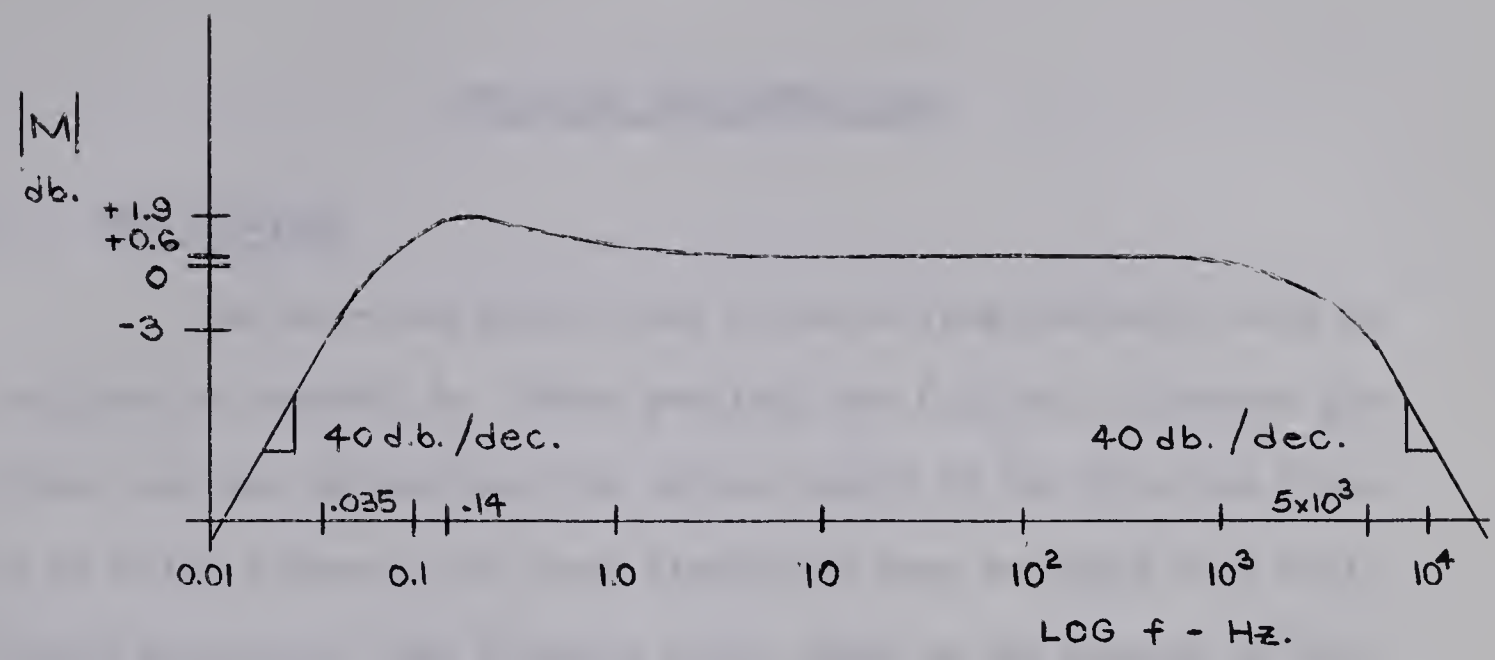

FIGURE 9. TOTAL SYSTEM RESPONSE CURVE

CHAPTER TWO

HOT-WIRE CONSIDERATIONS

2.1 THE HOT-WIRE

The hot-wire element was prepared from Wollaston wire as outlined in Appendix A. After etching, the 0.35 mil. diameter platinum core was exposed and the active length of the wire was found to be 0.135 inches. The above dimensions were measured by a calibrated microscope, the diameter being taken as the average of several readings. The following constants of platinum wire are used in later calculations:

S, specific heat = 0.0324 cal./gm.^{o}C

d, density = 352 gm./in.^{3}

α_o, temperature coefficient of resistance at $0^{o}C = 0.00363/^{o}C$

ρ_o, resistivity at $0^{o}C = 3.88 \times 10^{-6}$ ohm-inches

The resistivity of the wire at 20^{o}C is given by

$$\rho_{20} = \rho_o(1+\alpha_o T) \qquad (2.1)$$

as 4.7×10^{-6} ohm-inches or 5.32 ohm - C.M./inch, and the resistance of the hot-wire element at 20^{o}C is given by

$$R_a = \rho_{20}\frac{L}{A} \qquad (2.2)$$

as 5.42 ohms.

2.2 THE HOT-WIRE TRANSFER CHARACTERISTIC

A test was performed to determine the hot-wire resistance behavior for variations in wire current with mass air flow as a parameter. For this test, the hot-wire assembly was mounted in the

flow tube, and air was supplied to the flow tube via a Taylor mass flowmeter. The reference flowmeter had previously been calibrated against a reliable prover tank. The hot-wire characteristic is shown in Figure 10.

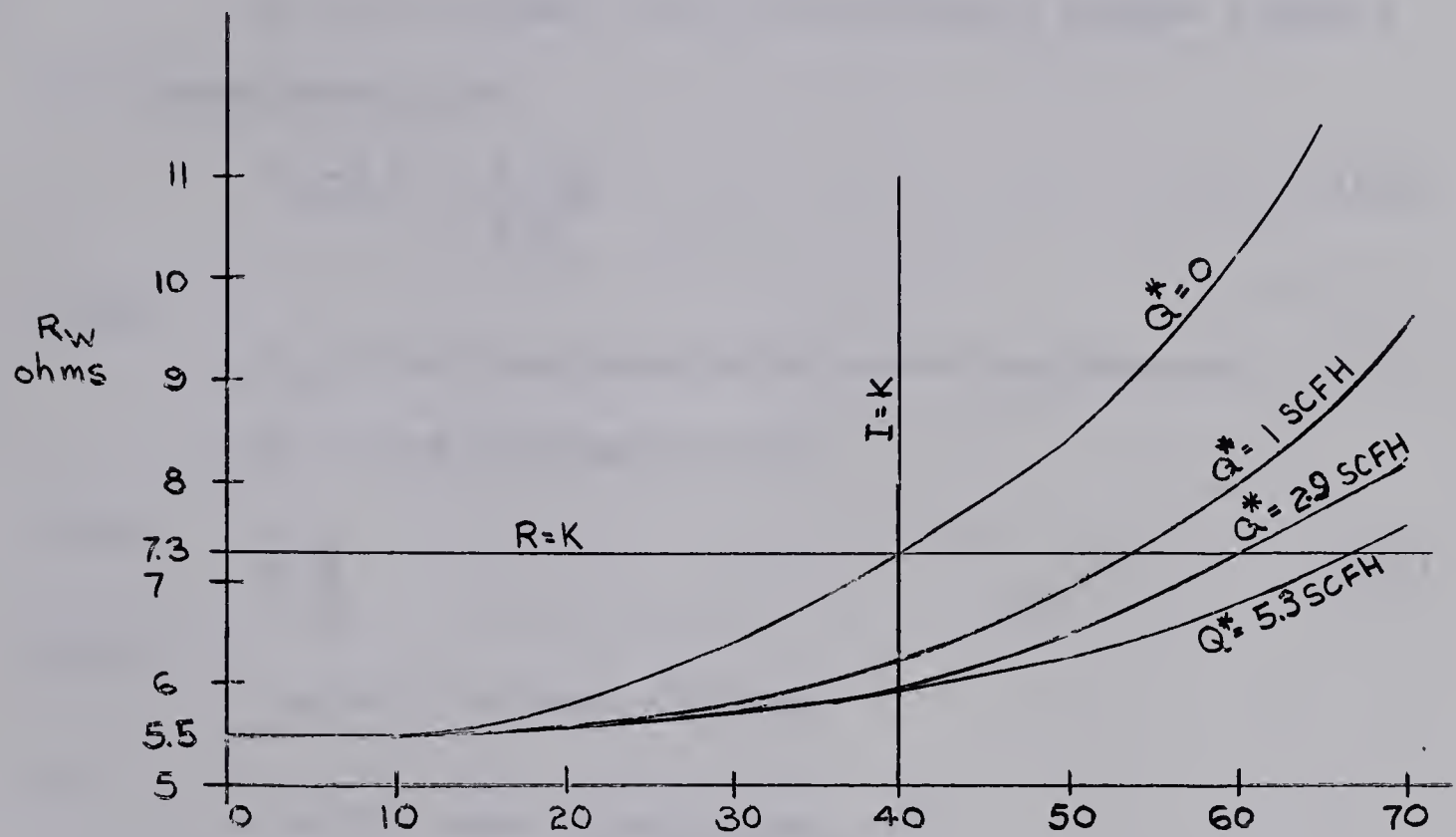

FIGURE 10. HOT-WIRE TRANSFER CHARACTERISTIC

2.3 THE HOT-WIRE HEAT BALANCE EQUATION

A heat balance equation for fine heated wires in an air stream is given by King's Law[5] as

$$I^2_w R_w = (K+D\sqrt{dU})\ (T_w - T_a) \qquad (2.3)$$

where

I_w = wire current, amps

R_w = wire resistance, ohms

K,D= King's Law constants

d = air density, lb./ft.^{3}

U = air velocity, ft./hour

T_w = wire temperature, ^oC

T_a = air stream temperature, ^oC

In utilizing equation 2.3, it was assumed that heat is transferred from the wire to the air stream by convection alone and that only the velocity component normal to the wire affects this heat exchange.

If it is assumed that wire resistance changes linearly with temperature, then

$$(T_w - T_a) = \frac{R_w - R_a}{R_o \alpha_o} \tag{2.4}$$

where

R_a = wire resistance at air stream temperature

R_o = wire resistance at 0^oC.

Since

$$U = \frac{Q}{A} \tag{2.5}$$

where

Q = air flow rate, $ft.^3$/hour

and

A = flow tube entrance area, $ft.^2$

and if

d*= air density at 20^oC and 14.7 psia.

and d = air density at 20^oC and stream absolute pressure

then equation 2.3 becomes

$$\frac{I^2_w R_w 10^{-3}}{R_w - R_a} = K' + D' \sqrt{\frac{d}{d^*} Q} \tag{2.6}$$

where I_w is given in mA., and the equation is given in units of mW./ohm.

Assuming that the air stream temperature is constant at 20^oC, then

$$\frac{d}{d^*} Q = \frac{PQ}{14.7} = Q^* \tag{2.7}$$

where P = air stream absolute pressure

Q*= air flow in SCFH.

The modified King's Law constants of equation 2.6 are

$$K' = \frac{K}{R_o \alpha_o} \quad mW./ohm \tag{2.8}$$

$$D' = \frac{D}{R_o \alpha_o} \sqrt{\frac{d^*}{A}} \tag{2.9}$$

2.4 HOT-WIRE OPERATING MODE

Two methods of operating a hot-wire for the measurement of air flow exist. In the first method, the hot-wire is operated at a constant current and resistance variations due to changes in air flow are utilized. If a wire bias current of 40 ma. is assumed in Figure 10, then the curve of Figure 11 shows the variation of hot-wire voltage with $\sqrt{Q^*}$, the effective input.

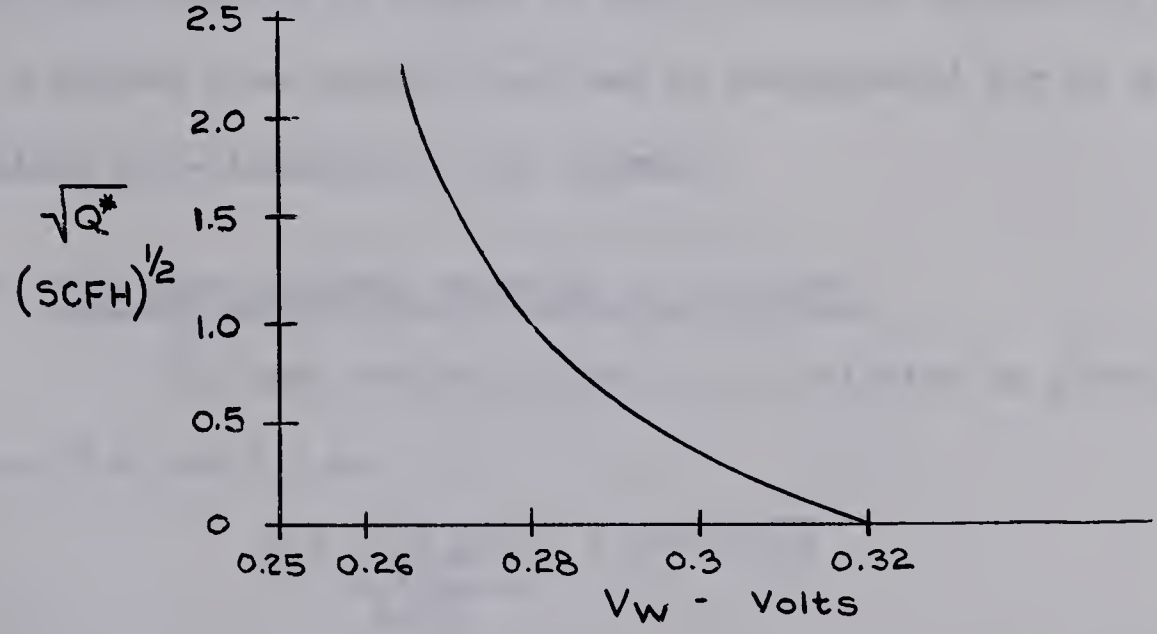

FIGURE 11. CONSTANT CURRENT HOT-WIRE OPERATION

The second method calls for operation of the hot-wire at a constant temperature, or constant resistance. Again, if a wire bias current of 40 mA. is assumed in Figure 10, then the curve of Figure 12 shows the variation of hot-wire current with $\sqrt{Q^*}$.

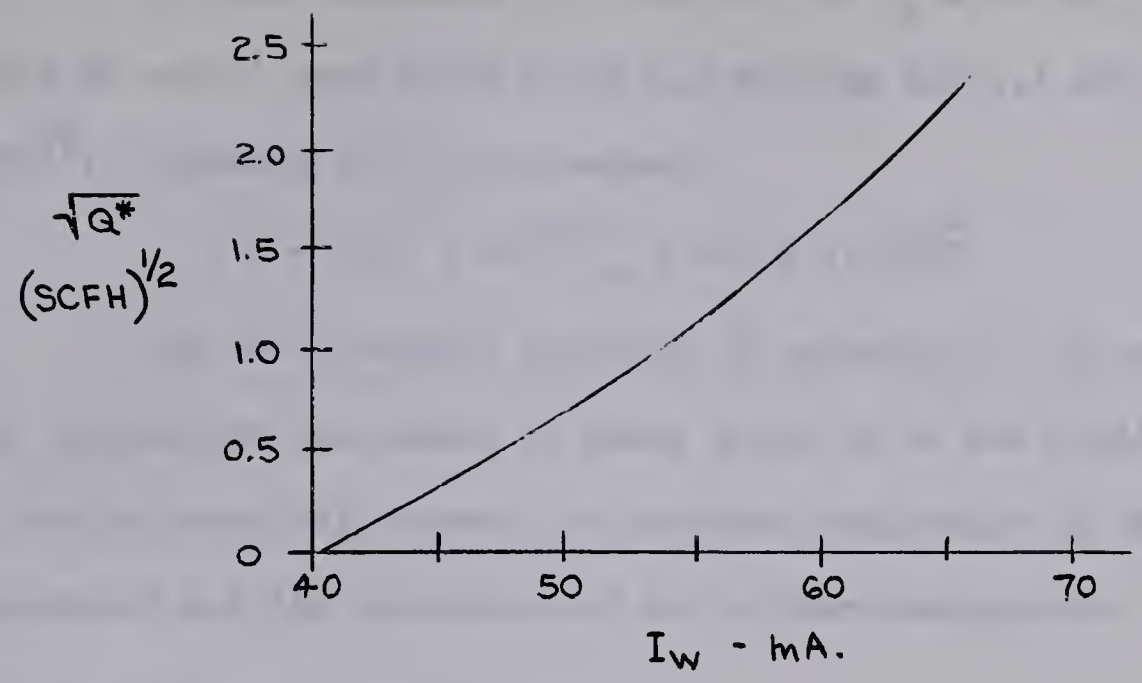

FIGURE 12. CONSTANT TEMPERATURE HOT-WIRE OPERATION

Comparing Figures 11 and 12, constant temperature operation is seen to be preferable for the metering of large scale flows. The non-linearity of Figure 12 may be further reduced by operating at a higher bias current, and may be compensated for by a complimentary non-linearity at the output.

2.5 THE HEAT TRANSFER FUNCTION OF VELOCITY

The heat transfer function of velocity is given by equations 2.6 and 2.7 as

$$H = \frac{I^2_w R_w 10^{-3}}{R_w - R_a} = K' + D' \sqrt{Q^*} \qquad (2.10)$$

The modifed King's Law constants may be evaluated by utilizing equation 2.10 and Figure 10. If a bias current, I_B, of 40 mA. is assumed at zero flow, this assumption implies that R_w must be maintained at 7.3 ohms.

$$K' = \left.\frac{I^2_B R_w 10^{-3}}{R_w - R_a}\right|_{Q^* = 0} \qquad (2.11)$$

$$D' = \left.\frac{I^2_B R_w 10^{-3}}{R_w - R_a}\right|_{Q^* = 1} - K' \qquad (2.12)$$

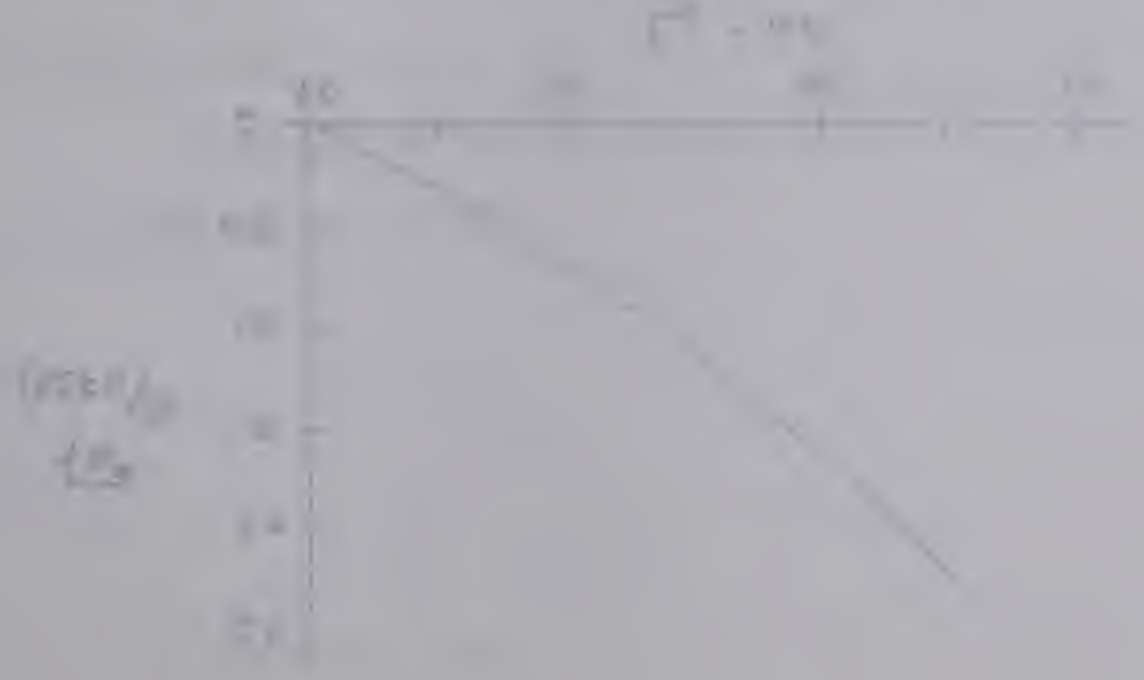

Solving equations 2.11 and 2.12 at I_B = 40 mA., the constants K' and D' were found to be 6.5 mW./ohm and 5.1 mW./ohm/$(SCFH)^{\frac{1}{2}}$. Equation 2.10 then becomes

$$H = 4.06 \times 10^{-3} I^2_w = 6.5 + 5.1\sqrt{Q^*} \qquad (2.13)$$

The heat transfer function of velocity, H, of equation 2.13, determines the amount of power given up to the fluid stream per ohm differential between the hot-wire resistance at operating temperature and its resistance at air stream temperature.

2.6 THE HOT-WIRE TIME CONSTANT

The thermal lag of a fine heated wire in an air stream is given by Dryden[6] as

$$\tau_w = \frac{4.2\ MS(R_w - R_a)}{I^2_w R_a R_o \alpha_o} \text{ sec.} \qquad (2.14)$$

where M = wire mass in grams

I_w = wire current in amps.

Equation 2.14 may be rearranged into

$$\tau_w = \left[\frac{4.2 d\pi^2 D^4 S}{16\ R_o \alpha_o} \times 10^6\right] \frac{R_w - R_a}{I^2_w R_a} \text{ sec.} \qquad (2.15)$$

where D = wire diameter in mils.

Equation 2.14 has also been defined by Grant and Kronauer[7] as

$$\tau_w = \frac{CR}{H} \text{ sec.} \qquad (2.16)$$

where

$$C = \frac{4.2\ MS}{R_o \alpha_o} \quad \frac{\text{joules}}{\text{ohm}}, \text{ heat capacity} \qquad (2.17)$$

$$H = \frac{I^2_w R_w 10^{-6}}{R_w - R_a} \quad \frac{\text{watts}}{\text{ohm}} \qquad (2.18)$$

I_w = wire current in Ma. (equations 2.15 and 2.18)

and

$$R = \frac{R_w}{R_a} \tag{2.19}$$

Equations 2.16 through 2.19 are utilized in the analysis of the hot-wire system in Chapter Four.

By substituting proper values into equation 2.15, it may be rewritten as

$$\tau_w = 31.5 \frac{R_w - R_a}{I^2_w R_a} \tag{2.20}$$

Solving equation 2.20 at I_w = 40 mA., yields, τ_w = 6.59×10^{-3} sec. and f_w = 24.1 Hz.

According to Schubauer and Klebanoff[8], the true time constant may be higher than that calculated due to end effects. They state that at an L/D ratio of 200, the true time constant may be 10 to 20% higher. The L/D ratio for the wire used is 360.

Tests were performed in order to determine the effect on the wire 3db down frequency of various static air flows and wire currents. The tests were performed by inserting the wire into one arm of a balanced Wheatstone bridge and impressing a 5 mA. peak to peak signal onto the wire bias current. Bridge unbalance voltage was taken as the system output. The results of these tests are shown in Figure 13.

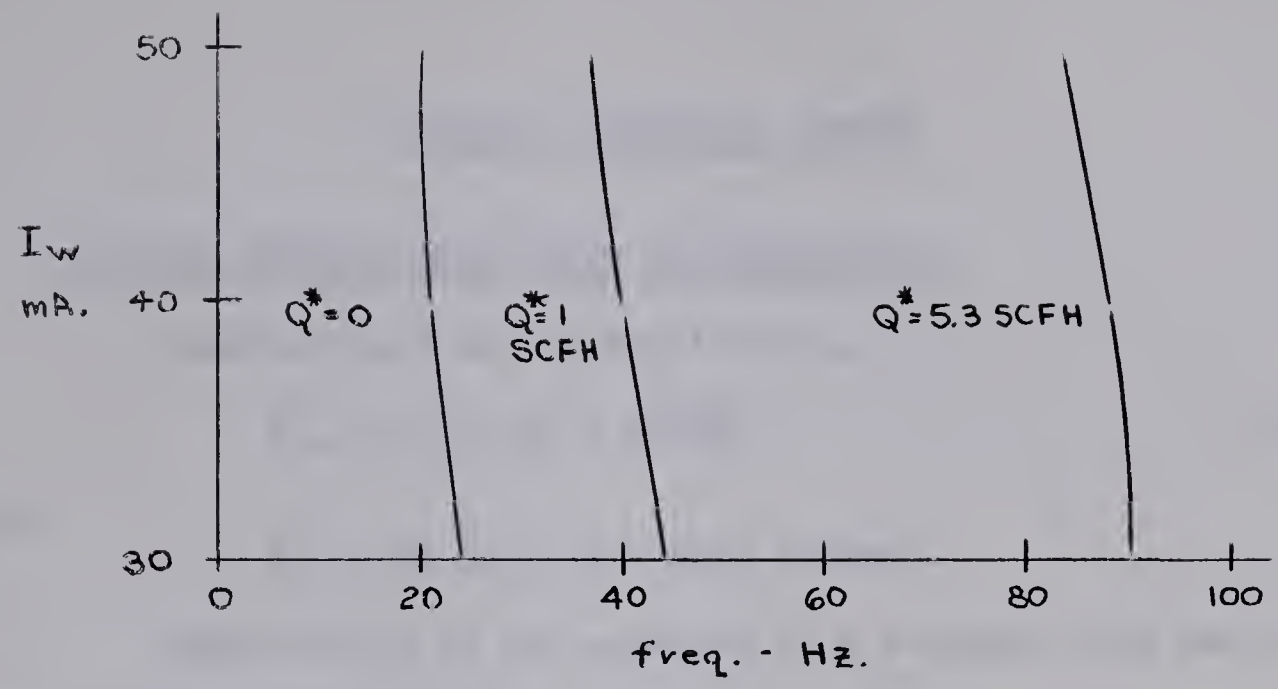

FIGURE 13. HOT-WIRE CORNER FREQUENCY TEST

CHAPTER THREE

THE FLOW MEASURING SYSTEM

3.1 CONSTANT TEMPERATURE SYSTEM CONSIDERATIONS

Equation 2.13 may be rewritten as

$$I^2_w = I^2_b + 1.26 \times 10^3 \sqrt{Q^*} \qquad (3.1)$$

where

I_b = 40 mA., wire bias current.

Equation 3.1 is the equation of a straight line and is shown plotted in Figure 14.

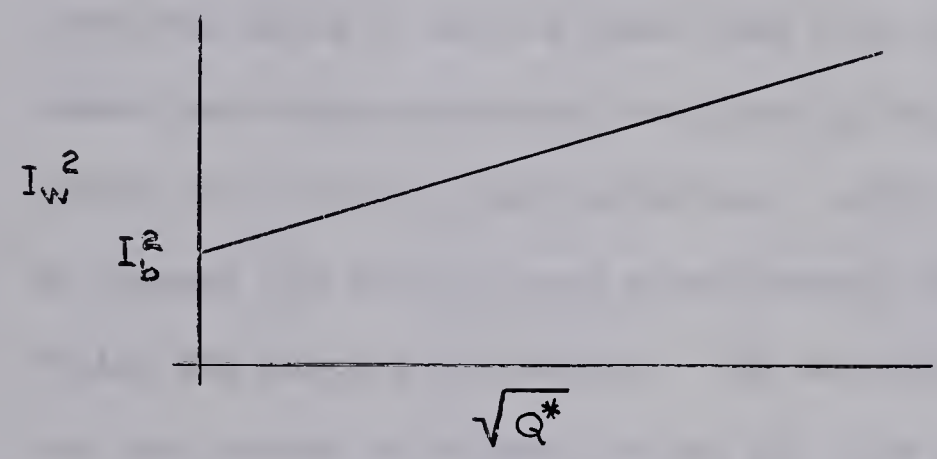

FIGURE 14. CONSTANT TEMPERATURE SYSTEM EQUATION

The control circuit has basically two functions to perform. The first is to meet the equality of equation 3.1, and the second is to extend the hot-wire corner frequency. The wire corner frequency is extended by a factor equal to the loop gain of the system. This is accomplished in view of the fact that the hot-wire has a time constant in the forward path due to H, and the same time constant in the feedback path due to I_w.

HOT-WIRE BRIDGE

The hot-wire may be operated in either the grounded

arm or the floating arm of the bridge (Figures 15a and 15b).

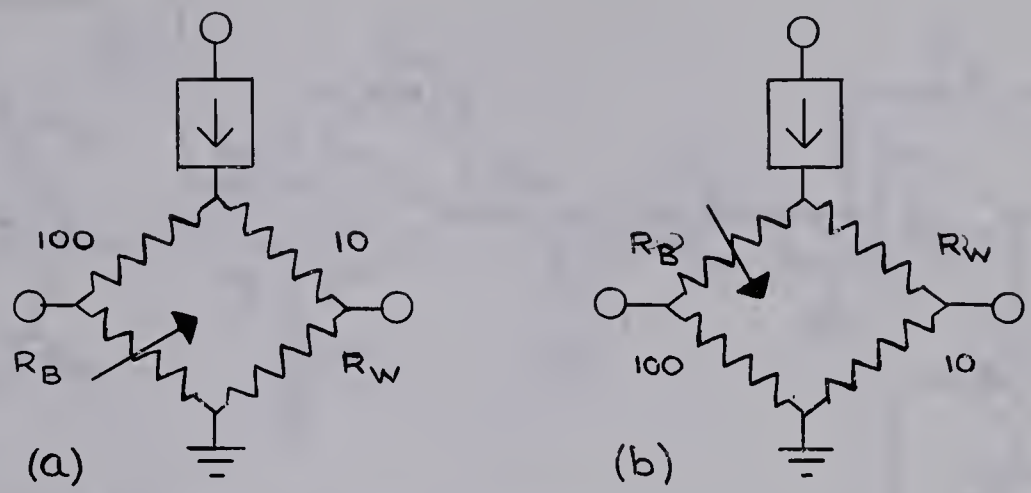

FIGURE 15. HOT-WIRE BRIDGE

The floating arm configuration of Figure 15b is preferred since it may be shown that this circuit has a common mode ratio advantage over that of Figure 15a by a factor of 3 for air flow variations. Both the circuits of Figures 15a and 15b have approximately the same CM ratios for current variations. The calculated CM ratios for the circuit of Figure 15b for air flow and for current variations are 2.3 and 0.23 respectively, where $CMR = V_D/V_C$.

3.2 THE CONTROL CIRCUIT

Figure 16 shows the hot-wire control circuit in detail. Amplifier A_1 is an operational amplifier with a high common mode rejection ratio. Components R_9 and C_1 together form a low pass filter, which was found necessary for common mode stability. Amplifier A_2 is also an operational amplifier. The loop gain of the system may be adjusted by means of potentiometer R_{10}.

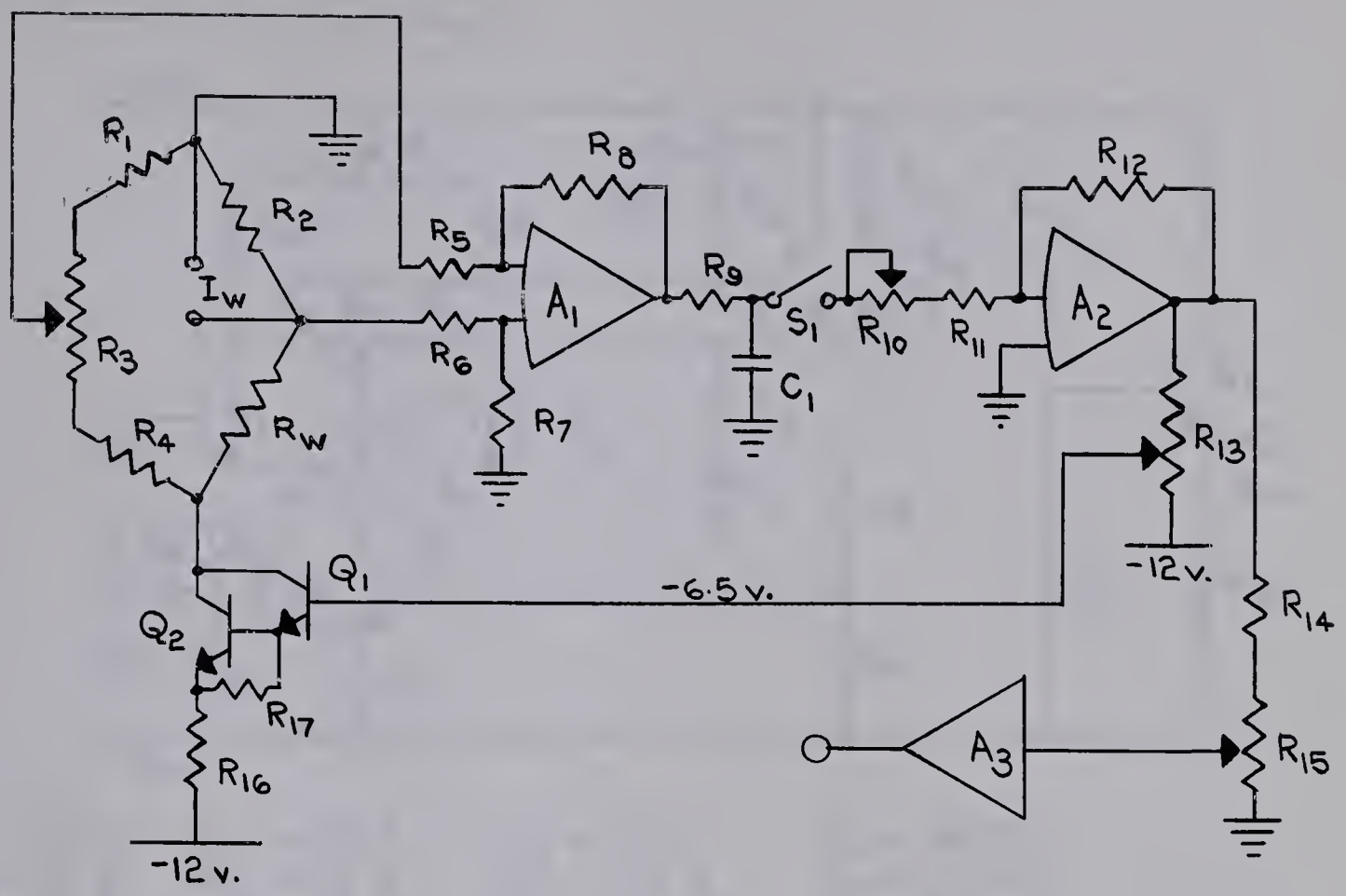

R_1 = 100	R_6 = 1 K	R_{11} = 1 K	R_{16} = 100
R_2 = 10	R_7 = 1 M	R_{12} = 82 K	R_{17} = 1.2K
R_3 = 100	R_8 = 1 M	R_{13} = 5 K	C_1 = 0.06Mf.
R_4 = 56	R_9 = 220	R_{14} = 6.8K	Q_1 = 2N3707
R_5 = 1 K	R_{10} = 10 K	R_{15} = 1 K	Q_2 = BFY-51

FIGURE 16. HOT-WIRE CONTROL CIRCUIT

Potentiometer R_{13}, the output emitter resistor of amplifier A_2, serves as a bridge current adjustment when switch S_1 is open, and acts as an output zeroing adjustment when switch S_1 is closed, as in normal operation. Transistors Q_1 and Q_2 together form a Darlington Compound which acts as the current source for the bridge. Potentiometer R_3 balances the bridge when S_1 is open, and serves as the bridge current adjustment when S_1 is closed. Potentiometer R_{15} acts as a variable attenuator for control circuit output signal entering the linearizing amplifier, A_3. Current through the hot-wire is measured by the voltage drop across R_2, a 10 ohm resistor.

3.3 THE BRIDGE AMPLIFER (A_1)

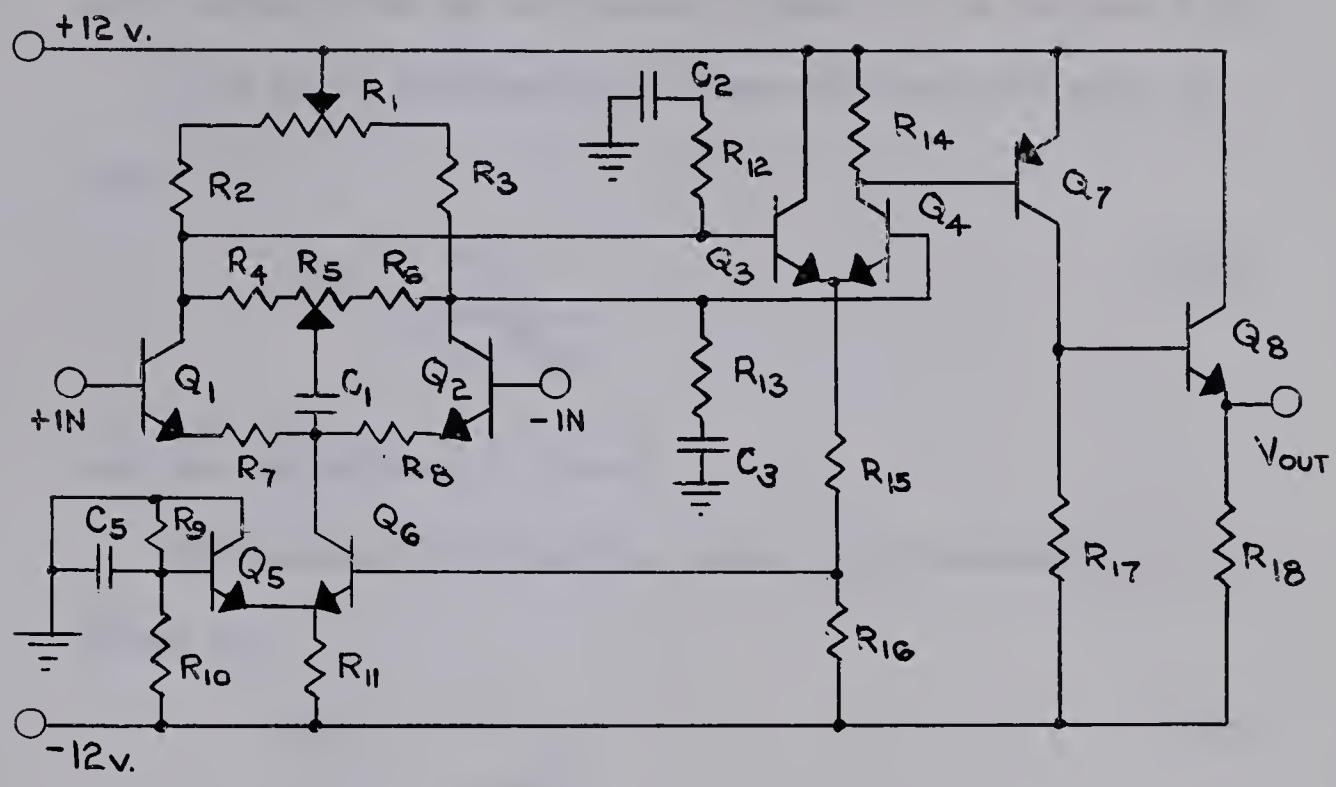

R_1	= 10 K	R_9	= 27 K	R_{17}	= 12 K	Q_4	= 2N3707
R_2	= 47 K	R_{10}	= 27 K	R_{18}	= 5.6 K	Q_5	= TI 412
R_3	= 47 K	R_{11}	= 12 K	C_1	= 2.5 pf.	Q_6	= TI412
R_4	= 56K	R_{12}	= 680	C_2	= 0.002Mf.	Q_7	= 2N3703
R_5	= 100 K	R_{13}	= 680	C_3	= 0.002Mf.	Q_8	= 2N3707
R_6	= 56 K	R_{14}	= 6.8 K	Q_1	= 2N3707	C_5	= 0.01Mf.
R_7	= 1 K	R_{15}	= 3.3 K	Q_2	= 2N3707		
R_8	= 1 K	R_{16}	= 3.3 K	Q_3	= 2N3707		

FIGURE 17. BRIDGE AMPLIFIER SCHEMATIC

BIAS CONDITIONS

Referring to Figure 17, R_1 adjusts the emitter of Q_8 to zero volts. Q_5 and Q_6 together deliver 0.45 mA. to R_{11}. Assuming that Q_5 and Q_6 share this current equally, then each operates at 0.225 mA. If Q_1 and Q_2 operate at equal currents, then each operates at approximately 0.11 mA. The collectors of Q_1 and Q_2 will then be biased at 6.15 V., forcing Q_3 and Q_4 to operate at 0.85 mA. each. Q_8 is biased to operate at 2.1 mA. and Q_7 at 1.05 mA.

OPEN LOOP DIFFERENTIAL FREQUENCY RESPONSE

Gain and corner frequency calculations for the differ-

ential response of the bridge amplifier are based on the same assumptions as previously presented in Section 1.3.

The first differential stage differential gain is given by

$$A_{12} \doteq \frac{-R_{L_2}}{h_{ib_2}+R_{e_2}} \tag{3.2}$$

and was calculated to be -8.

The second differential stage single-ended gain is given by

$$A_{34} \doteq \frac{-R_{L_4}}{2\,h_{ib_4}} \tag{3.3}$$

and was calculated to be -8.5.

The third stage gain is given approximately by

$$A_7 \doteq \frac{-R_{L_7}}{h_{ib_7}} \tag{3.4}$$

and was found to be -460.

The unloaded gain of the emitter follower stage is given as

$$A_8 \doteq \frac{1}{1+\frac{h_{ib_8}}{R_{18}}} \tag{3.5}$$

and was found to be unity.

The open loop differential gain, as given by

$$A_{0L} \doteq A_{12}\cdot A_{34}\cdot A_7\cdot A_8 \tag{3.6}$$

was found to be -3.1×10^4 or 90 db.

The first interstage time constant, τ_{24}, is given as

$$\tau_{24} \doteq R_{L_2} \left[(1-A_{34})\, C_{ob} + C_{e_4} \right] \text{ sec.} \qquad (3.7)$$

and was found to be 0.27×10^{-5} sec.

The second interstage time constant, τ_{47}, is given by

$$\tau_{47} \doteq R_{L_4} \left[C_{e_7} + (1-A_7) C_{ob} \right] \text{ sec.} \qquad (3.8)$$

and was calculated to be 0.145×10^{-5} sec.

The third interstage time constant, τ_{78}, is given by

$$\tau_{78} \doteq R_{L_7} C_{ob} \text{ sec.} \qquad (3.9)$$

and was found to be 0.72×10^{-7} sec.

The uncompensated open loop differential response curve, based on the above calculations is given in Figure 18. The corner frequencies, related to the above time constants were found to be:

f_{24} = 60 kHz, f_{47} = 110 kHz, and f_{78} = 2.2 MHz.

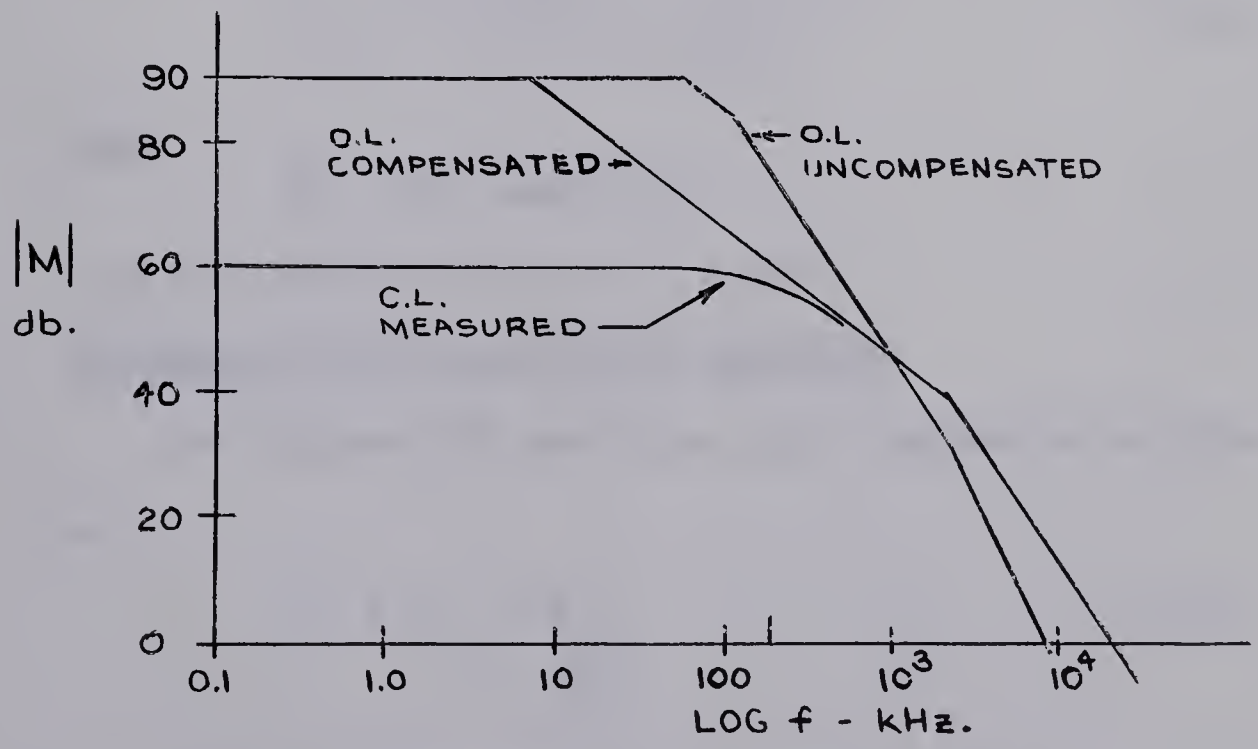

FIGURE 18. BRIDGE AMPLIFIER DIFFERENTIAL RESPONSE

For stable closed loop operation at a gain of 60db, the amplifier response was modified by the addition of components R_{12}, R_{13}, C_2 and C_3. The modified time constants are given as

$$\tau'_{24} \doteq R_{L_2} C_3 \text{ sec.} \qquad (3.10)$$

and

$$\tau''_{24} \doteq R_{13} C_3 \text{ sec.} \qquad (3.11)$$

and were calculated to be 0.2×10^{-4} sec. and 0.14×10^{-5} sec. respectively. The corresponding corner frequencies were found to be:

$$f'_{24} = 8 \text{ kHz (lag) and } f''_{24} = 115 \text{ kHz (lead).}$$

The compensated open loop differential response curve is also shown in Figure 18.

DIFFERENTIAL INPUT IMPEDANCE

The differential input impedance is given approximately as

$$Z_{iD} \doteq 2 \left[\beta_2 (h_{ib_2} + R_8)\right] \qquad (3.12)$$

where

$$\beta_2 = 300 \text{ (measured)}$$

Z_{iD} was calculated to be 175 K ohms.

DIFFERENTIAL OPEN LOOP OUTPUT IMPEDANCE

The differential open loop output impedance is given as

$$Z_o \doteq h_{ib_8} + \frac{R_{17}}{\beta_8} \qquad (3.13)$$

where $\beta_8 = 100$ (measured)

and was calculated to be 130 ohms.

COMMON MODE FREQUENCY RESPONSE

The common mode gain and frequency response, for the bridge amplifier, were calculated with the aid of Figure 19, the common mode equivalent circuit.

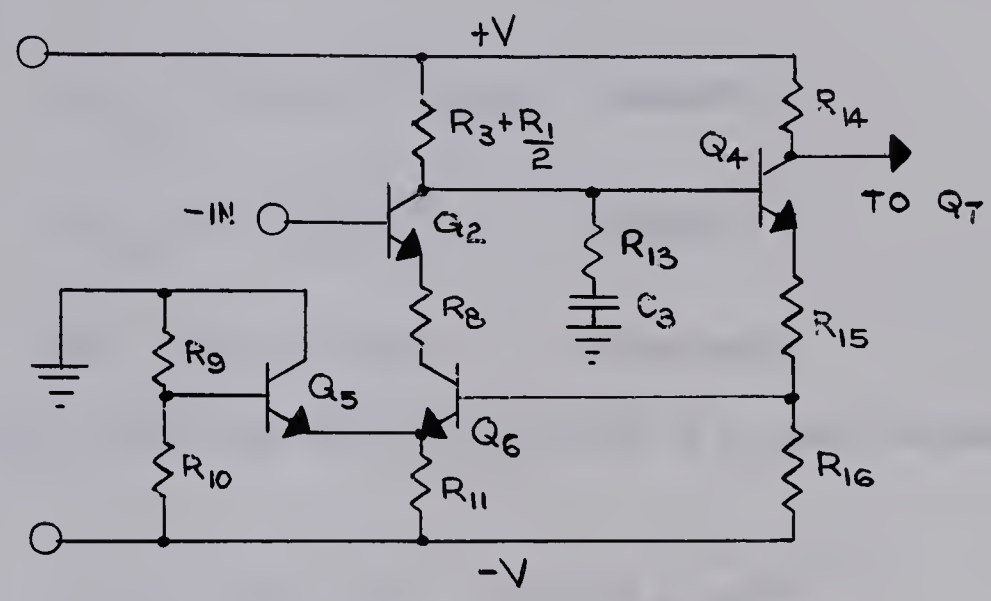

FIGURE 19. COMMON MODE EQUIVALENT CIRCUIT

The common mode gain without common mode feedback is given by

$$A_{cm} \doteq \frac{R_{L_2} \cdot R_{L_4} \cdot R_{L_7}}{4(R_8 + Z_{o_6})(R_{15} + R'_{16})h_{ib_7}} \tag{3.14}$$

where

$$R'_{16} = R_{16} // \left[\beta_6(h_{ib_6} + R_{e_6})\right] \tag{3.15}$$

$$R_{e_6} = h_{ib_5} + \frac{R_9 // R_{10}}{\beta_5} \tag{3.16}$$

and

$$\frac{1}{Z_{oe}} = Y_{oe} = h_{ob} + \frac{h_{ob} Z_B + h_{rb}}{\frac{h_{ib} + Z_e + Z_B}{\beta}} \tag{3.17}$$

Utilizing equation 3.17, the output admittance of the current source, Q_6, is given as

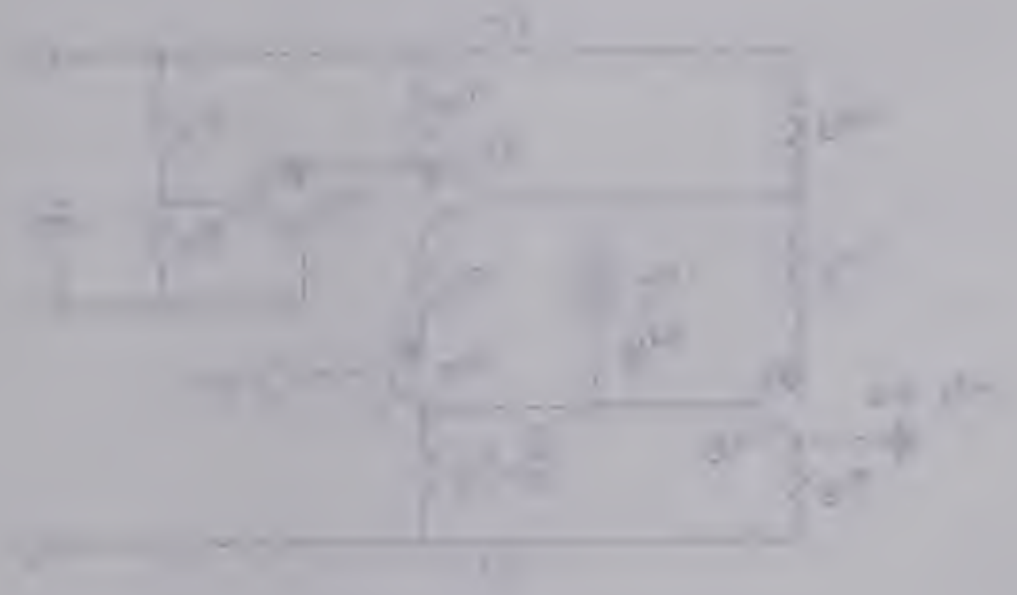

$$Y_{o_6} = \frac{h_{ob_6}+h_{ob_6}R_{16}+h_{rb_6}}{h_{ib_6}R_{e_6}+\frac{R_{16}}{\beta_6}} + j\omega\left[\frac{C_{ob_6}+C_{ob_6}R_{16}}{h_{ib_6}+R_{e_6}+\frac{R_{16}}{\beta_6}}\right] \qquad (3.18)$$

where

$$h_{ob_6} = 0.5 \times 10^{-7} \text{ mhos} \quad \text{(assumed)}$$

$$h_{rb_6} = 0.5 \times 10^{-4} \quad \text{(assumed)}$$

$$\beta_5 = \beta_6 = 120 \quad \text{(measured)}$$

Using equations 3.14 through 3.18 Y_{o_6} was calculated to be

$$Y_{o_6} = 5.8 \times 10^{-7} + j\omega\, 55.2 \times 10^{-12}$$

and the open loop common mode gain, A_{cm}, was found to be 0.12.

The common mode loop gain, based on Figure 19, is given as

$$A_L = \frac{R_{L_2}R'_{16}}{(h_{ib_6}+R_{e_6})(R_{15}+R'_{16})} \qquad (3.19)$$

and was calculated to be 28.

The closed loop low frequency common mode gain is given as

$$A_{cm}' = \frac{A_{cm}}{1+A_L} \qquad (3.20)$$

and was found to be 4.1×10^{-3} or -48 db.

To find the shape of the common mode response curve, it was necessary to inspect the common mode gain of the input transistor, Q_2, of Figure 19.

$$A_2 = \frac{Z_{L_2}}{h_{ib_2} + R_8 + Z_{o_6}} \tag{3.21}$$

where

$$Z_{L_2} = R_{L_2} // \left[R_{13} + \frac{1}{j\omega C_3} \right] \tag{3.22}$$

Then

$$A_2 = \frac{R_{L_2} // \left[R_{13} + \frac{1}{j\omega C_3} \right]}{h_{ib_2} + R_8 + \frac{1}{5.8 \times 10^{-7} + j\omega\, 5.5 \times 10^{-11}}} \tag{3.23}$$

Inspecting equation 3.23, it is seen that both the neumerator and the denominator contain a lag and a lead corner frequency. In the neumerator, $f^N_{Lag} = \frac{0.16}{R_{L_2} C_3} = 2.4$ kHz and $f^N_{Lead} = \frac{0.16}{R_{13} C_3} = 117$ kHz are the two corner frequencies, whereas, in the denominator, $f^D_{Lead} = \frac{0.16 h'_{ob}}{C'_{ob}} = 1.7$ kHz and $f^D_{Lag} = \frac{0.16}{(h_{ib_2} + R_8) C'_{ob}} = 2.3$ MHz are the other two corner frequencies. Since Z_{L_2} of equation 3.22 appears in both A_{cm} and A_L of equation 3.20, the lag corner frequency f^N_{Lag} must be modified by the loop gain to $f^{N*}_{Lag} = 700$ kHz.

The lag corner frequencies, f_{47} and f_{78}, as previously calculated, are also valid for the common mode response curve.

Based on the preceding calculations, the common mode response curve is shown in Figure 20.

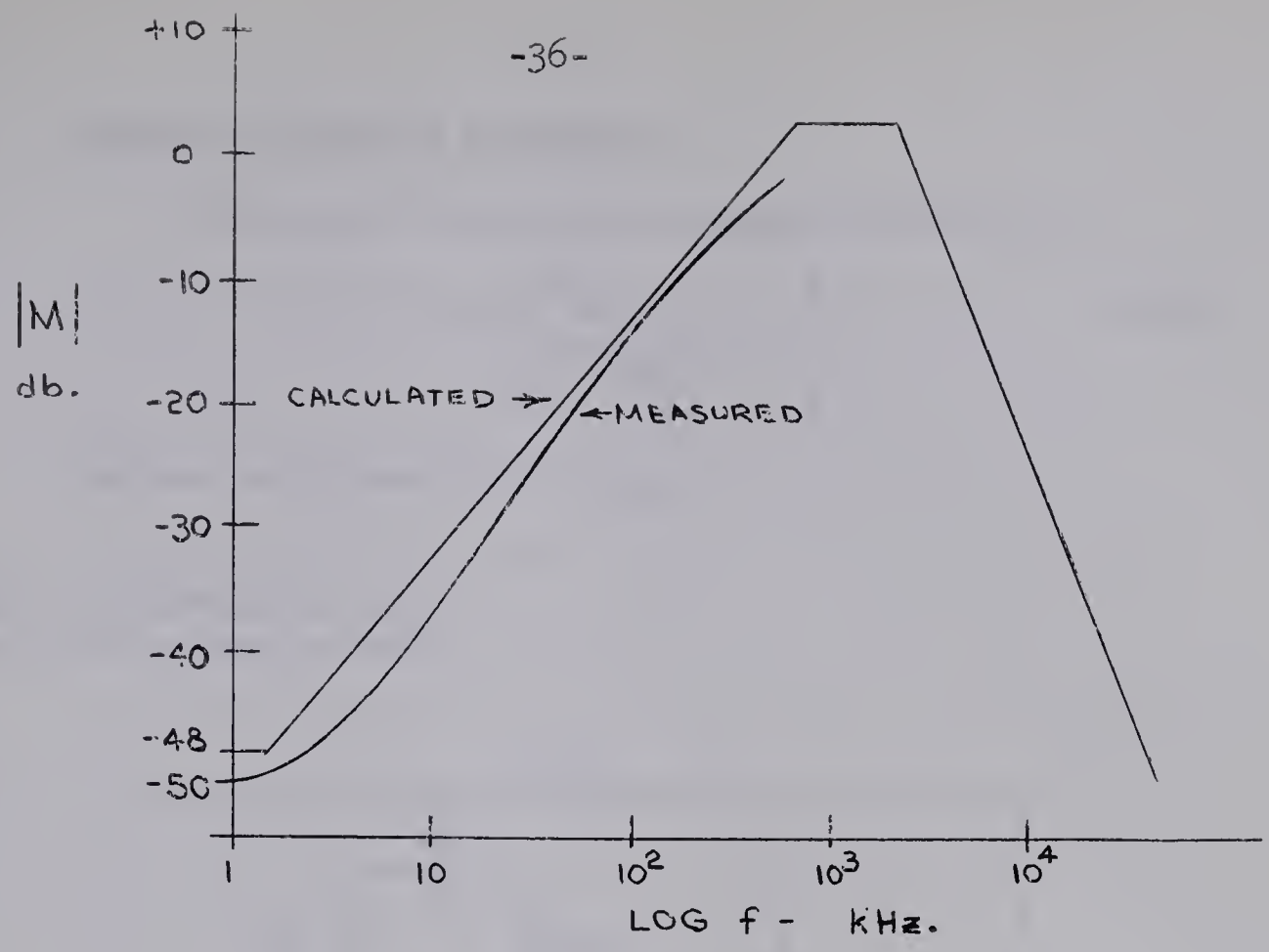

FIGURE 20. COMMON MODE FREQUENCY RESPONSE

The circuit consisting of R_4, R_5, R_6, and C_1, was added to the amplifier input stage to cancel the effects produced by a slight mismatch of the input transistors. By the adjustment of R_5, an unbalanced common mode signal may be fed back to the collectors of Q_1 and Q_2 in such a manner as to cancel unwanted differential to common mode gain signals appearing there. This circuit has a negligible effect on the differential frequency response curve.

MEASURED CLOSED LOOP RESPONSE CURVES

Figure 18 shows the measured differential frequency response curve obtained by applying single-ended signals between either the positive or the negative input and ground.

Figure 20 shows the measured common mode frequency response, with R_5 adjusted, and with the signal applied between both inputs and ground.

CLOSED LOOP OUTPUT IMPEDANCE

The closed loop output impedance is given by

$$Z_o' \doteq Z_o // \left[\frac{(R_5+R_8)\, Z_o}{R_5 A_{oL}} \right] \qquad (3.23)$$

and was calculated to be 4 ohms.

3.4 THE LOOP AMPLIFIER (A_2)

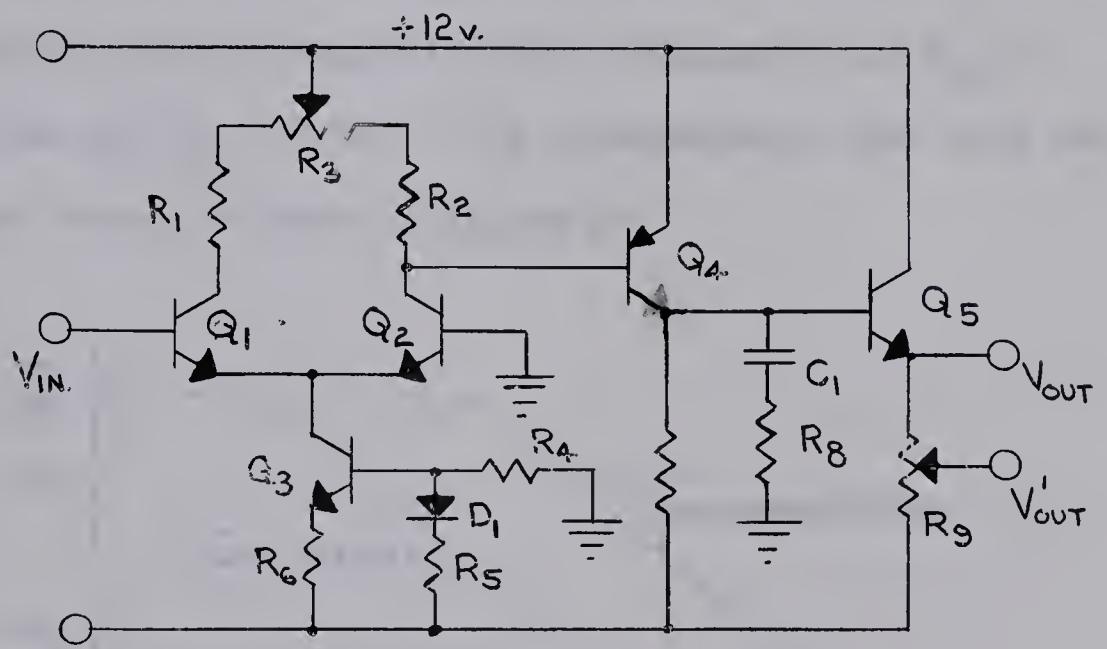

R_1 = 220	R_5 = 5.6 K	R_9 = 5 K	Q_2 = TI411
R_2 = 2 K	R_6 = 5.6 K	C_1 = 0.0067 μf.	Q_3 = TI411
R_3 = 220	R_7 = 2.7 K	D_1 = 1020	Q_4 = 2N3702
R_4 = 5.6 K	R_8 = 330	Q_1 = TI411	Q_5 = 2N3707

FIGURE 21. LOOP AMPLIFIER SCHEMATIC

BIAS CONDTIONS

Referring to Figure 21, R_3 adjusts the emitter of Q_5 to zero volts, causing Q_5 to deliver 2.4 mA. to R_9. Q_4 then is forced to operate at 4.7 mA. The current source, Q_3, is biased to operate at 1 mA. Assuming that Q_1 and Q_2 share the current supplied by Q_3, then each operates at 0.5 mA.

OPEN LOOP GAIN AND FREQUENCY RESPONSE

Utilizing the assumptions as outlined in Section 1.3, and equations 1.17, 1.18 and 1.19, the amplifier stage gains and open loop gain were calculated to be: $A_{12} \doteq 6.1$, $A_4 \doteq -450$, $A_5 \doteq 1$, and $A_{oL} = -2750$ or 68.8db.

The interstage time constants, as calculated from equations 1.20 and 1.21 were found to be: $\tau_{14} = 0.18 \times 10^{-5}$ sec. and $\tau_{45} = 0.19 \times 10^{-7}$ sec. The corresponding corner frequencies were calculated as: $f_{14} = 90$ kHz and $f_{45} = 8$ Mhz. The uncompensated open loop response curve is shown in Figure 22.

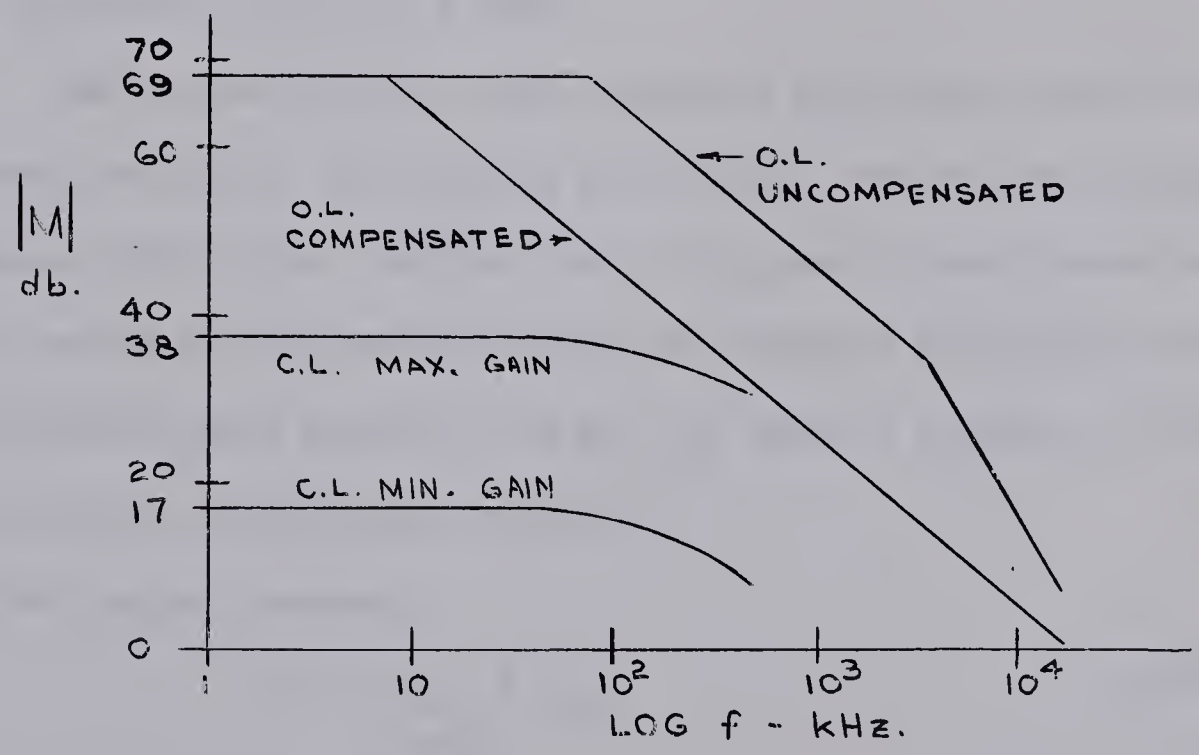

FIGURE 22. LOOP AMPLIFIER RESPONSE CURVES

Components C_1 and R_8 were added to the amplifier circuit to compensate the response curve for stable closed loop operation. The modified time constants caused by this addition were found to be: $\tau'_{45} \doteq R_7C_1 = 0.19 \times 10^{-4}$ sec. and $\tau''_{45} = R_8C_1 = 0.23 \times 10^{-5}$ sec. The corner fre-

quencies resulting from these time constants were calculated as: f'_{45} = 8.5 kHz (lag) and f''_{45} = 70 kHz (lead). The compensated open loop response curve, based on the preceding calculations, is shown in Figure 22. Figure 22 also shows the measured closed loop frequency response curves at both maximum and minimum gains.

3.5 THE CURRENT SOURCE

Referring to Figure 16, when the system is in closed loop operation with the hot-wire biased at 40 mA., the current source load is given as

$$R_L = (R_w+R_2)//(R_1+R_2+R_3) \qquad (3.25)$$

and was calculated to be 16.2 ohms.

The current source, then, supplies the bridge with 42.7 mA., causing a 0.69 V. drop across the bridge. The emitter of Q_2 is biased at -7.7 volts, and the bases of Q_2 and Q_1 are biased at -7 volts and -6.5 volts respectively. Q_1 supplies the bridge with 0.6 mA. while Q_2 must provide 42.1 mA. Q_2 must be capable of dissipating 300 mW. under these conditions.

For the Darlington Compound:

$$h_{ib}^{*} = \frac{h_{ib_1}}{\beta_2} + h_{ib_2} \qquad (3.26)$$

$$\beta^{*} = \beta_1 \cdot \beta_2 \qquad (3.27)$$

where

$$\beta_1 = 240 \text{ and } \beta_2 = 160 \text{ (measured)}.$$

The current source input impedance is given as

$$Z_i \doteq \beta^{*}(h_{ib}^{*}+R_{16})//\frac{1}{h_{ob_1}} \qquad (3.28)$$

and was found to be in the megohm range.

Since the impedance levels at the input and output of the current source are relatively low, the frequency response of the compound was considered flat up to and beyond the frequencies of interest.

3.6 THE LOW PASS NETWORK

Referring to Figure 16, the low pass network, composed of R_9, R_{10}, R_{11} and C_1, will have a time constant and an attenuation factor given by

$$\tau_{LP} \doteq C_1 \left[R_9 // (R_{10}+R_{11}) \right] \tag{3.29}$$

$$\gamma = \frac{R_{10}+R_{11}}{R_9+R_{10}+R_{11}} \tag{3.30}$$

The time constants, at maximum and minimum loop gains were found to be 1.2×10^{-5} sec. and 1.5×10^{-5} sec. whereas the corresponding corner frequencies were calculated as 13 kHz and 11 kHz. The attenuation factors at maximum and minimum gains were calculated to be 0.83 and 0.98 respectively.

CHAPTER FOUR

ANALYSIS OF THE HOT-WIRE BRIDGE AND CONTROL SYSTEM

4.1 GENERAL CLOSED LOOP CONSIDERATIONS

Figure 23 shows a simplified schematic of the hot-wire bridge and control loop.

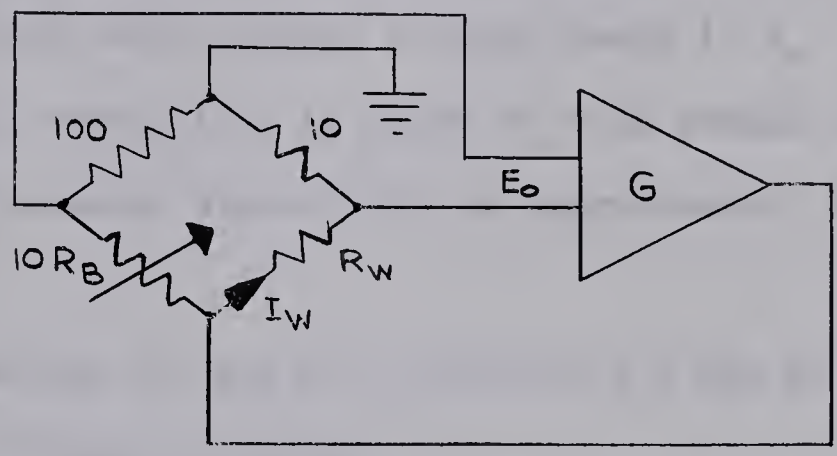

FIGURE 23. SIMPLIFIED BRIDGE AND CONTROL LOOP SCHEMATIC

In the closed loop, if G is large, the bridge is always near balance, and the bridge output voltage may be written as

$$E_o = I_W(R_W - R_B) \tag{4.1}$$

where R_B is the value of R_w that balances the bridge. The hot-wire current is given as

$$I_W = I_B - GE_o \tag{4.2}$$

where I_B is the hot-wire current that flows when the bridge is balanced at zero air flow, and G is the loop transconductance, including current division at the bridge. On the basis of equations 4.1 and 4.2, the following relationships were obtained:

$$I_W = \frac{I_B}{1+G(R_W-R_B)} \tag{4.3}$$

and

$$R_W = \frac{\phi-1+GR_B}{G} \tag{4.4}$$

where

$$\phi = \frac{I_B}{I_W} \tag{4.5}$$

From equation 4.3, it may be seen that, if G is large, a small change in R_W will produce a large change in I_W. Equation 4.4 indicates that, again, if G is large, R_W will remain nearly constant with air flow changes, since ϕ will be approximately 0.6 when Q^* = 5 SCFH.

Equations 2.3 and 2.4 of Section 2.3 may be combined to yield the heat balance equation

$$I_W^2 R_W = (R_W-R_a)H \tag{4.6}$$

where H is the heat transfer function of velocity for the wire. Combining equations 4.4 and 4.6 yields

$$\frac{I_W^2}{H} = \frac{1-R_aG}{\phi-1+GR_B} \tag{4.7}$$

Equation 4.7 indicates that for large values of G, I_W^2 is proportional to H in steady-state closed loop operation.

4.2 THE LINEARIZED HOT-WIRE FLUCTUATION EQUATION

In dynamic operation of the hot -wire, equation 4.6 must be modified[8] by the addition of a heat capacity term C, such that,

$$I_W^2 R_W = (R_W-R_a)H + C\frac{dR_W}{dt} \tag{4.8}$$

To linearize this equation, all variables are divided into their long term steady-state (bar) components, and their fluctuation (prime) components.

$$I_w = \bar{I}_w + I_w'(t)$$
$$R_w = \bar{R} + R_w'(t)$$
$$R_a = \bar{R} + R_a'(t)$$
$$H = \bar{H} + H'(t) \qquad (4.9)$$

Combining equations 4.8 and 4.9 produces the steady-state equation:

$$\bar{I}_w^2 \bar{R}_w = (\bar{R}_w - \bar{R}_a)\bar{H} \qquad (4.10)$$

Neglecting all products of primed quantities, and subtracting out equation 4.10 from the combined equation of 4.8 and 4.9 yields the linearized fluctuation equation:

$$\frac{R_w'}{\bar{R}_w} + CR\,\frac{\bar{H}}{\bar{I}_w}\,\frac{d(R_w'/\bar{R}_w)}{dt} = 2(R-1)\frac{I_w'}{\bar{I}_w} + \frac{R_a'}{\bar{R}_a} - \frac{(R-1)H'}{\bar{H}} \qquad (4.11)$$

where

$$R = \frac{\bar{R}_w}{\bar{R}_a}$$

The R.H.S. of equation 4.11 contains the hot-wire input terms, while the L.H.S. of the equation contains the hot-wire output terms. The input term $R_a'/\bar{R}_a$ was neglected in the following analysis, since it was assumed that the laboratory compressed air temperature remains essentially constant.

In analyzing the closed loop system in detail, the method of transfer functions was chosen. Dropping the superscript bars

from the steady state terms, the bridge input transfer functions based on equation 4.11, were found to be

$$\left.\frac{R_w'}{H'}\right|_{I_w' = 0} = \frac{-R_w(R-1)}{H(1+S\tau_w)} \qquad (4.12)$$

for an H' input

and

$$\left.\frac{R_w'}{I_w'}\right|_{H' = 0} = \frac{2R_w(R-1)}{I_w(1+S\tau_w)} \qquad (4.13)$$

for an I_w' input

where

$$\tau_w = \frac{CR}{H}$$

4.3 SYSTEM BLOCK DIAGRAM AND TRANSFER FUNCTIONS

In developing the system transfer functions and block diagram, several simplifying assumptions were made, namely:

(i) The H' input signal produces only a differential signal at the bridge output terminals.

(ii) The bridge amplifier, A_1, is represented by two separate transfer functions. The differential transfer function rejects common mode signals completely, and the common mode transfer function rejects differential signals completely. This assumption implies that a differential loop and a common mode loop exist, and that both loops are independent of each other insofar as analysis is concerned.

(iii) All system blocks are represented by constants with or without a single pole and/or zero. The system block

diagram is shown in Figures 24a and 24b.

HOT-WIRE BRIDGE TRANSFER FUNCTIONS

Combining equations 4.5 and 4.7 yields

$$H = \frac{KI_B^2}{\phi^2} = \frac{H_o}{\phi^2} \qquad (4.14)$$

where K is the constant of proportionality of equation 4.7, and H_o is the heat transfer function of velocity of the hot-wire at zero air flow when $I_w = I_B$ or when $\phi = 1$. Since equation 4.4 states that $R_w \doteq R_B$, and adopting the notation of equations 4.1, 4.5, and 4.14, equations 4.12 and 4.13 are rewritten as

$$\frac{R_w'}{H'} = \frac{-K_1\phi^2}{1+S\tau_w}$$

where

$$K_1 = \frac{R_B(R-1)}{H_o} \qquad (4.15)$$

and

$$\frac{R_B'}{I_w'} = \frac{K_2\phi}{1+S\tau_w}$$

where

$$K_2 = \frac{2R_B(R-1)}{I_B} \qquad (4.16)$$

and where $\tau_w = \phi^2\tau_w' \qquad (4.17)$

where

$$\tau_w' = \frac{CR}{H_o}$$

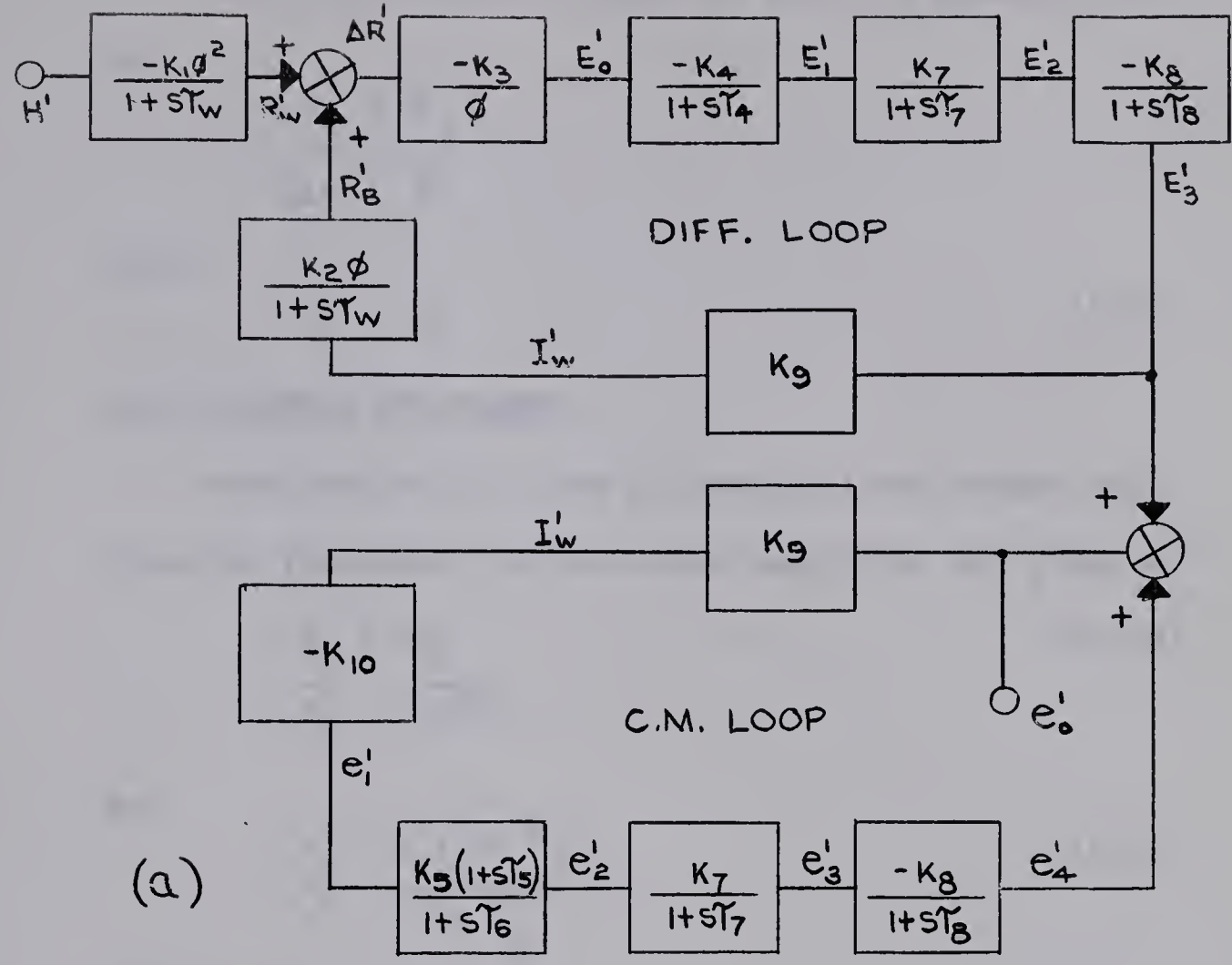

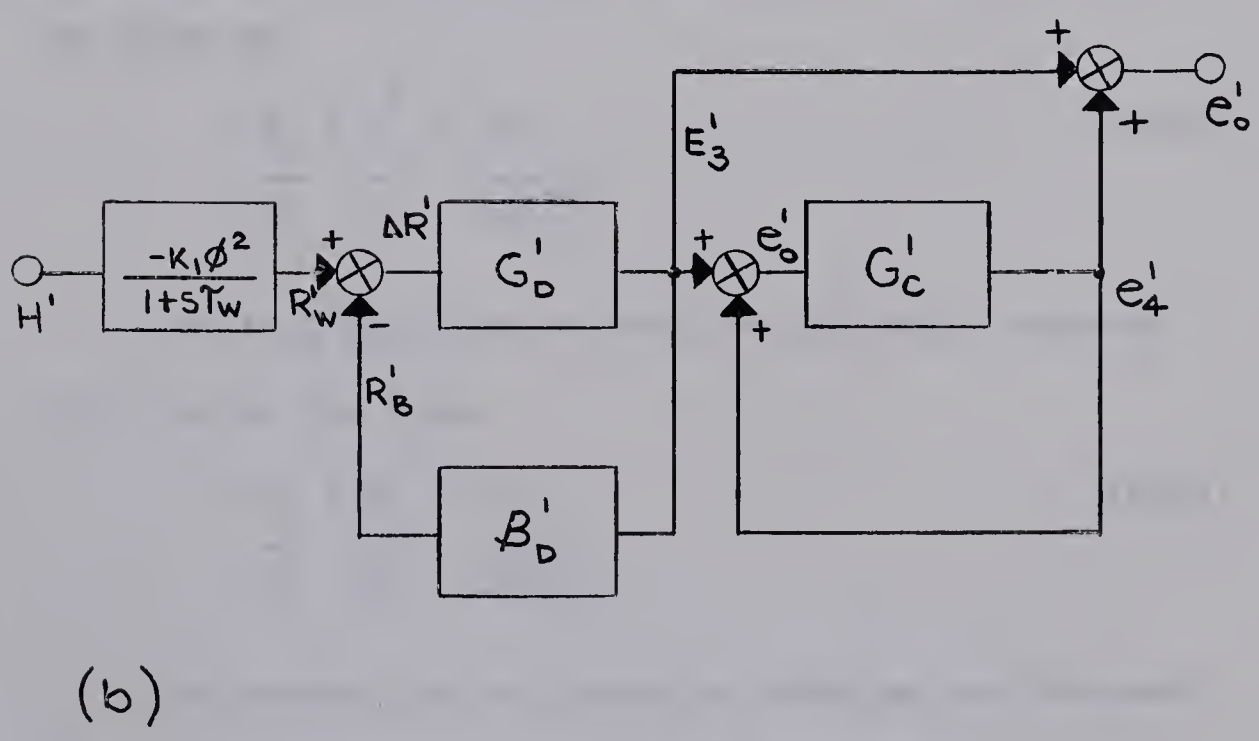

FIGURE 24. BRIDGE AND CONTROL CIRCUIT BLOCK DIAGRAMS

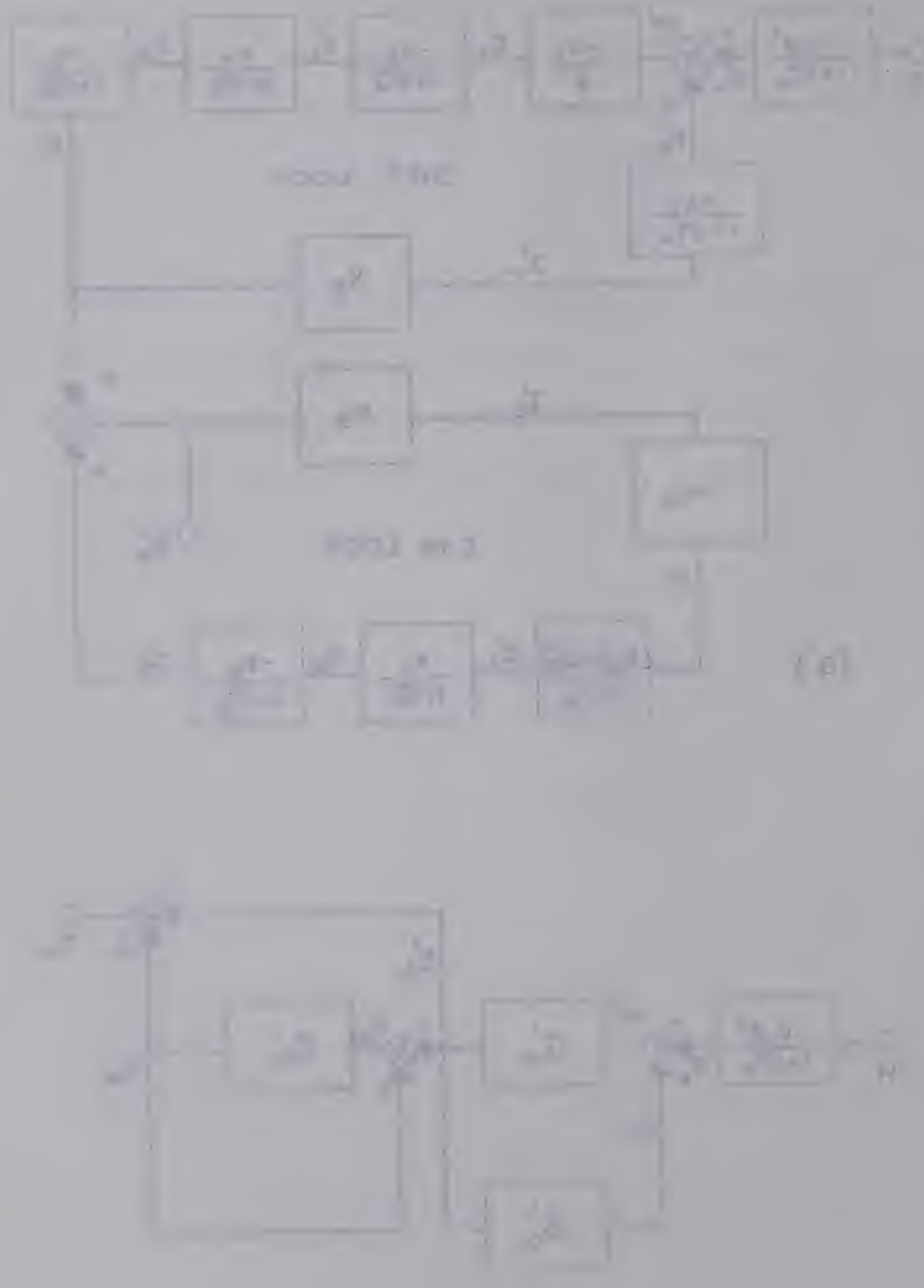

The bridge output voltage is given by equation 4.2, as

$$\frac{E_o'}{\Delta R'} = \frac{-K_3}{\phi}$$

where

$$K_3 = I_B \tag{4.18}$$

LOOP TRANSFER FUNCTIONS

From Section 3.3, the differential and common mode transfer functions for the bridge amplifier are given as

$$\frac{E_1'}{E_o'} = \frac{-K_4}{1+S\tau_4} \tag{4.19}$$

and

$$\frac{e_2'}{e_1'} = \frac{K_5(1+S\tau_5)}{1+S\tau_6} \tag{4.20}$$

respectively.

From Section 3.6, the lag network transfer function is given as

$$\frac{E_2'}{E_1'} = \frac{e_3'}{e_2'} = \frac{K_7}{1+S\tau_7} \tag{4.21}$$

The loop amplifier of Section 3.4 has a transfer function of the form

$$\frac{E_3'}{E_2'} = \frac{e_4'}{e_3'} = \frac{-K_8}{1+S\tau_8} \tag{4.22}$$

The current source transfer function, as discussed in Section 3.5, is given by a constant as

$$\frac{I_w'}{E_3'} = \frac{I_w'}{e_o'} = K_9 \tag{4.23}$$

where

$$K_9 = \frac{\theta}{\alpha R_{16}}$$

Referring to Figure 16, θ is the attenuation factor between the output voltage of amplifier A_2, and the base voltage of Q_1. This factor was taken to be 0.46 . $\alpha I_w'$ is the total bridge current fluctuation, the factor α being taken as 1.07.

Current fluctuations in the hot-wire bridge, as well as producing the differential voltage E_o', also produce a common mode voltage, e_1', given as

$$\frac{e_1'}{I_w'} \doteq -K_{10} \qquad (4.24)$$

where

$$K_{10} = R_2$$

4.4 EVALUATION OF SYSTEM CONSTANTS

Based on calculations and test results, for the case when I_B = 40 mA., the system constants were evaluated and are listed as follows:

$K_1 = 0.37 \ \frac{\text{ohms}}{\text{mW./ohm}}$ (calc.)

$K_2 = 1.2 \times 10^2 \ \frac{\text{ohms}}{\text{amp}}$ (calc.)

$K_3 = 4 \times 10^{-2}$ amps (test)

$K_4 = 9.8 \times 10^2$ (test)

$K_5 = 3.2 \times 10^{-3}$ (test)

$K_7 = 0.83$ (calc. for max. gain)

$K_7 = 0.98$ (calc. for min. gain)

$K_8 = 80$ (tested for max. gain)

$K_8 = 7.4$ (tested for min. gain)

$K_9 = 4.3 \times 10^{-3}$ mhos (calc.)

$K_{10} = 10$ ohms

$\tau'_w = 7.3 \times 10^{-3}$ sec. (test)

$\tau_4 = 8 \times 10^{-7}$ sec. (test)

$\tau_5 = 6.4 \times 10^{-5}$ sec. (test)

$\tau_6 = 2 \times 10^{-7}$ sec. (test)

$\tau_7 = 1.2 \times 10^{-5}$ sec. (calc. for max. gain)

$\tau_7 = 1.5 \times 10^{-5}$ sec. (calc. for min. gain)

$\tau_8 = 8 \times 10^{-7}$ sec. (test)

4.5 THE ROUTH CRITERION STABILITY TESTS

Without the lag network, the Routh Criterion yields the following requirements for both differential loop and common mode loop stability

$$K'_D \leq \frac{2\tau'_w \phi^2}{\tau_4} \tag{4.25}$$

where K'_D is the differential loop gain, and

$$K'_c \leq \frac{\tau_6 + \tau_8}{\tau_5} \tag{4.26}$$

where K'_c is the common mode loop gain. The above requirements dictate that:

$$K'_D \leq 1.8 \times 10^4 \text{ for } \phi = 1,$$

$$K'_D \leq 6.6 \times 10^3 \text{ for } \phi = 0.6,$$

and

$$K'_c \leq 1.5 \times 10^{-2}.$$

For the maximum loop gain case, the differential and common mode

gains were calculated to be: $K_D' = 1.6 \times 10^3$ and $K_c' = 1.1 \times 10^{-2}$. The Routh Criterion indicates that the system is stable without compensation, however, when tested, the system was found to be unstable at the maximum loop gain, but stable at reduced gains. Since the calculated common mode gain is close in value to that indicated by the Routh Criterion, it was assumed that the system was unstable in the common mode at maximum gain.

With the lag network in the loop, the new stability requirements are given by:

$$K_D \leq \frac{\phi^2 \tau_w'}{2\tau_4} \tag{4.27}$$

and

$$K_c \leq \frac{\tau_7}{\tau_5} \tag{4.28}$$

The above requirements dictate that: $K_D \leq 4.6 \times 10^3$ for $\phi = 1$, $K_D \leq 1.7 \times 10^3$ for $\phi = 0.6$, and $K_c \leq 0.19$. At maximum loop gain, the revised differential and common mode gains were calculated to be: $K_D = 1.3 \times 10^3$ and $K_c = 0.92 \times 10^{-2}$. The system, when tested, was found to be stable up to and including values of $\phi = 0.50$, or $I_w = 80$ mA.

4.6 THE SYSTEM TRANSFER FUNCTION

Referring to Figure 24a and 24b, the common mode transfer function, $G_c = \frac{G_c'}{1-G_c'}$, was calculated to be

$$G_c \doteq \frac{\frac{K_c}{1-K_c}(1+s\tau_5)}{(1+s\tau_9)(1+s\tau_{10})} \tag{4.29}$$

where

$$\frac{K_c}{1-K_c} \doteq K_c = 0.92 \times 10^{-2}$$

$$\tau_9 = 1.1 \times 10^{-6} \text{ sec.}$$

and

$$\tau_{10} = 1.2 \times 10^{-5} \text{ sec.}$$

The common mode response curve, according to equation 4.29 is shown in Figure 25.

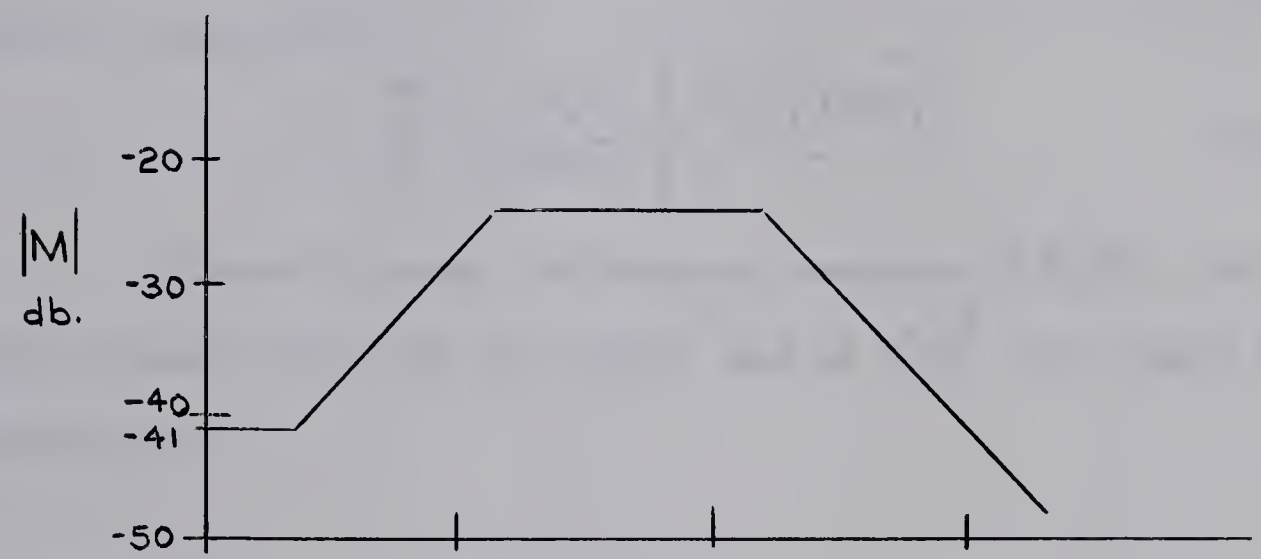

FIGURE 25. COMMON MODE RESPONSE

Again, referring to Figures 24a and 24b the differential transfer function, $G_D = \frac{G_D'}{1+\mathcal{B}_D' G_D'}$, was found to be

$$G_D \doteq \frac{\left[K_D^*/\phi\right](1+S\tau_w)}{(1+S\tau_{11})\left(\frac{S^2}{\omega_n^2}+\frac{2\zeta}{\omega_n}S+1\right)} \qquad (4.30)$$

where

$$\frac{K_D^*}{\phi} = \frac{-(K_3/\phi).K_4.K_7.K_8}{1+K_D} \qquad (4.31)$$

The constants of equations 4.30 and 4.31 were calculated as

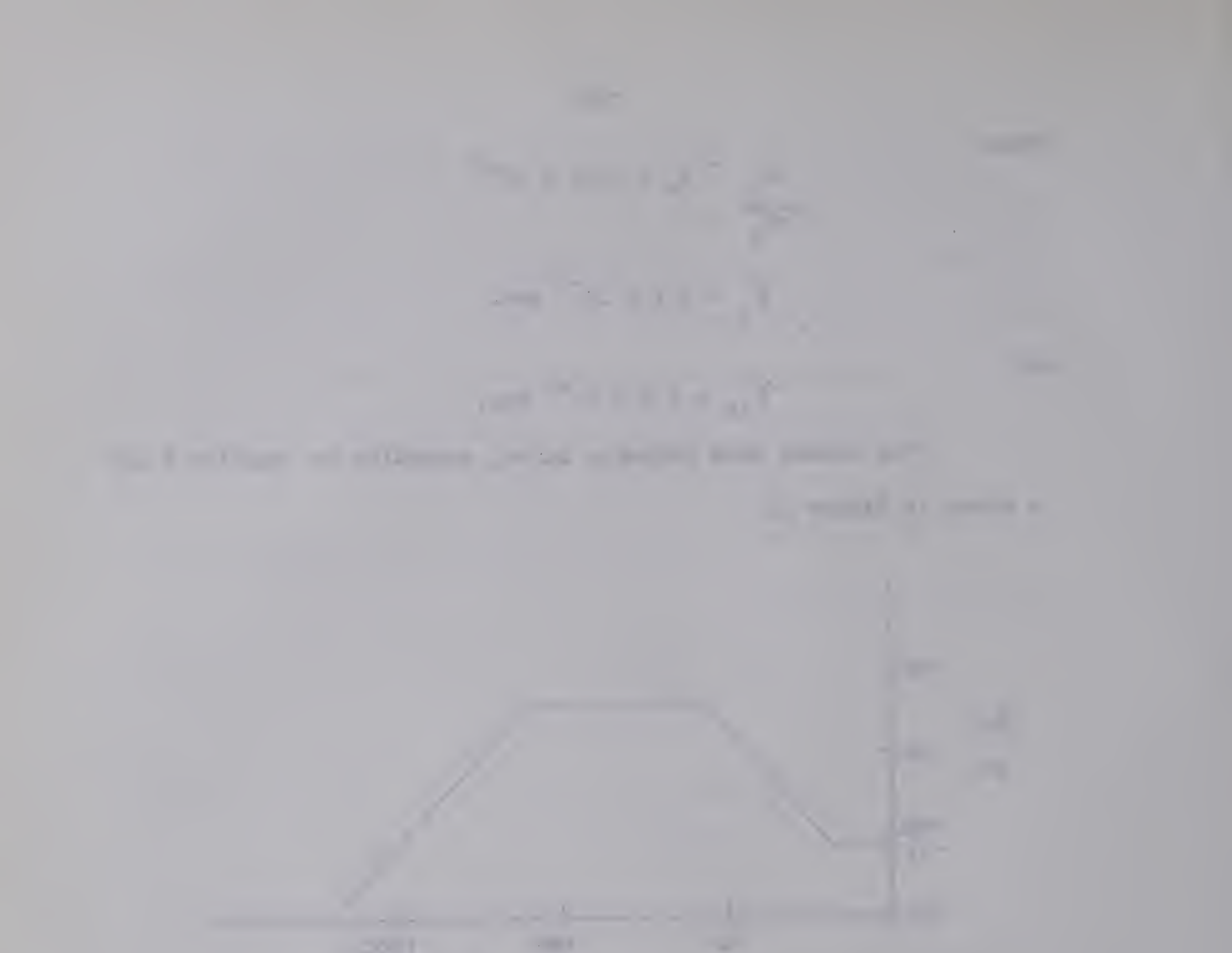

$$K_D^* = -2$$

$$\left.\begin{aligned} \tau_{11} &= 1.8 \times 10^{-6} \text{ sec.} \\ \omega_n &= 1.34 \times 10^5 \text{ r/s} \\ \xi &= 0.2 \end{aligned}\right\} \phi = 1$$

$$\left.\begin{aligned} \tau_{11} &= 1.6 \times 10^{-6} \text{ sec.} \\ \omega_n &= 2 \times 10^5 \text{ r/s} \\ \xi &= 0.05 \end{aligned}\right\} \phi = 0.6$$

Referring to Figure 24, the overall system transfer function was found to be

$$\frac{e_o'}{H'} = \left[\frac{-K_1\phi^2}{1+S\tau_w}\right] \cdot G_D \cdot \left[1+G_c\right] \qquad (4.32)$$

Figure 26 shows the frequency response of E_3'/H', the differential signal portion of the output, and of e_4'/H', the common mode contribution.

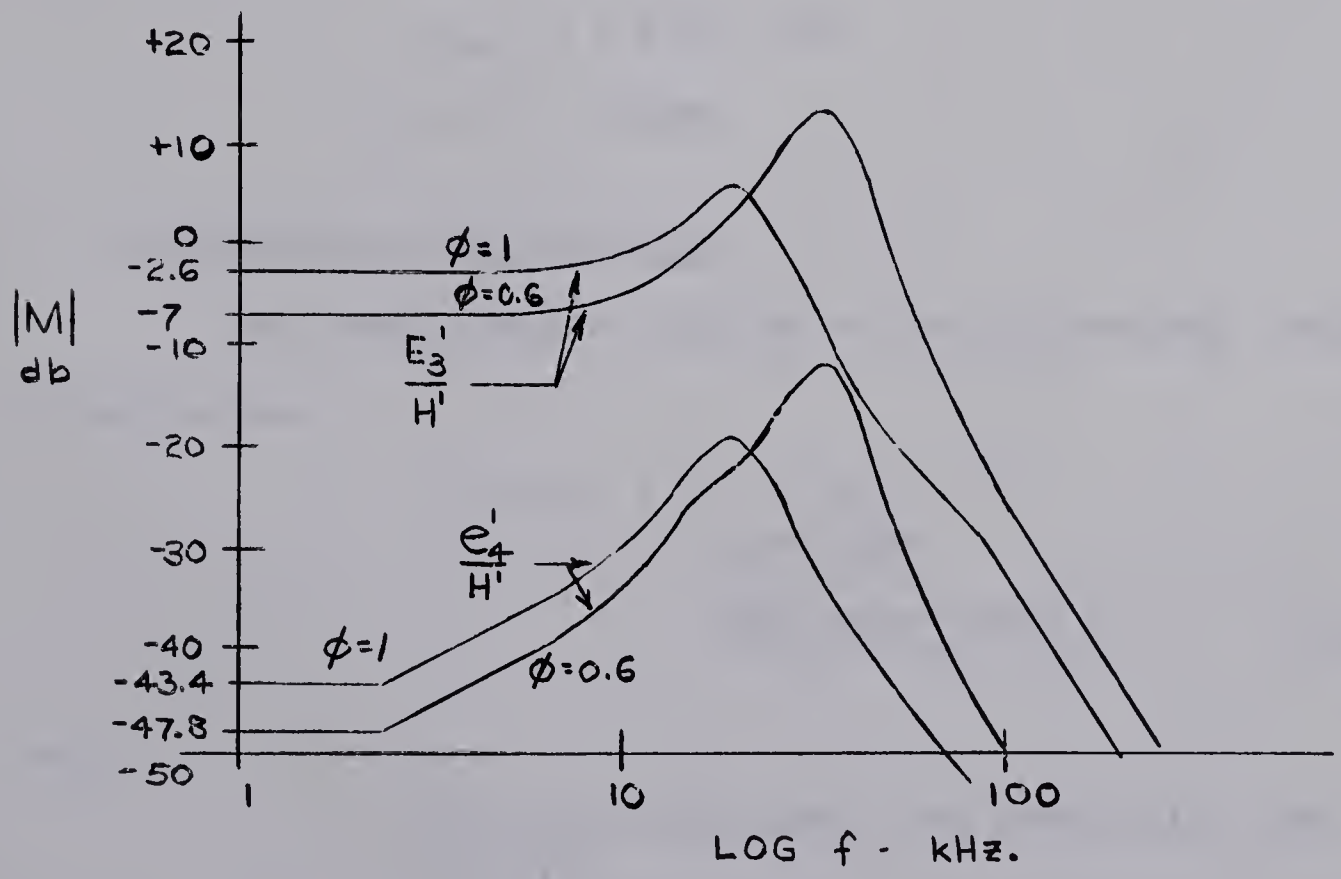

FIGURE 26. SYSTEM DIFFERENTIAL AND COMMON MODE RESPONSES

Since the common mode response was found at all frequencies to be less than 10% of the magnitude of the differential response, then the common mode portion was neglected, giving

$$\frac{E_3'}{H'} \doteq \frac{e_o'}{H'} \doteq \frac{K_1 K_D^* \phi}{(1+S\tau_{11})\left[\frac{S^2}{\omega_n^2} + \frac{2\zeta}{\omega_n} S+1\right]} \qquad (4.33)$$

where

$$K_1 K_D^* = 0.74 \ \frac{\text{volts}}{\text{mW./ohm}}$$

Utilizing the relationships: $M_p = \frac{1}{2\zeta\sqrt{1-\zeta^2}}$ and $\omega_p = \omega_n\sqrt{1-2\zeta^2}$, the system may be described as follows:

for $\phi = 1$ $\quad M_p = 8$ db.

$\omega_p = 1.3 \times 10^5$ r/s

B.W.= 28 kHz

and for $\phi = 0.6$ $\quad M_p = 20$ db

$\omega_p = 2 \times 10^5$ r/s

B.W. = 48 kHz

4.7 DIFFERENTIAL LOOP ROOT LOCUS

The characteristic equation of the differential loop may be written as

$$1 + GH = 1 + \frac{\frac{K_D}{\tau_w \tau_7 \tau_4^2}}{(S+S_1)(S+S_2)(S+S_3)^2} \qquad (4.34)$$

where $\frac{K_D}{\tau_w \tau_7 \tau_4^2}$, the static loop sensitivity, was evaluated as $1.78 \times 10^{19} \ K_D/\phi^2$ and where

$$S_1 = 137/\phi^2$$

$$S_2 = 8.3 \times 10^4$$

and

$$S_3 = 1.25 \times 10^6$$

In plotting the root locus, four asymptotes at angles $\pm \pi/4$ and $\pm 3\pi/4$ were found. The asymptotic real axis intersection was calculated to be at $S = -6.45 \times 10^5$, and the real axis break away point was found to be at $S = -4 \times 10^4$. The imaginary axis crossings were found to occur at $S = \pm j2.3 \times 10^5$. Figure 27 shows the root locus plot, which remains essentially the same for $\phi = 0.6$ and for $\phi = 1$. At $\phi = 0.6$, the pole S_1 moves from S= -137 to S= -381, but in relation to the other poles, this is an insignificant movement.

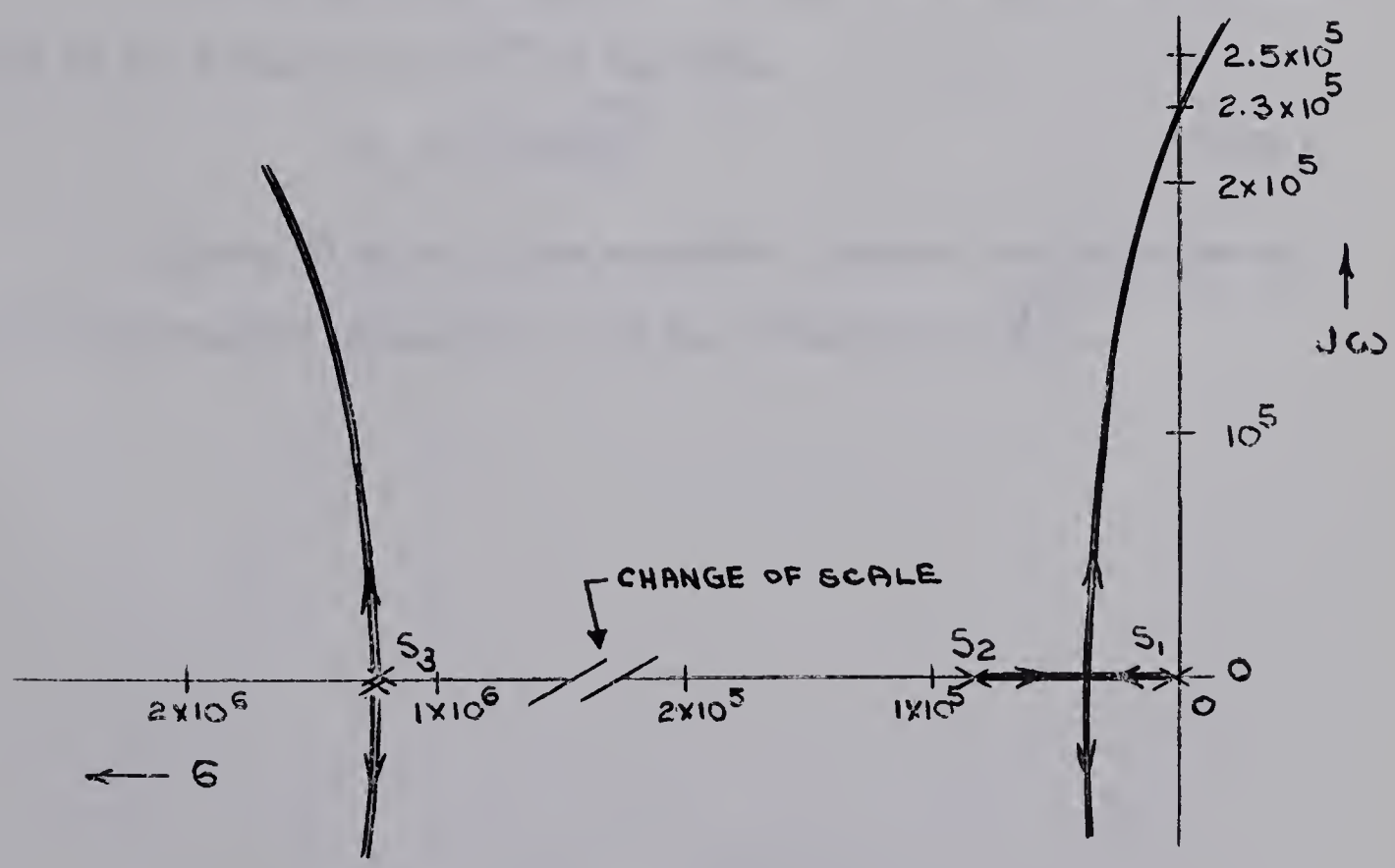

FIGURE 27. DIFFERENTIAL LOOP ROOT LOCUS

The static loop sensitivity, however, changes from 1.78 x 10^{19} K_D to 4.95 x 10^{19} K_D as ϕ changes from 1 to 0.6, and, as such,

affects system stability. Only the pair of roots near the origin need be considered regarding stability, since the other pair tends asymptotically to infinity in a stable direction. From the root locus diagram, the break away gains were calculated as: 141 for ϕ = 1 and 51 for ϕ = 0.6. The gains at the imaginary axis crossing were found to be 4.4×10^3 for ϕ = 1 and 1.5×10^3 for ϕ = 0.6. The gains for ζ = 0.707 were calculated to be 182 for ϕ = 1 and 66 for ϕ = 0.6.

4.8 BRIDGE AND CONTROL SYSTEM TEST

A static test was performed on the hot-wire bridge and control system. A known steady-state air flow was applied to the flow tube and the output voltage was noted as shown in Figure 28.

Utilizing equations 2.13 and 4.33, the output voltage was found to be a function of Q^* of the form

$$e_o = 3.77\phi\sqrt{Q^*} \tag{4.35}$$

Figure 28 shows close agreement between the experimental and the calculated values for e_o/ϕ as a function of $\sqrt{Q^*}$.

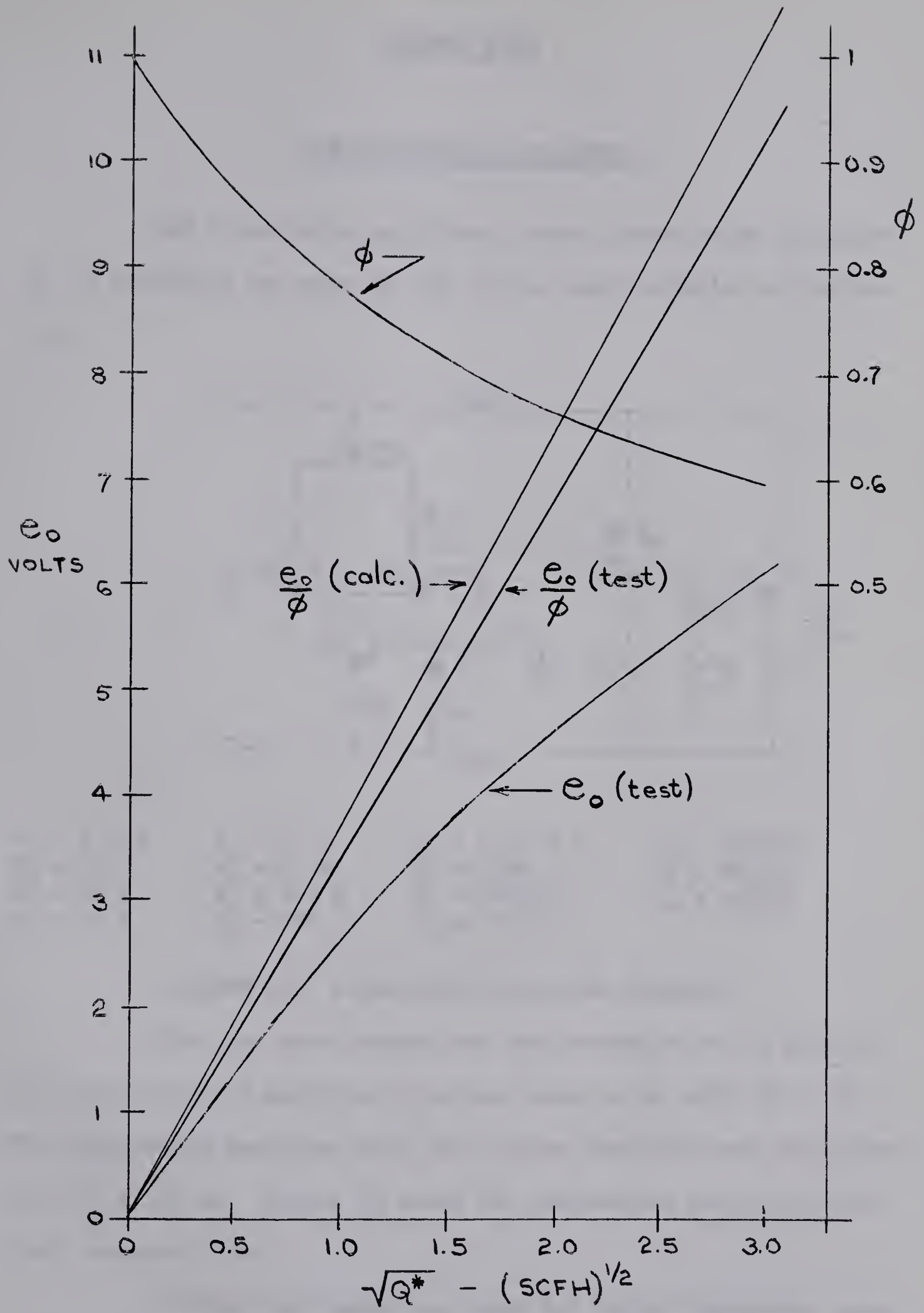

FIGURE 28. SYSTEM STATIC TEST

CHAPTER FIVE

THE LINEARIZING AMPLIFIER

The linearizing amplifier circuit, shown below in Figure 29, is basically the same as that of the loop amplifier of Section 3.4.

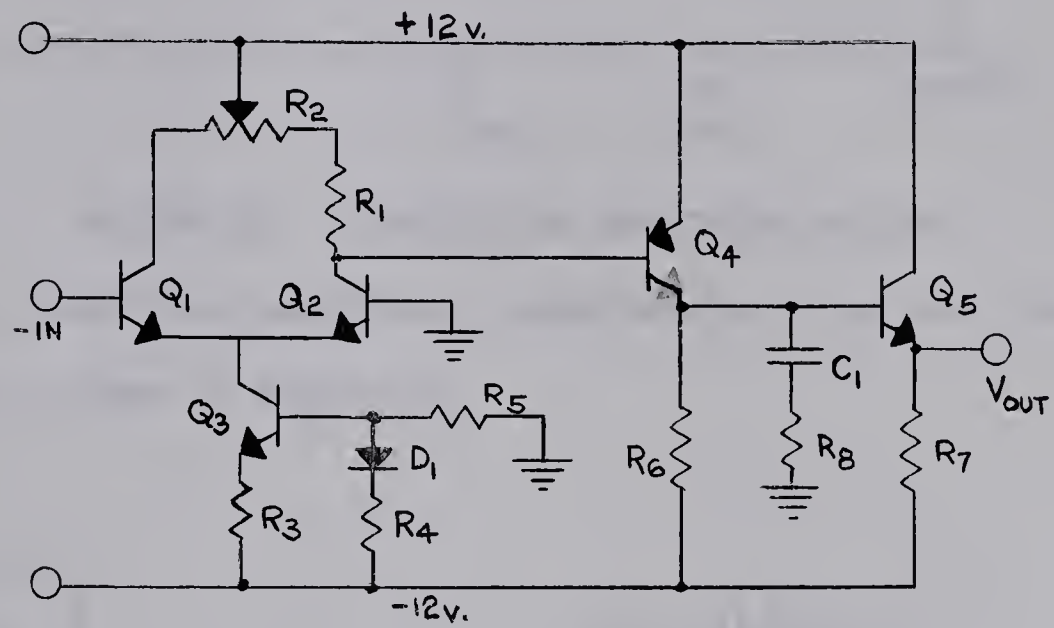

R_1 = 6.8 K	R_5 = 56 K	C_1 = 0.05 μf.	Q_3 = 2N3707
R_2 = 10 K	R_6 = 27 K	D_1 = 1020	Q_4 = 2N3702
R_3 = 56 K	R_7 = 4.7 K	Q_1 = 2N3707	Q_5 = 2N3707
R_4 = 56 K	R_8 = 470	Q_2 = 2N3707	

FIGURE 29. LINEARIZING AMPLIFIER SCHEMATIC

Using the same assumptions and procedures as in Section 3.4, the open loop amplifier gain was found to be -4270 or 73 db. The compensated amplifier open loop corner frequency was calculated as, f'_{45} = 120 Hz. Figure 30 shows the compensated amplifier open loop response curve.

The open loop amplifier input and output impedances were calculated and found to be: $Z_i \doteq$ 330 K ohms and $Z_o \doteq$ 21 ohms.

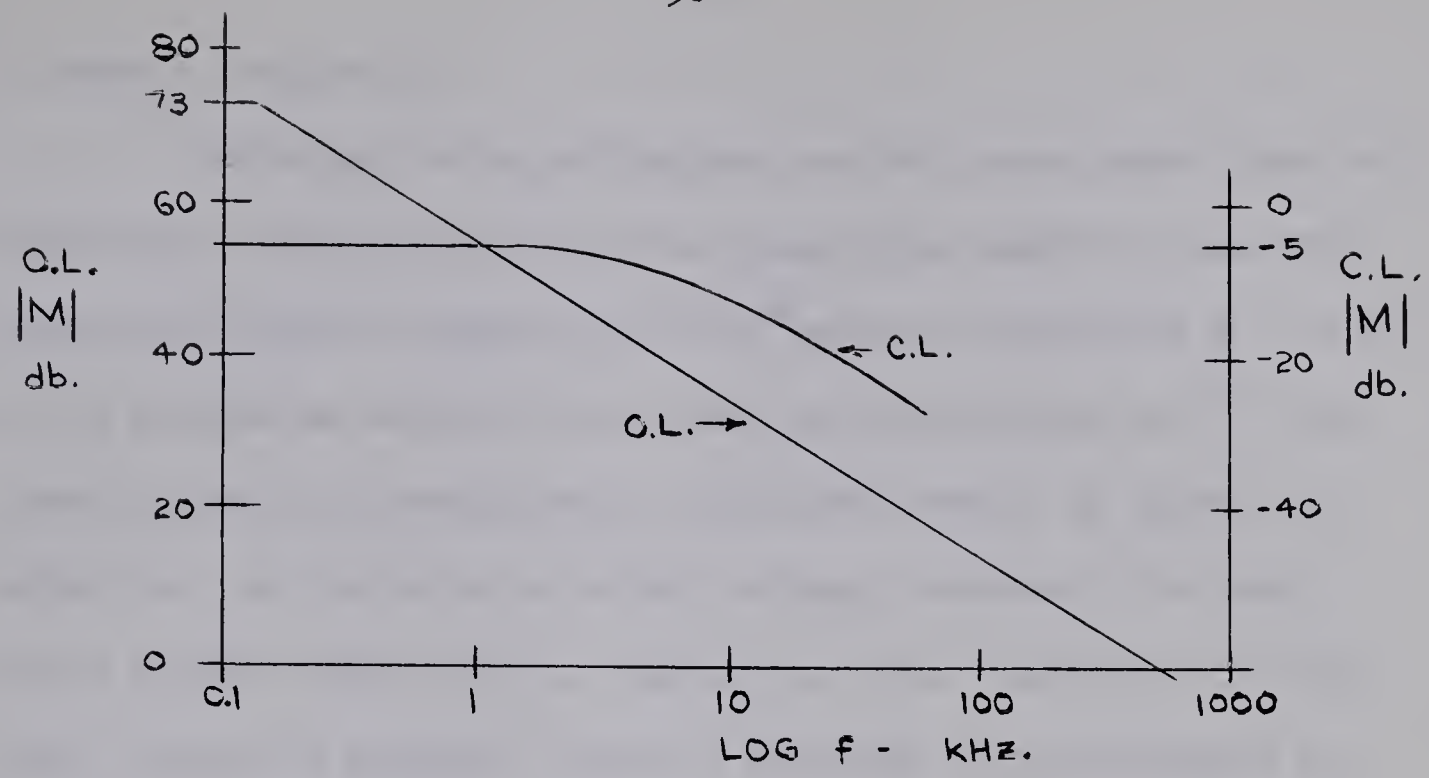

FIGURE 30. LINEARIZING AMPLIFIER RESPONSE

The linearizing amplifier, complete with input and feedback networks is shown in Figure 31.

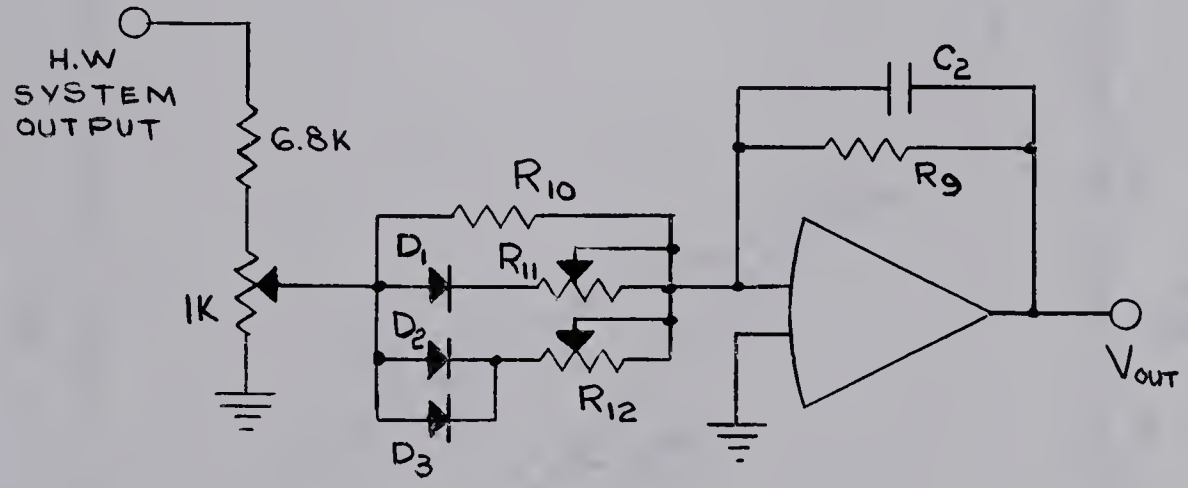

R_9 = 33 K R_{12} = 100 K D_2 = TI71
R_{10} = 56 K C_2 = 0.001 Mf. D_3 = TI71
R_{11} = 100 K D_1 = TI71

FIGURE 31. CLOSED LOOP LINEARIZING AMPLIFIER

The closed loop frequency response of the amplifier was determined from test, with only R_{10} in the input circuit, and with R_9 and C_2 in the feedback path. The tested closed loop response

is shown in Figure 30.

Referring to the bridge and control system static test of Figure 28, it may be seen that the linearizing amplifier must compensate for both the square root of Q^* and for the factor ϕ , in order to produce an output voltage that is proportional to Q^*. This linearization is accomplished by the input network of diodes and resistors. As the hot-wire output voltage increases, the input diodes conduct more current, causing the total resistance of the input circuit to decrease towards a limiting value determined by the resistor settings. As a result, the overall gain of the linearizing amplifier will vary as the input voltage.

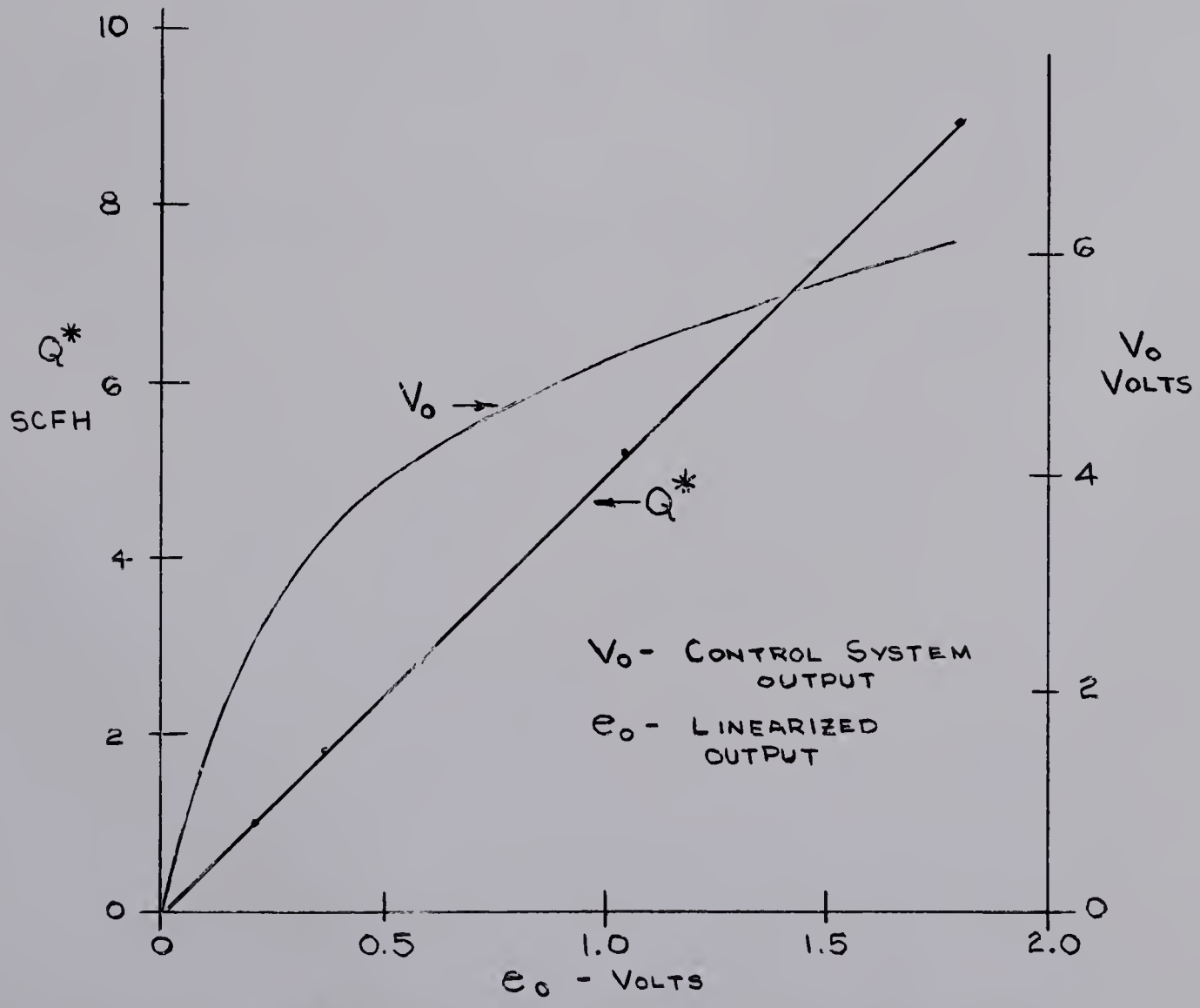

FIGURE 32. AMPLIFIER AND SYSTEM TRANSFER CHARACTERISTIC

Figure 32 shows the amplifier transfer characteristic with resistors R_{11} and R_{12} of Figure 31 properly adjusted for the best overall system linearization. This curve is identical in shape to the amplifier input resistance characteristic as a function of input voltage. Figure 32 also depicts the overall system transfer characteristic of e_o versus Q^*.

CHAPTER SIX

FLUID DEVICE STATIC AND DYNAMIC TESTS

6.1 THE PNEUMATIC RESISTOR

Corning Electronics manufactures a series of laminar flow resistors for use with fluid amplifiers. A feature of these resistors is their linear flow-pressure relationship. The resistors are available in values from 1 x 10^6(lb.-sec.)/ft.^{5} to 100 x 10^6 (lb.-sec.)/ft.^{5}. Adopting the definitions of Appendix D, a resistor of value 1 x 10^6 (lb.-sec.)/ft.^{5}. is equal to 4 SAR, whereas a resistor of value 100 x 10^6(lb.-sec.)/ft.^{5} is equal to 400 SAR.

Utilizing the hot-wire air flowmeter, and the Giannini air pressure transducer (Appendix C), the flow characteristics for both a 4 SAR (R=1) resistor and a 36 SAR (R=9) resistor, were plotted. These relationships are shown in Figure 33.

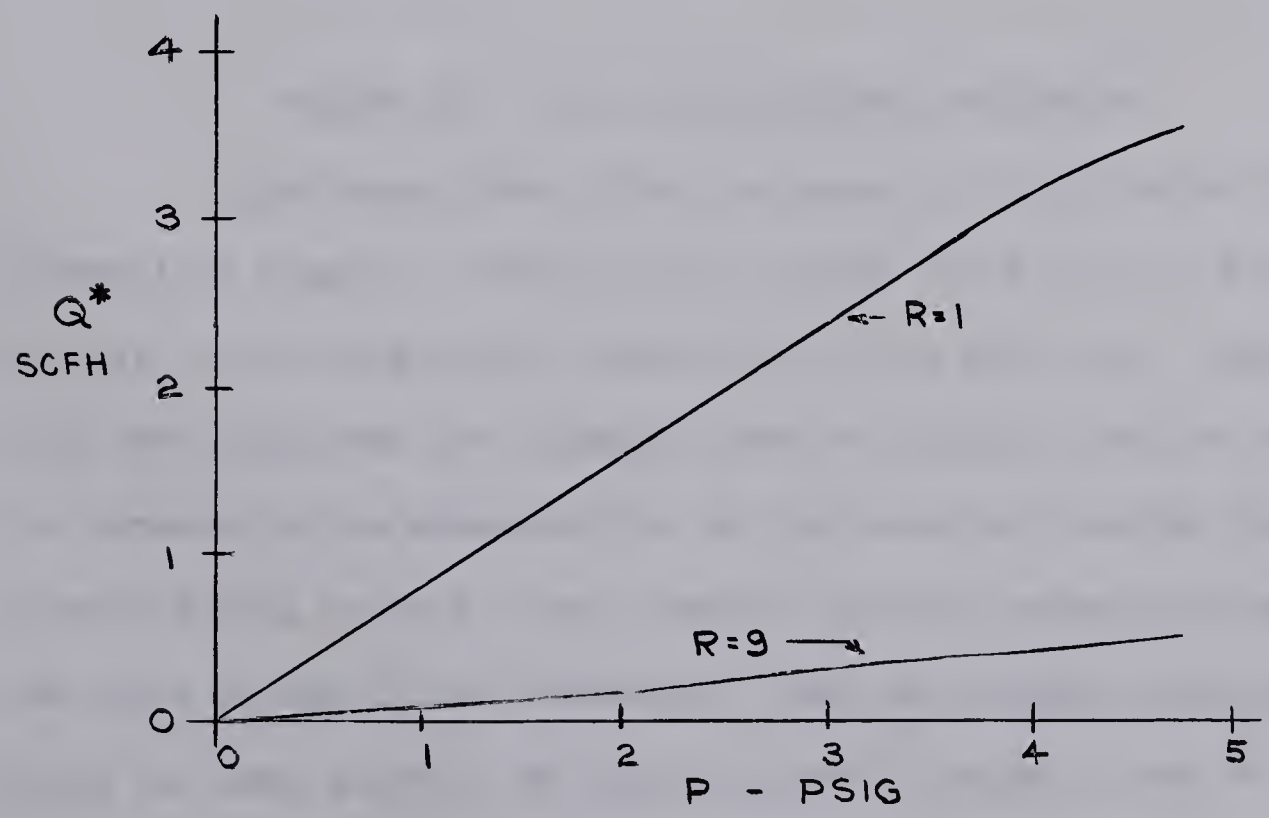

FIGURE 33. FLUID RESISTOR CHARACTERISTICS

Both resistors were found to be linear to a ± 3% maximum deviation from the best straight line, up to a differential pressure of 4.75 psi. The R=1 resistor was found to have a nominal value of 1.1 whereas the R=9 resistor was found to have a nominal value of 8.6.

6.2 THE PROPORTIONAL AMPLIFIER

Figure 34 shows the basic single stage proportional amplifier.

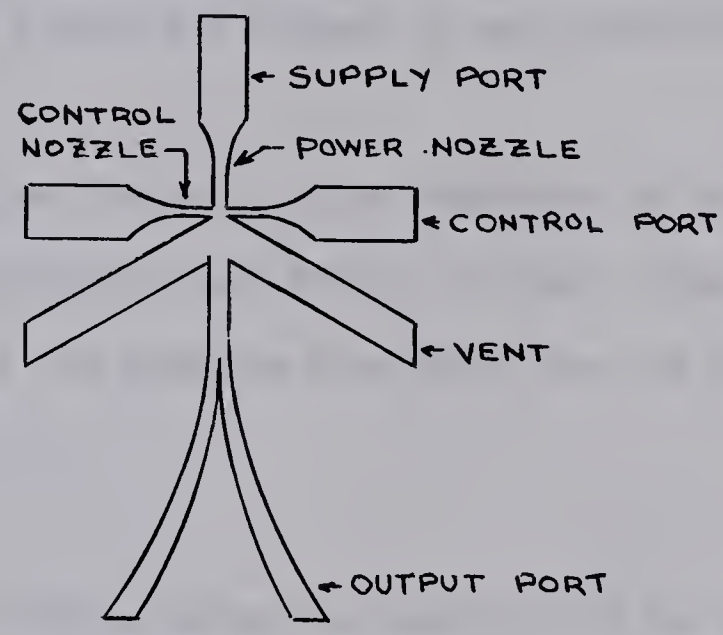

FIGURE 34. BASIC PROPORTIONAL AMPLIFIER

High energy fluid from the power jet is directed into the interaction region. Control or low energy fluid is also directed into this region from jets on each side of the power jet. The direction that the power jet assumes after interaction with the control jet depends on the momentum flux of the power jet and the forces exerted by the control jets. When the control pressures are equal, the power stream is not deflected. Then each output aperture collects the same quantity of fluid. A small change in one of the control pressures deflects the power stream and causes one output to

collect more fluid than the other. Since the output difference is greater than the control difference, this is a stage of amplification.

To prevent the power stream from locking-on to the walls of the interaction chamber, the chamber is vented by large vents near the control nozzles.

The deflecting force of the control stream may be generated in two ways. The force may be either a pressure force or a momentum flux force. Both forces are present in any porportional amplifier.

In general, the low frequency input impedance of an amplifier with predominantly pressure type force, is high. When the forces are predominantly of the momentum flux type, the low frequency input impedance is low.

STATIC TESTS

A number of static tests were carried out on the Corning standard proportional device. The results of these tests are shown plotted in Figures 35, 36, and 37.

Figure 35a shows the amplifier supply port characteristic.

Figure 35b depicts the amplifier control port characteristic with supply pressure as a parameter. The solid lines represent the L.H. control port impedance with the R.H. control port vented. The dashed lines indicate the increase in the L.H. control port impedance when the R.H. control port is blocked.

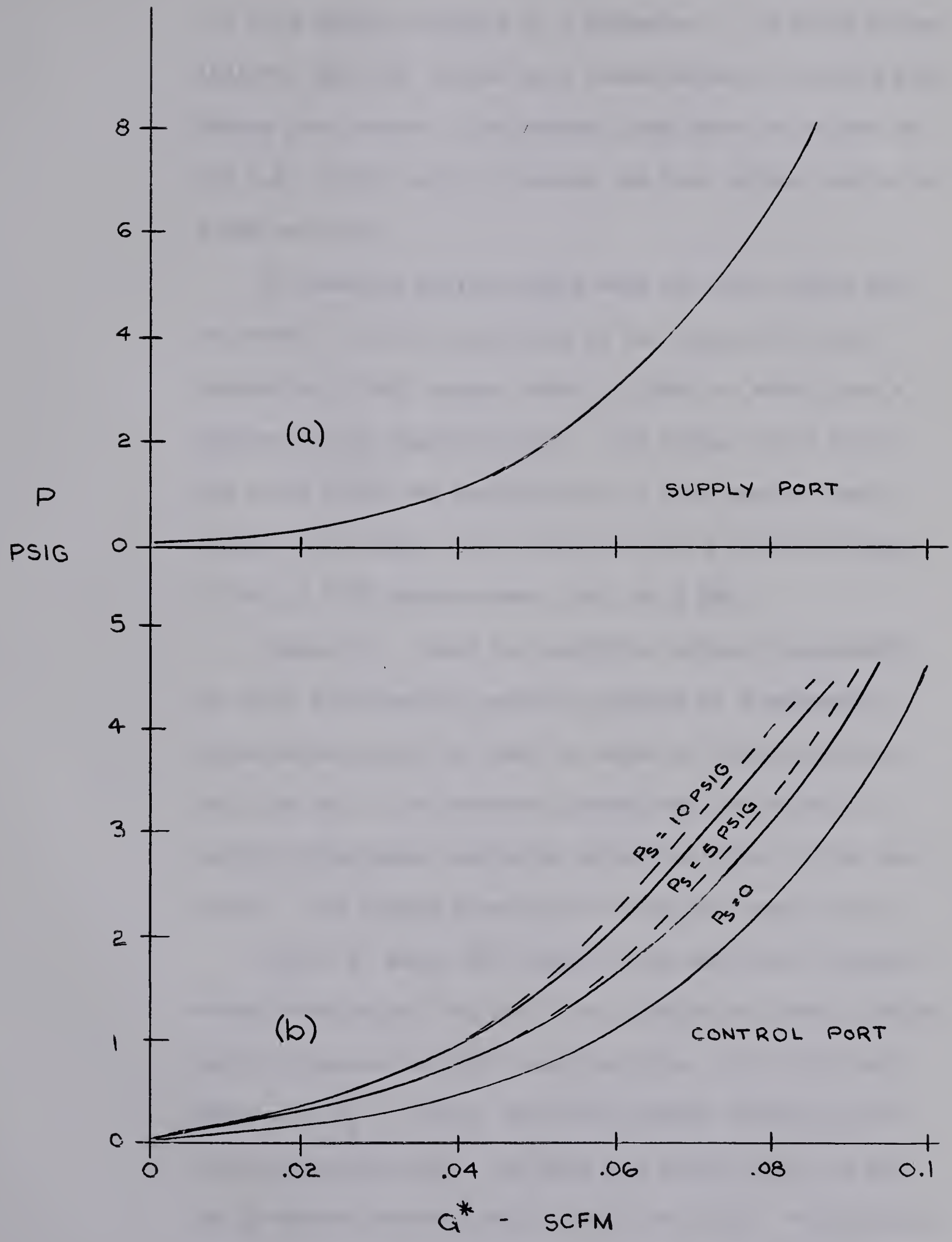

FIGURE 35. P.A. SUPPLY PORT AND CONTROL PORT CHARACTERISTICS

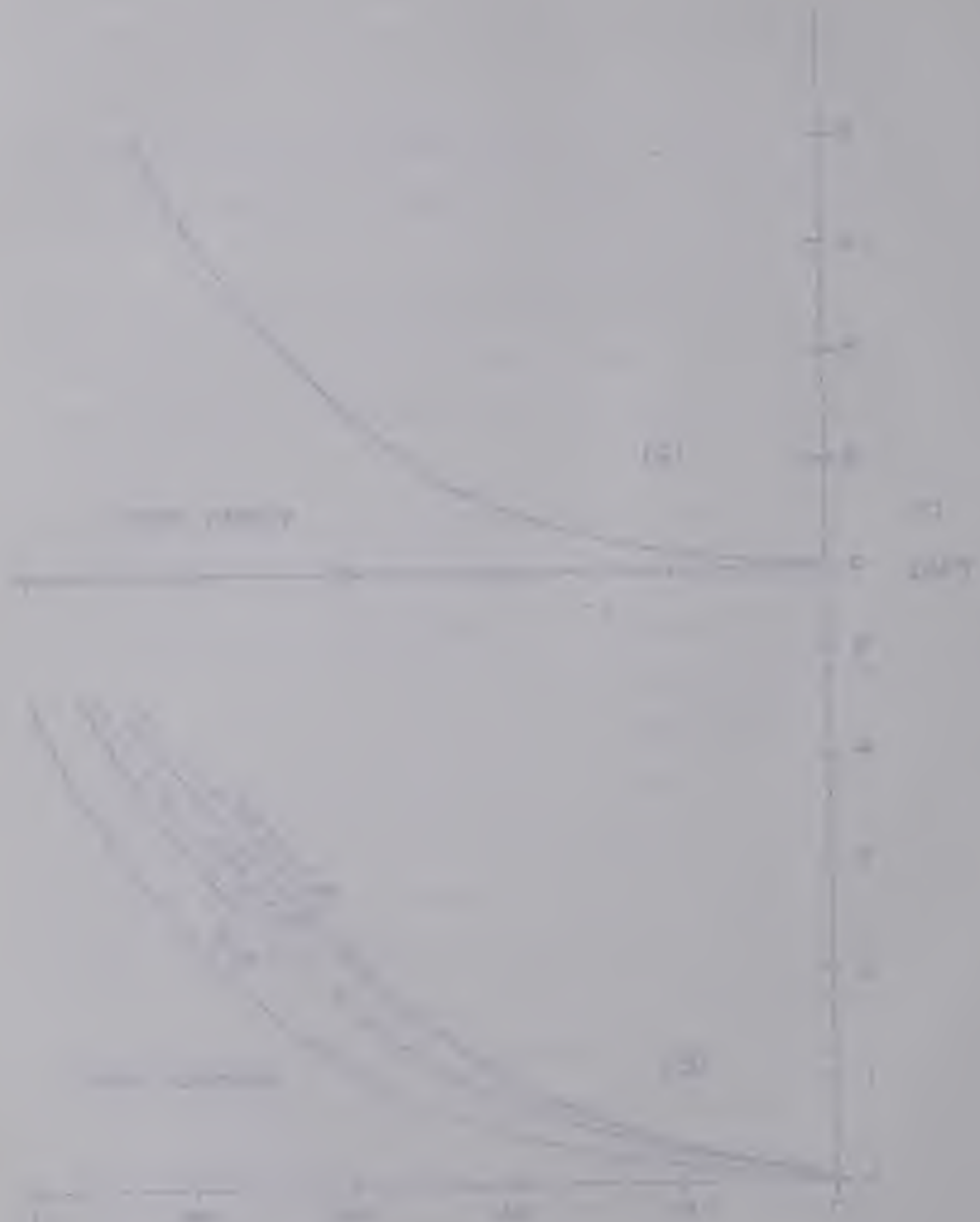

Figure 36a shows the amplifier output characteristic with supply pressure as a parameter. The solid lines indicate the L.H. output port characteristic with the R.H. output port vented. The dashed lines show the effect on the L.H. output port of loading the R.H. output port with 4 SAR resistor.

An unstable region exists when the R.H. output port is vented. As the resistance of the R.H. port is increased to 4 SAR, output noise is found to exist over a portion of the characteristic. The output noise below the noise limit was measured as 0.1 SCFH peak-to-peak, whereas the output noise above the noise limit was found to be 0.3 SCFH peak-to-peak, both at 5 kHz.

Figure 36b shows the amplifier output characteristic with differential control pressure as a parameter. An unstable region is found to exist on this characteristic as well. The measured output was loaded with a second proportional amplifier while the other output was vented. The supply pressure for this test was 5 psig.

Figure 37 shows the proportional amplifier transfer characteristic and the effect of loading and power nozzle supply pressure on this characteristic. Curve (a) was taken with P_s = 5 psig. and both outputs loaded by proportional amplifiers. The gain was found to be 3.2 and the pressure recovery was found to be 17.6%. An unstable area of operation was found to exist on the negative slope portion of the characteristic. Curve (b) shows the trans-

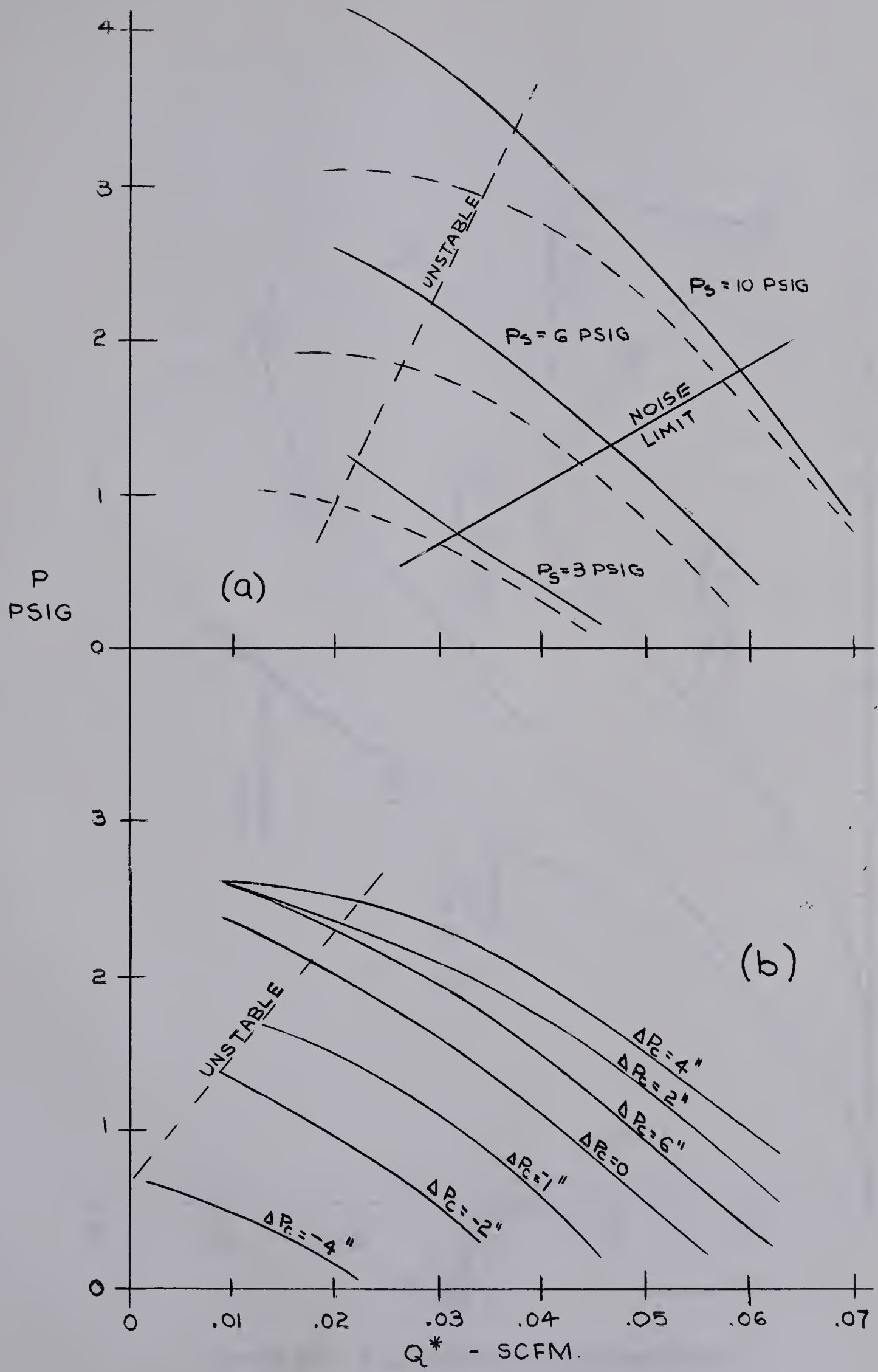

FIGURE 36. P.A. OUTPUT PORT CHARACTERISTICS

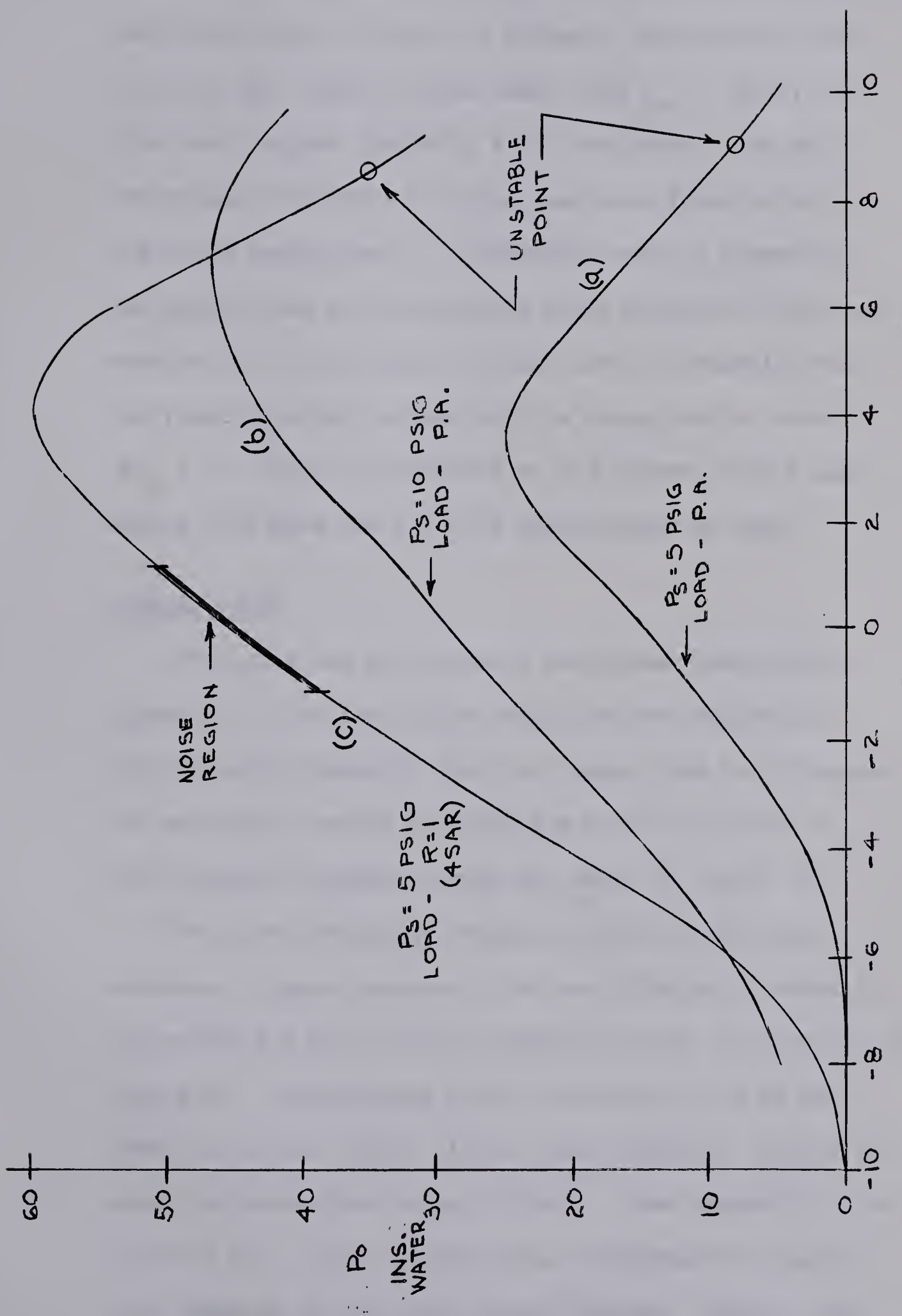

FIGURE 37. P.A. TRANSFER CHARACTERISTICS

fer characteristic with the same loading as for curve (a), but with P_s increased to 10 psig. The gain for this curve was found to be 3.25 and the pressure recovery was found to be 16.8%. Curve (c) was taken with P_s = 5 psig., but with both outputs loaded by 4 SAR resistors. The gain and pressure recovery for this case were found to be 5.6 and 43.2% respectively. An unstable area of operation was again noted on the negative slope portion of the characteristic. In addition, a noisy area of operation was now found to exist on the positive slope portion about $\Delta P_c = 0$. The noise measured at the output, when biased within this area was 0.3 SCFH peak-to-peak at 5kHz.

DYNAMIC TESTS

Utilizing the air pressure oscillator described in Appendix C, the proportional amplifier was subjected to two different frequency response tests. The test diagram, and equivalent output circuits are shown in Figure 38. The frequency response curves are shown in Figure 39.

The first frequency response test related output pressure to input pressure. This test diagram is shown in Figure 38a and the resulting response curve is curve (a) of Figure 39. The measured corner frequency of 20 Hz was found due to the output circuit time constant. Figure 38b shows the equivalent output circuit. From Appendix D, the 0.1 inch I.D. line resistance and inductance are negligible compared to the other circuit values. Again, from

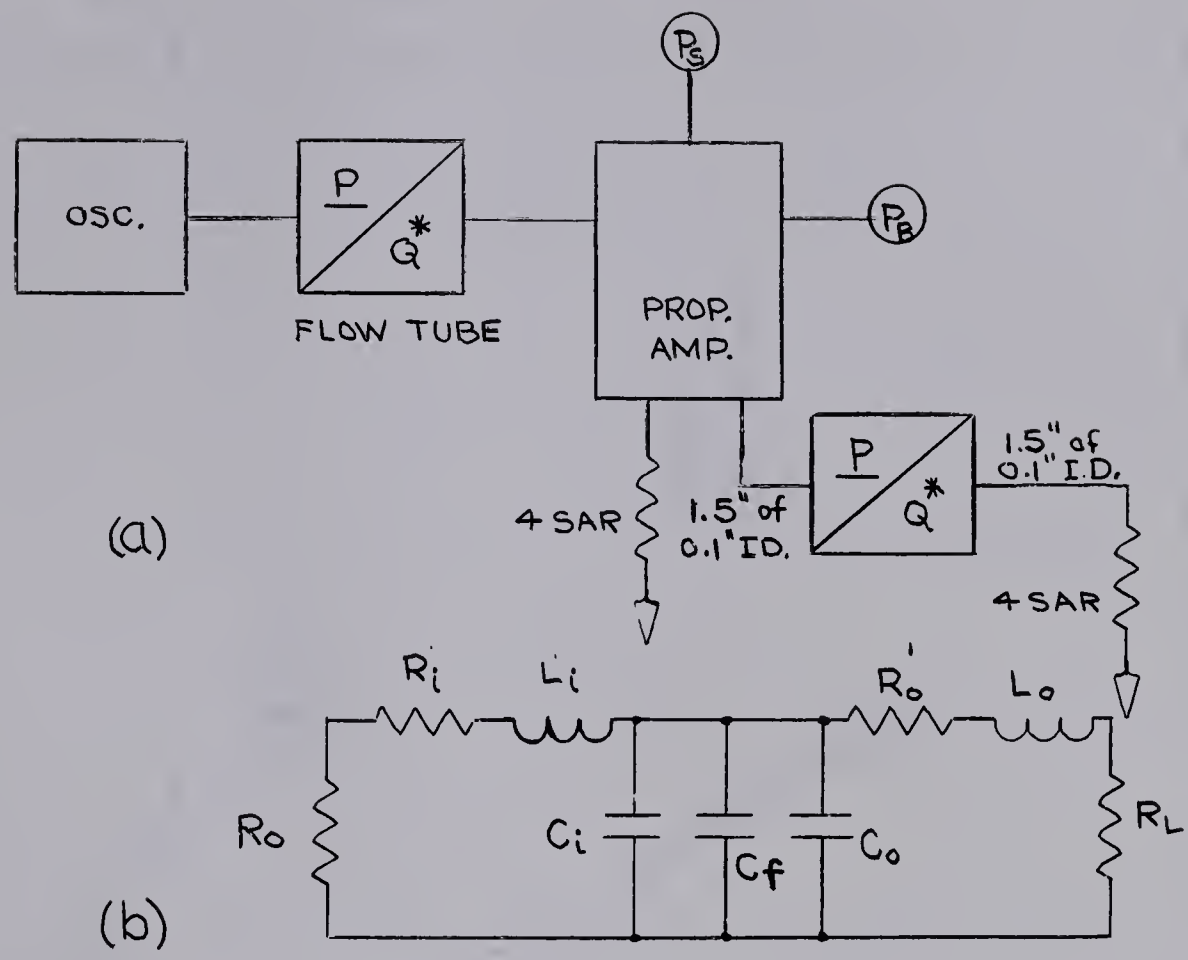

FIGURE 38. P.A. TEST DIAGRAMS

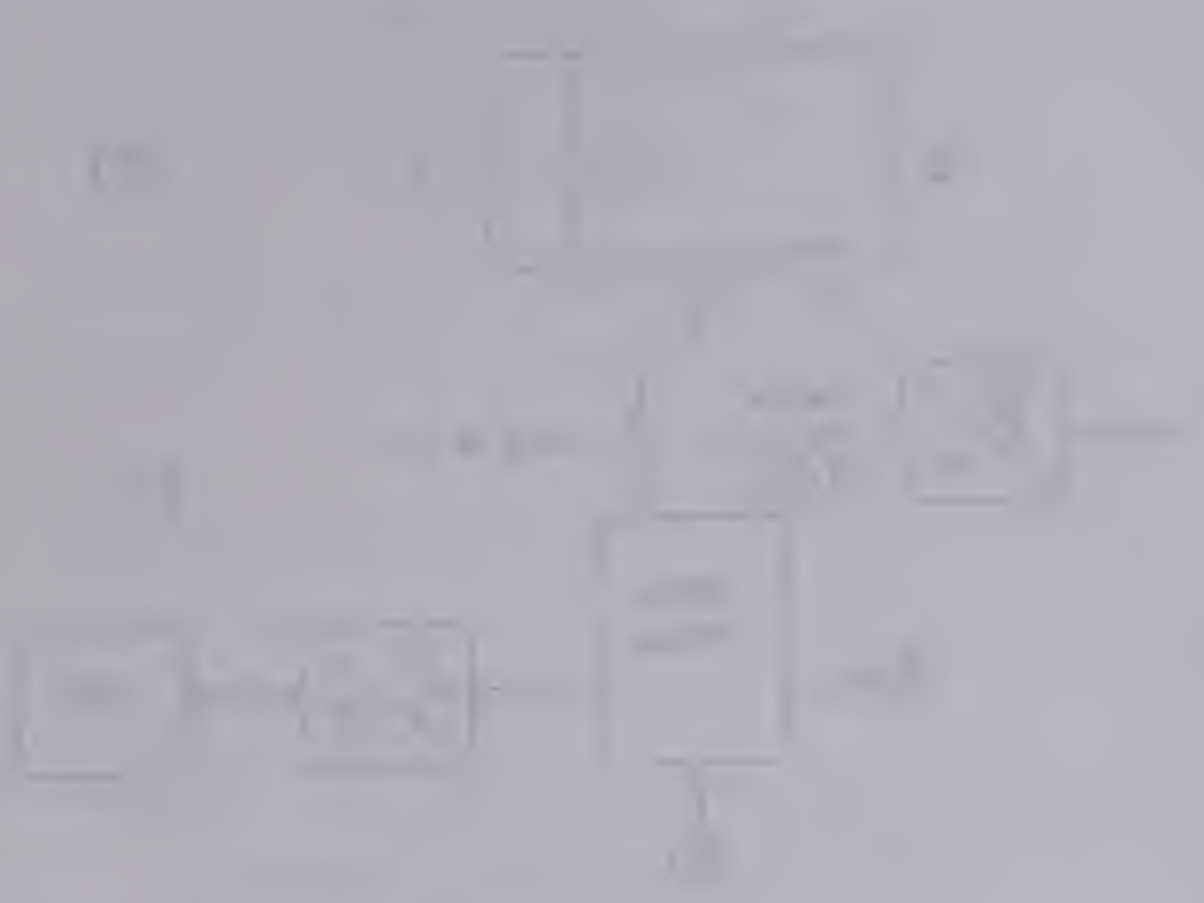

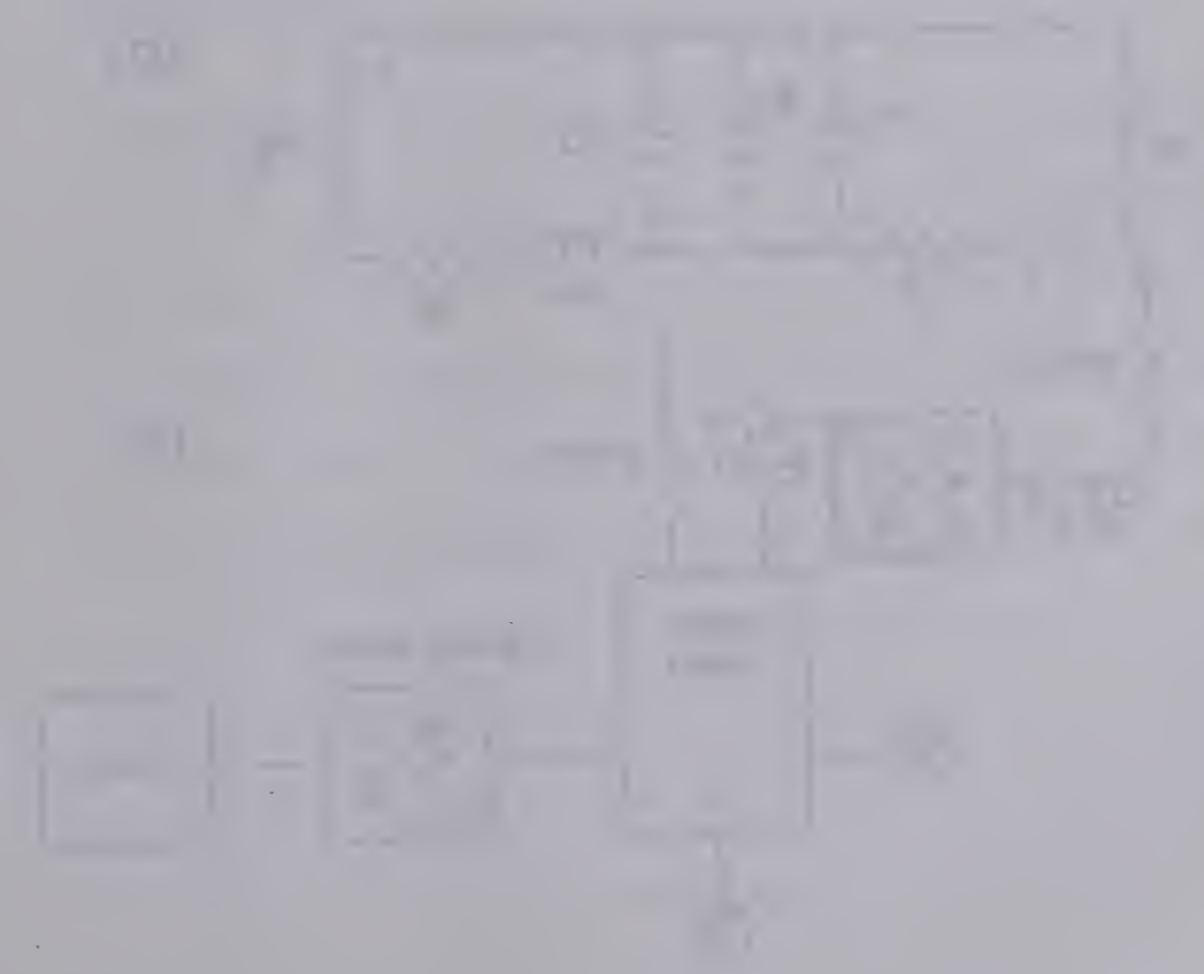

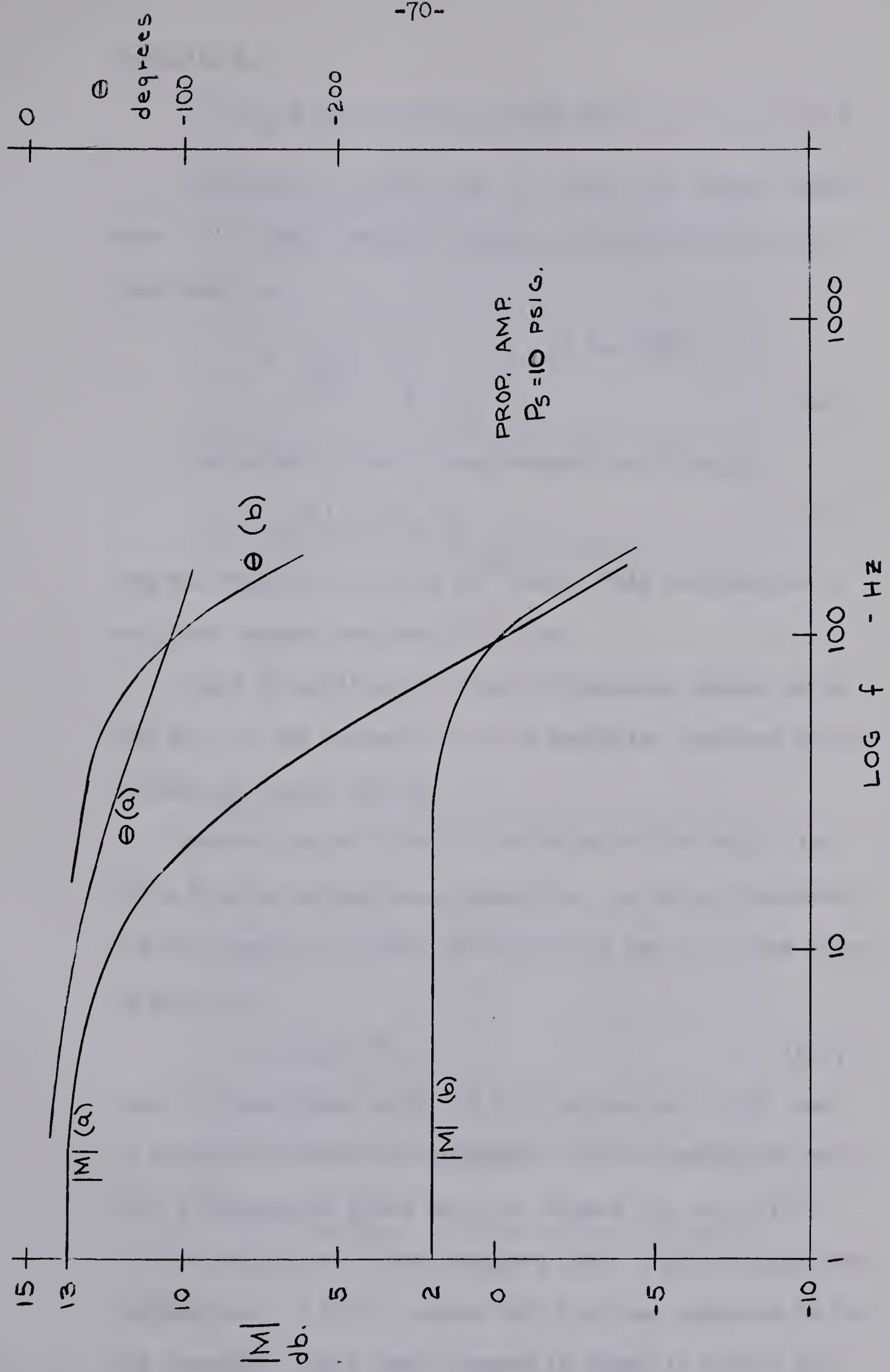

FIGURE 39. P.A. FREQUENCY RESPONSE

Appendix D,

$$C_T = C_f + C_i + C_o = 4.55 \text{ SAC} \tag{6.1}$$

Referring to Figure 36a, the amplifier output impedance, at 10 psig. supply pressure, about the bias point, was found as,

$$R_o = \left.\frac{P_o}{Q^*_o}\right|_{P_c = K} = 2.2 \text{ SAR} \tag{6.2}$$

The output circuit time constant is given by

$$\tau_o \doteq \left[R_o // R_L\right] C_T \tag{6.3}$$

and was found to be 6.4×10^{-3} sec. This corresponds to an upper corner frequency of 25 Hz.

Since no additional corner frequencies appear up to 200 Hz., it was assumed that the amplifier response curve is flat to beyond 200 Hz.

Belsterling and Tsui[9], calculated the delay time, for a similar proportional amplifier, to be approximately 0.4 milliseconds. Since the lag angle due to a time delay is given as

$$\theta = 360\, f\, \tau_D \tag{6.4}$$

then a linear phase shift of 1.5 degrees per 10 Hz. may be expected through the amplifier. This corresponds well with the measured phase shift of Figure 39, curve (a).

To verify the first response test, a second test was carried out, in which, output air flow was compared to input pressure. This test diagram is shown in Figure 38c and the output equivalent circuit is shown in Figure 38d.

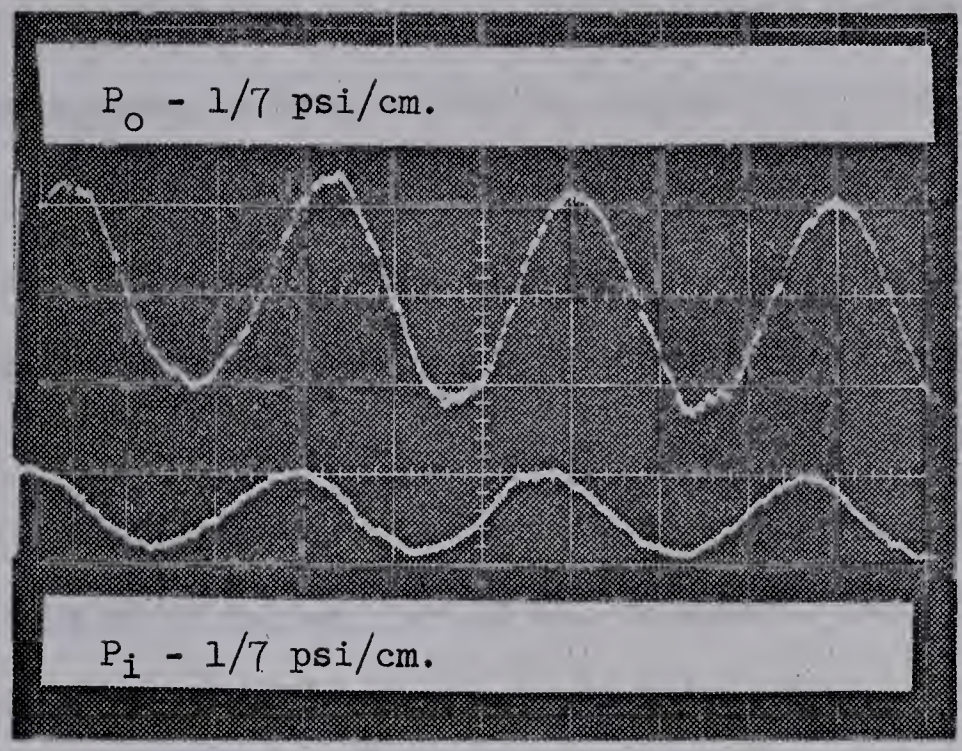

(a)

TIME - 10 ms./cm.

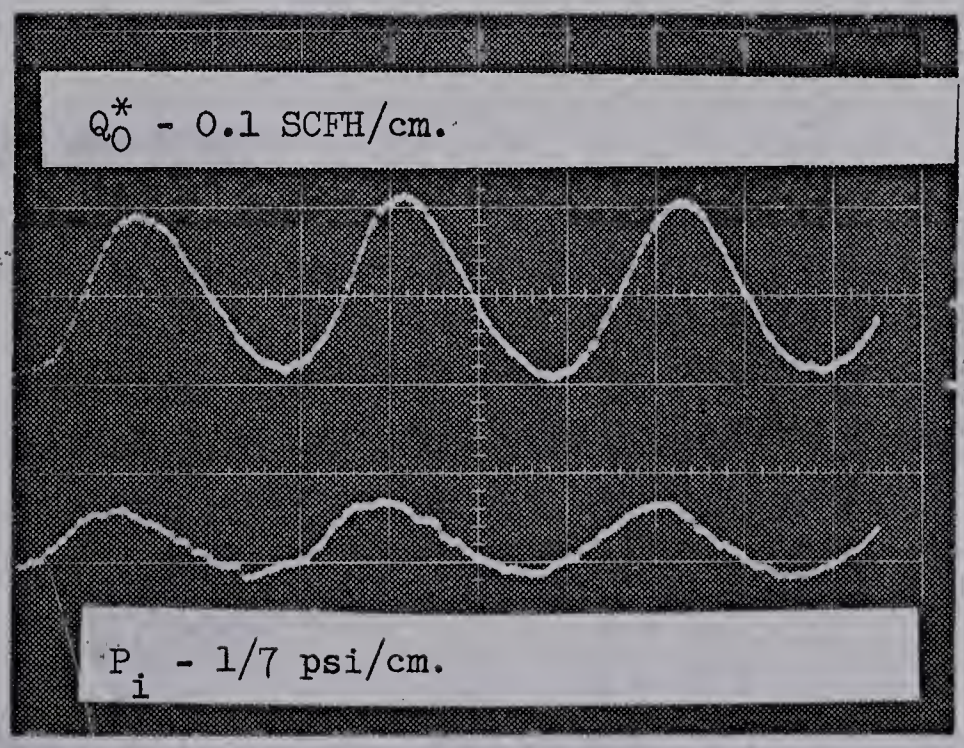

(b)

TIME - 10 ms./cm.

FIGURE 40. P.A. FREQUENCY RESPONSE PHOTOGRAPHS

From Figure 39, an upper corner frequency was now found to occur at 125 Hz. Again, neglecting line resistance and inductance in Figure 38d, an output time constant of 1.1×10^{-3} seconds was calculated. This corresponds to a predicted corner frequency of 140 Hz. Since the 4 SAR resistor was found to have a 1 millisecond delay time, the total delay time between input and output was now found to be 1.4 milliseconds. This time delay caused a linear lag angle of 5 degrees per 10 Hz. to occur. Referring to Figure 39, curve (b), the measured phase angles agree with this observation.

Figures 40a and 40b show photographs of typical input and output sine waves. Figure 40[a] shows output pressure and input pressure, while Figure 40b shows output flow and input pressure.

6.3 THE BISTABLE AMPLIFIER

The bistable amplifier is shown schematically in Figure 41.

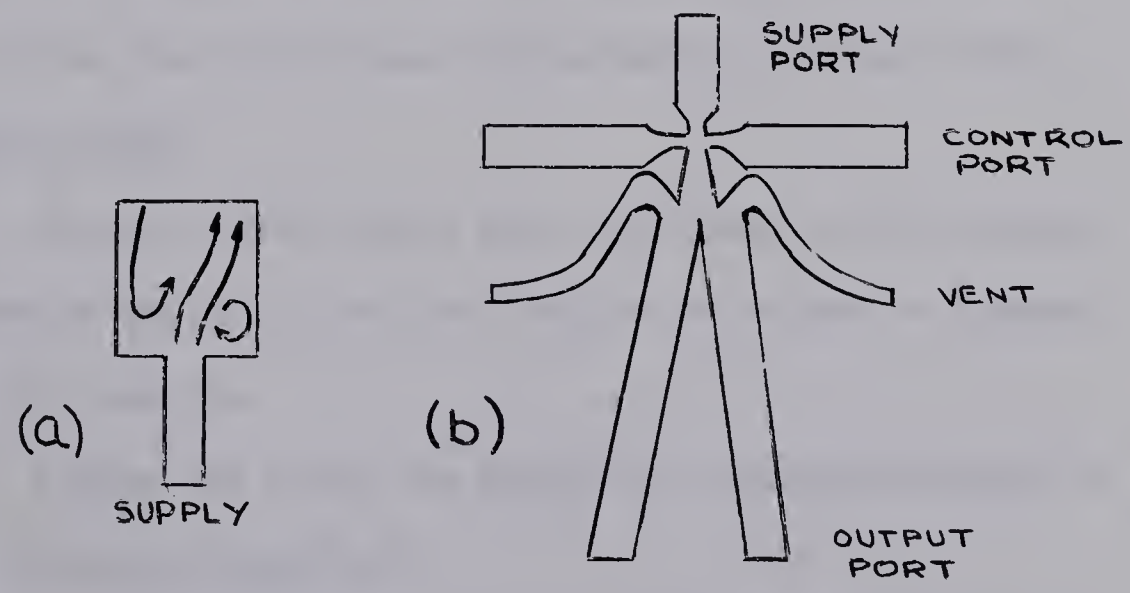

FIGURE 41. BISTABLE AMPLIFIER

A stream issuing from a nozzle between bounding walls (Figure 41a) entrains fluid from the interaction region, lowering the pressure in this region. The entrained fluid is replaced by a counterflow from the ambient pressure. Since this is an unstable situation, any turbulence will incline the stream closer to one wall than the other. As the stream moves towards one wall, the area available for counter flow to that side is reduced, creating a reduction in pressure on that side, and therefore a pressure difference across the stream. This pressure difference inclines the stream towards the low pressure region still further, and the stream is said to "lock-on" to that wall.

This situation exists in the bistable amplifier of Figure 41b. If the stream is assumed locked-on to the R.H. wall and an air flow is introduced into the separation bubble through the right control, the point of stream attachment to the wall will move downstream. When there is sufficient control flow to satisfy the entrainment, the stream will move to the center of the interaction region. Entrainment will lower the pressure on the left side of the stream, and the stream will attach to the left wall.

STATIC TESTS

Several static tests were performed on the Corning bistable amplifier and the results are shown in Figures 42, 43, and 44.

Figure 42a shows the supply port characteristics of the bistable amplifier.

Figure 42b shows the control port characteristics with supply pressure as a parameter. These curves were

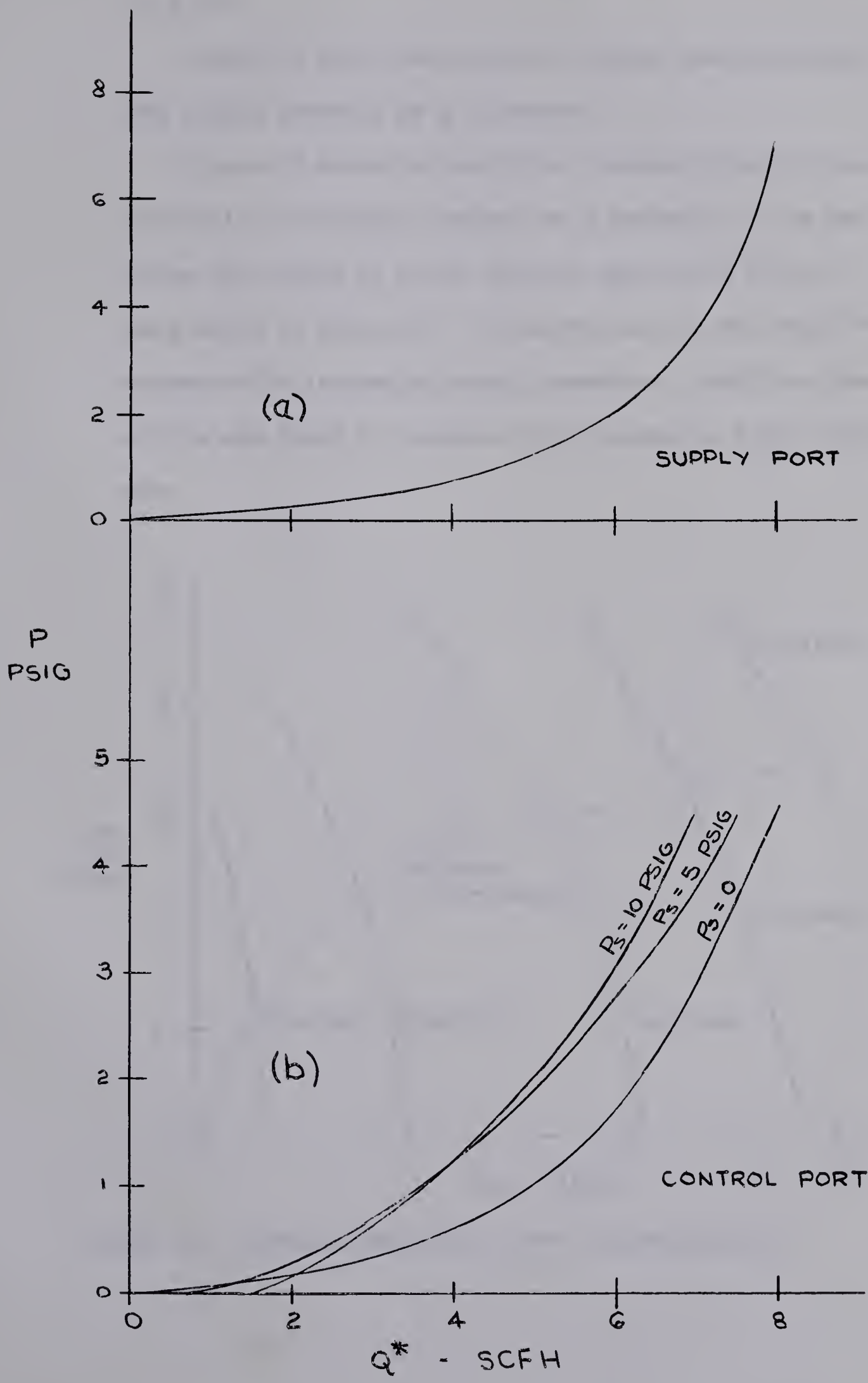

FIGURE 42. B.A. SUPPLY PORT AND CONTROL PORT CHARACTERISTICS

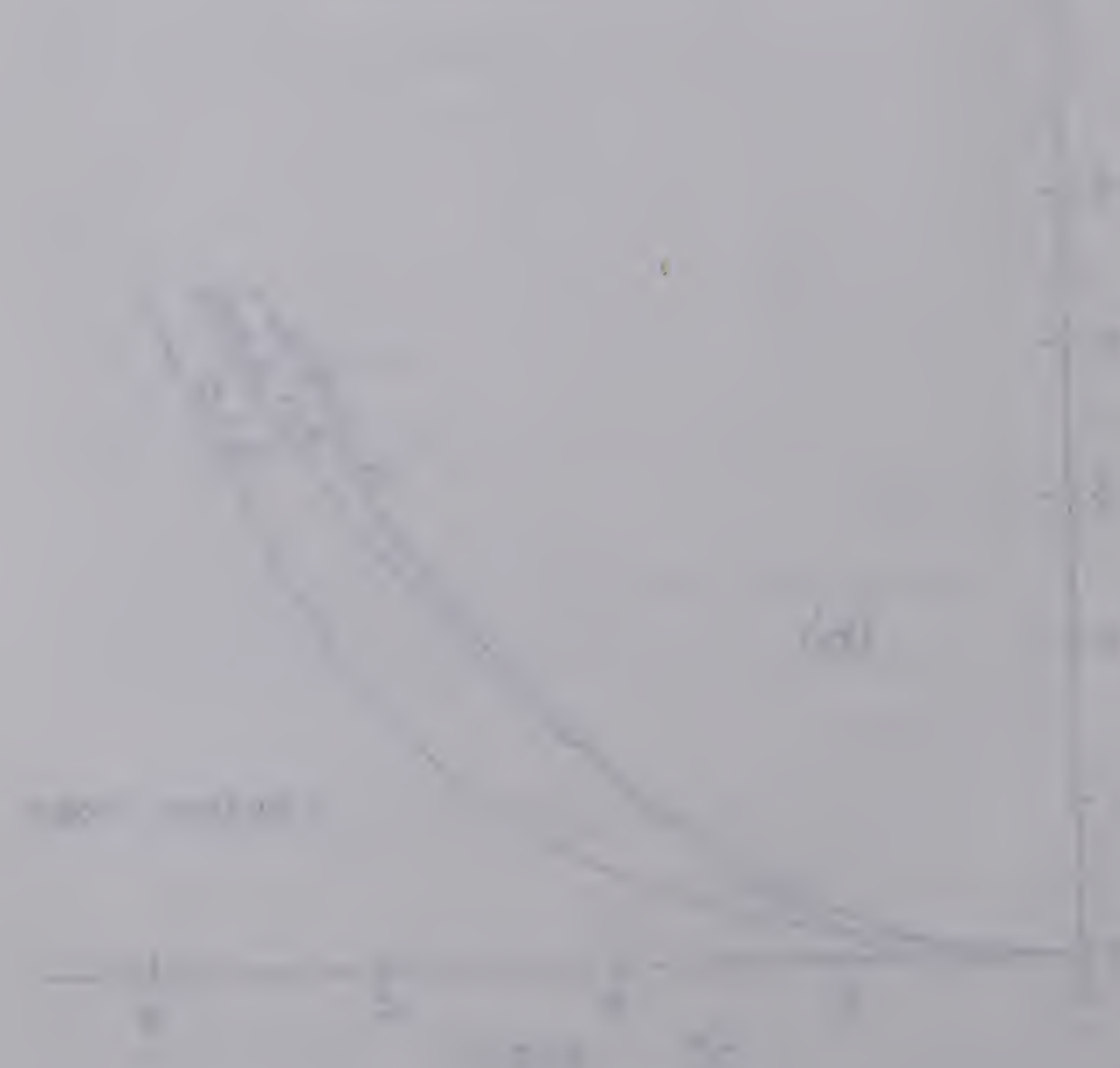

not affected by blocking of the other control or the output ports.

Figure 43 shows the amplifier output characteristics with supply pressure as a parameter.

Figure 44 shows the amplifier pressure transfer characteristic with supply pressure as a parameter. The amplifier was loaded by other bistable amplifiers for the tests shown in Figure 44. Pressure recovery was found to decrease with increasing supply pressure. Amplifier hysterisis was found to increase with increasing supply pressure.

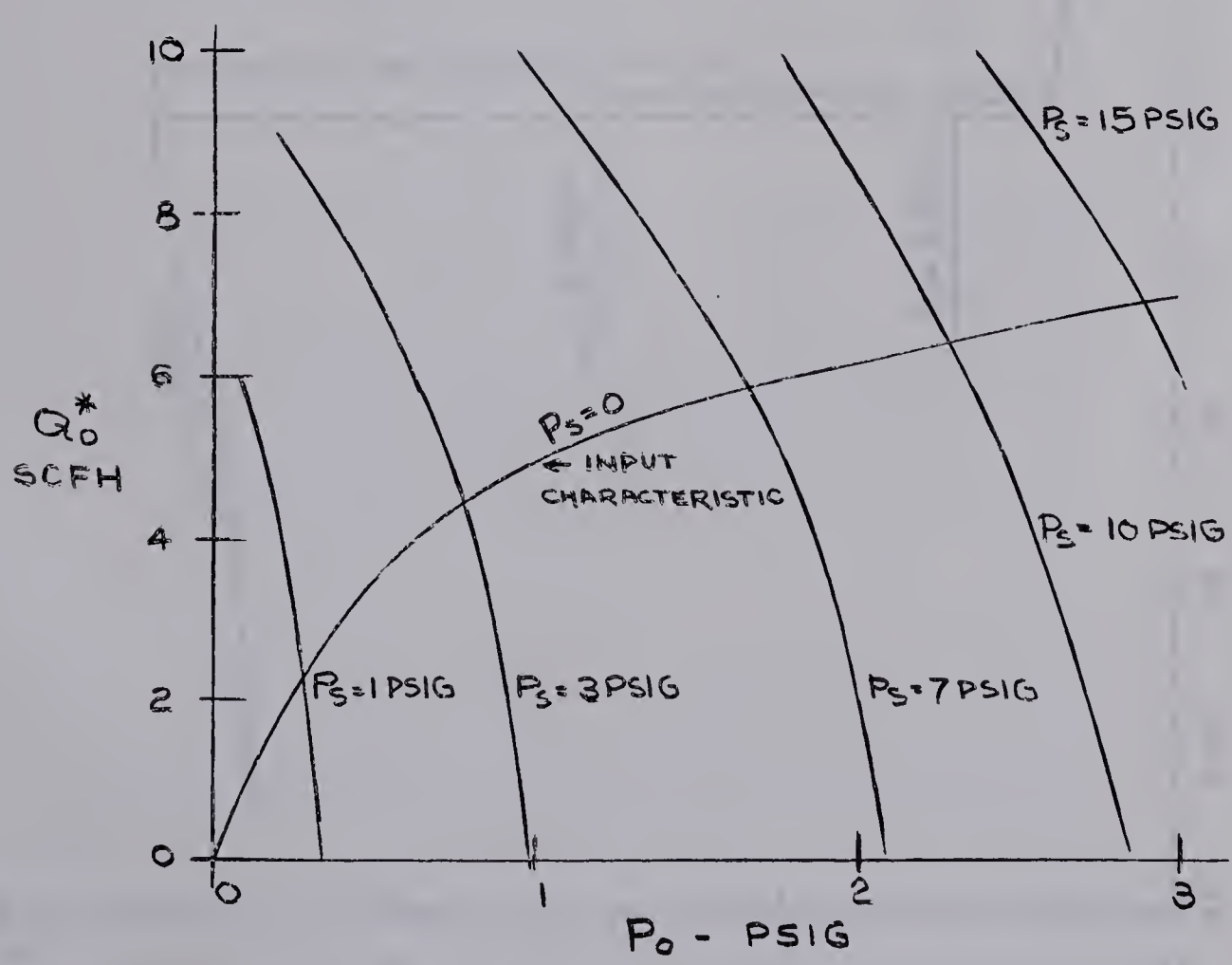

FIGURE 43. BISTABLE AMPLIFIER OUTPUT CHARACTERISTICS

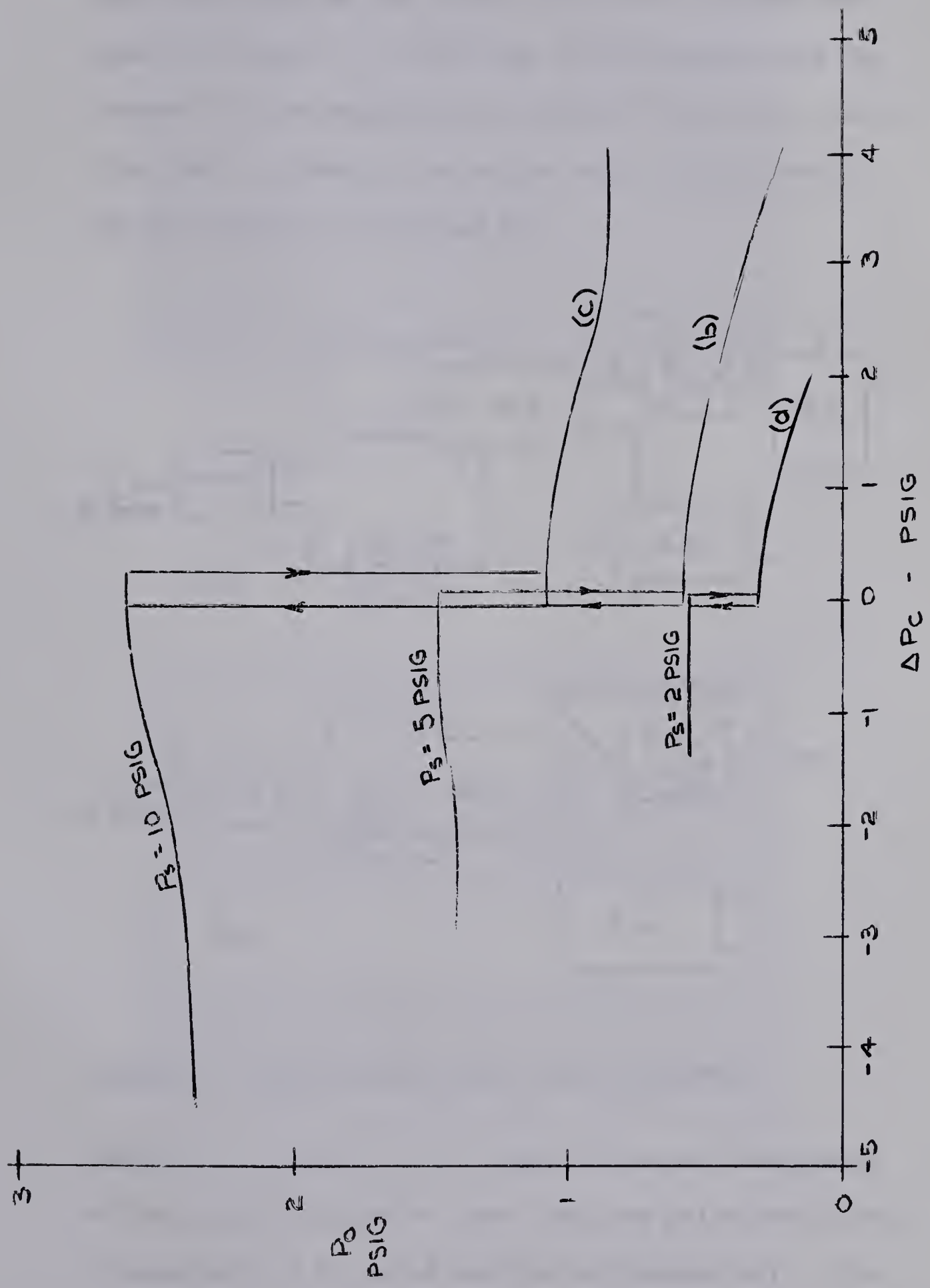

FIGURE 44. B.A. TRANSFER CHARACTERISTIC

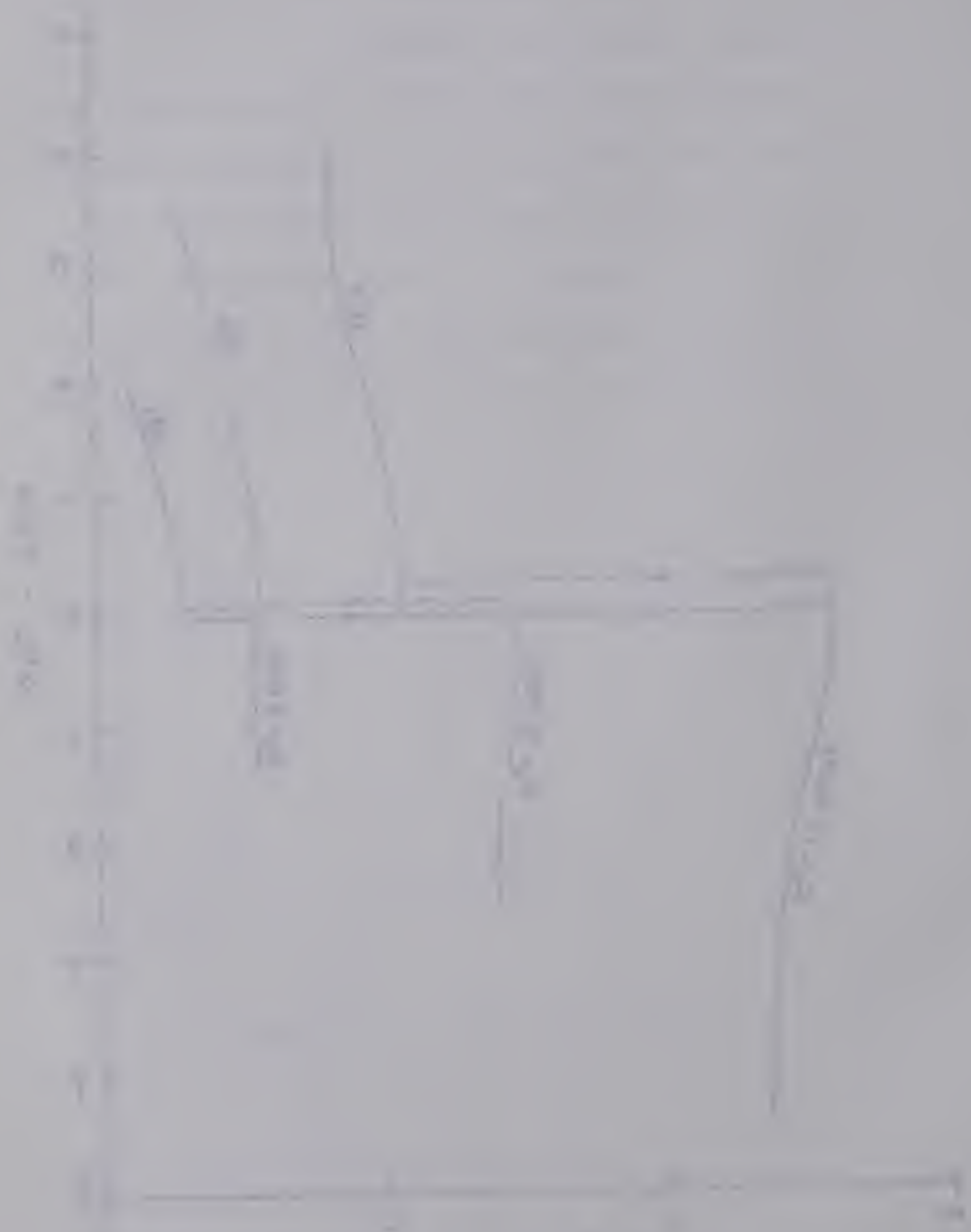

DYNAMIC TESTS

Using a Corning pneumatic clock timer, the bistable amplifier rise time was tested. The test diagrams are shown in Figure 45. A rise time of 1.2 milliseconds was observed for the amplifier as tested in Figure 45a. This rise time is primarily due to the output circuit which may be treated as in Section 6.2.

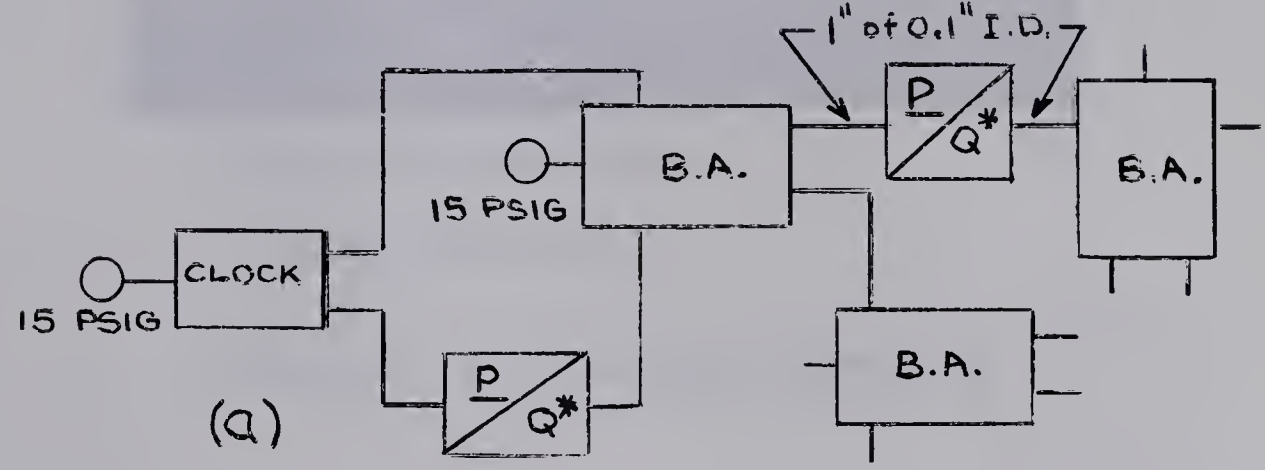

FIGURE 45. BISTABLE AMPLIFIER RISE TIME TESTS

Referring to Figure 43, the input and output resistances of the bistable amplifier about the bias point were found by equation 6.2 to be 0.4 and 3.4 SAR respectively. The total capacitance of the line and flow tube was calculated

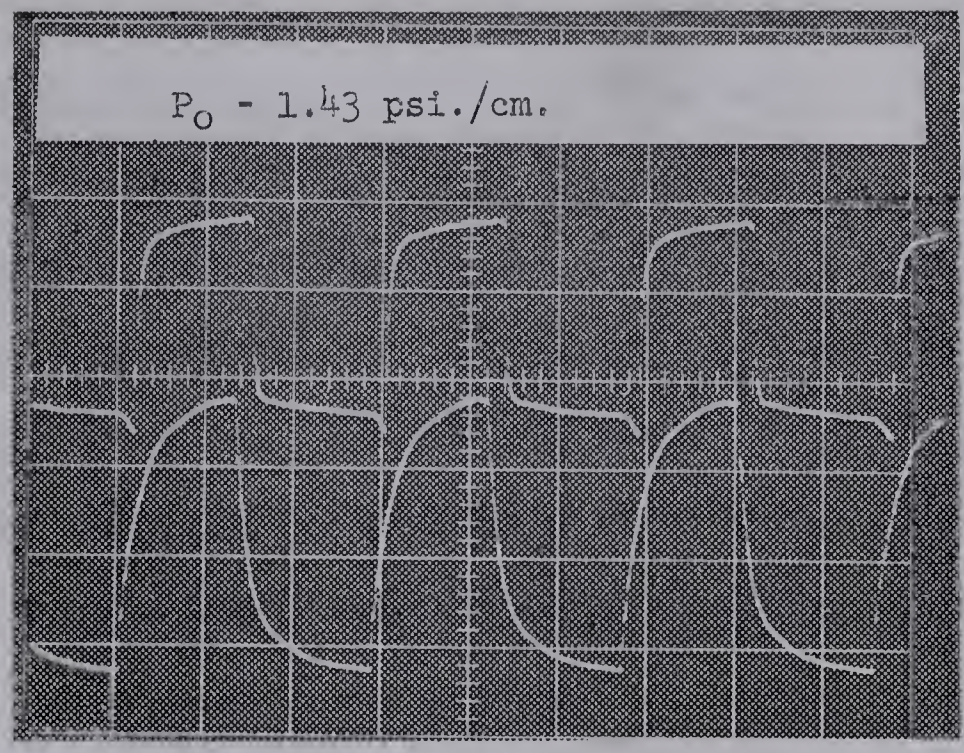

P_i - 1.43 psi./cm.

TIME - 20 ms./cm.

FIGURE 46. B.A. SWITCHING PHOTOGRAPH

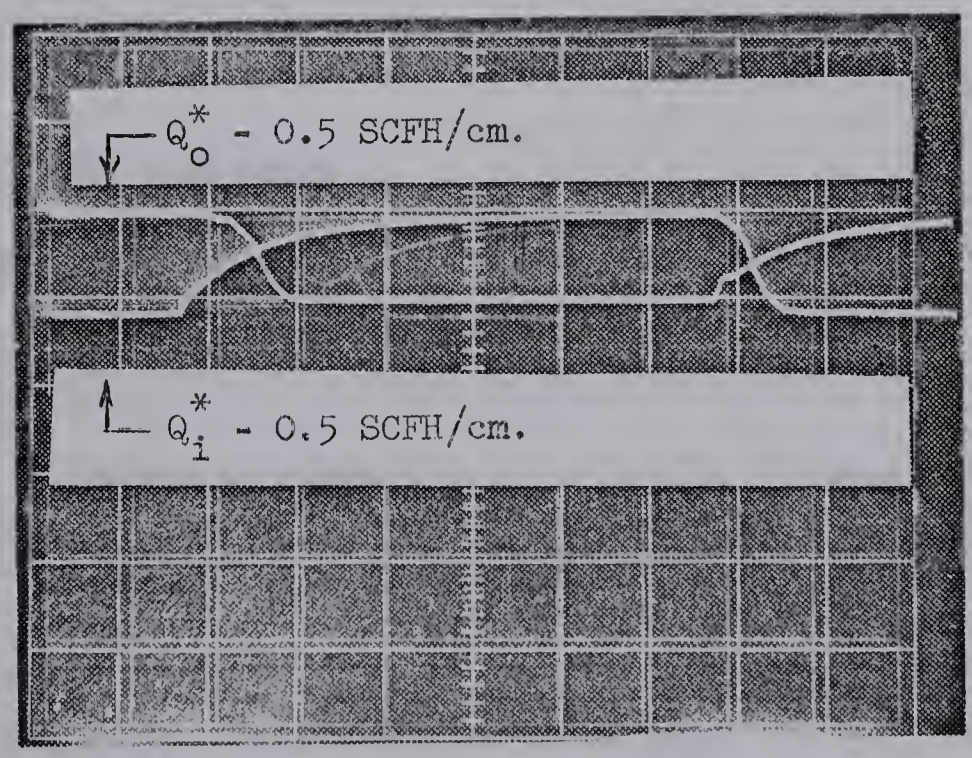

TIME - 20 ms./cm.

FIGURE 47. T.A. SWITCHING PHOTOGRAPH

to be 4 x 10^{-3} SAC. With these values, the output time constant was found to be 1.4 milliseconds.

The test of Figure 45b eliminated the output time constant, as the bistable amplifier was vented to atmosphere via the flow tube. With this test, the air flow rise time at the output was found to be 0.25 milliseconds, the amplifier rise time.

The bistable amplifier delay time was not measured, but was expected to be somewhat less than the proportional amplifier delay time due to the large control nozzle of the bistable device.

Figure 46 is a photograph showing the output air pressure of the bistable amplifier, and the control air pressure as provided by the Corning clock pulser. The test diagram is shown in Figure 45a.

6.4 THE TURBULENCE AMPLIFIER

A schematic of a turbulence amplifier is shown in Figure 48.

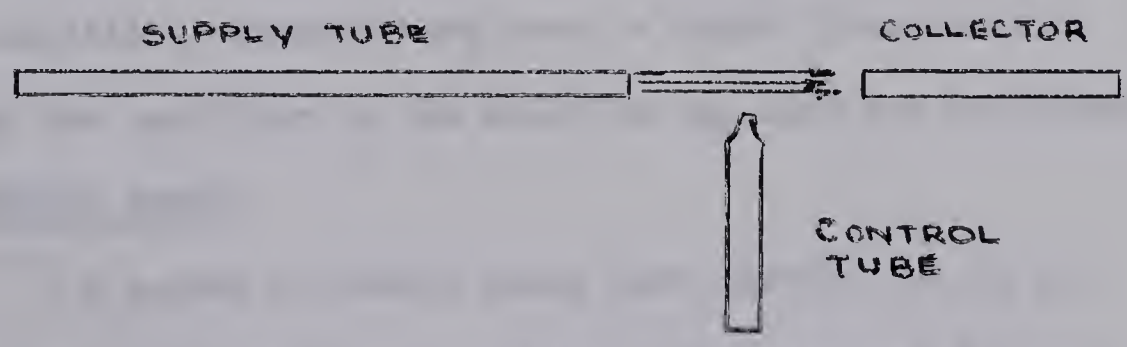

FIGURE 48. THE TURBULENCE AMPLIFIER

If a fluid stream is sent through a smooth-walled pipe, such that the Reynolds number, R_e, is less than 2000, the pipe's walls will induce laminar flow. This flow may then be projected over a distance of 100 times the I.D. of the supply pipe, in a laminar state. The distance over which the stream will remain laminar decreases as the velocity of the stream increases. A collector tube placed downstream of the flow and aligned with the supply tube will obtain a static pressure which is the result of the average velocity of the portion of the stream received. If turbulence occurs in the stream before the collector tube is reached, the pressure in the collector tube will drop because a smaller portion of the fluid stream enters the collector tube. If the fluid stream is laminar at the collector, but very near turbulence, then any small disturbance produced by the control nozzle will cause the fluid stream to become turbulent, before reaching the collector tube. In this manner, small pressure and flow variations at the control port control larger pressure and flow variations at the output. The turbulence amplifier is basically a switch and acts as a NOR element. The amplifier may have any number of control ports, but practical amplifiers commonly have four or eight. Transmission time through the amplifier is the order of one inch per millisecond.

STATIC TESTS

A number of static tests were carried out on an eight port turbulence amplifier. The results of these tests are shown in Figures 49, 50, and 51.

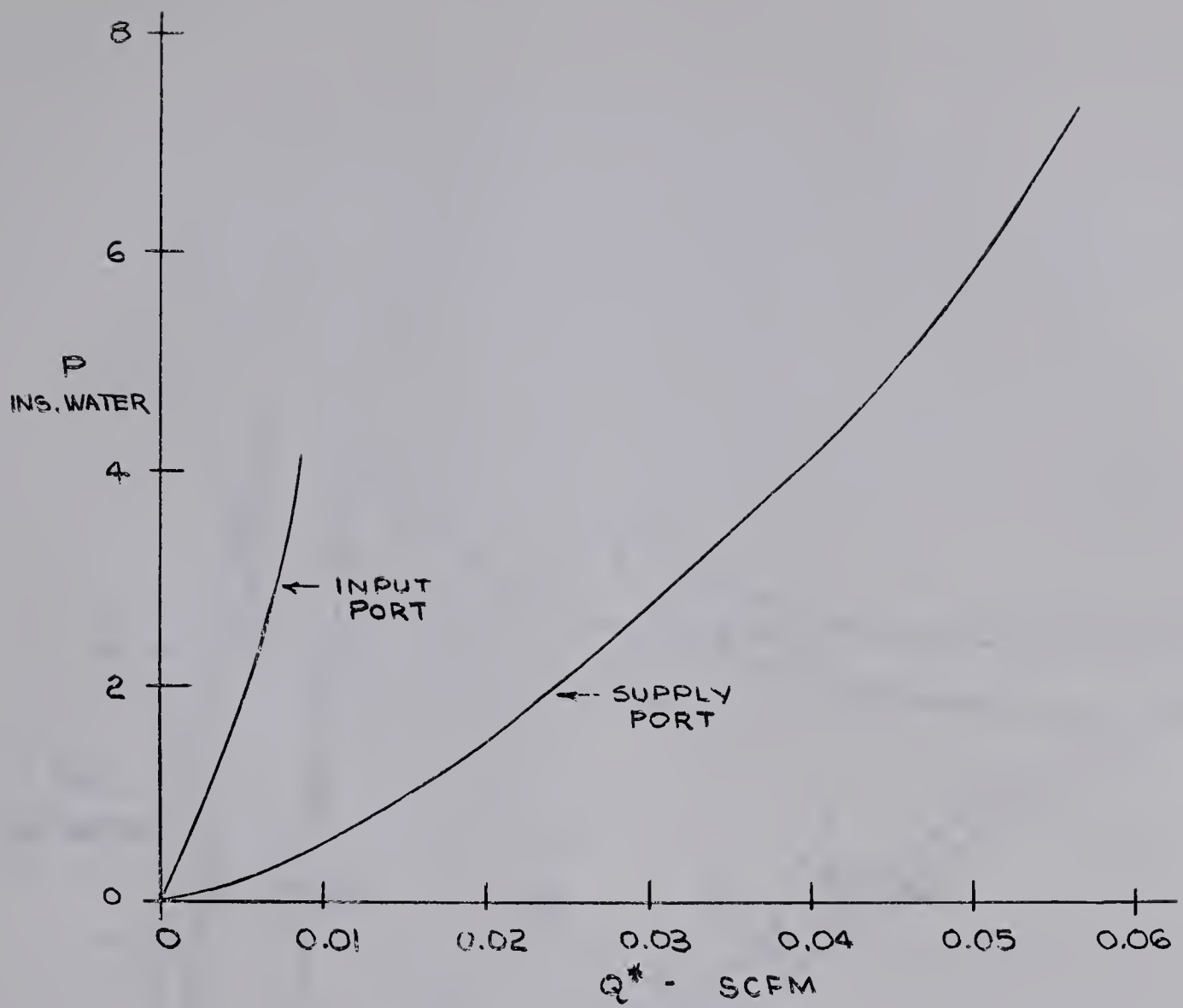

FIGURE 49. T.A. SUPPLY PORT AND CONTROL PORT CHARACTERISTICS

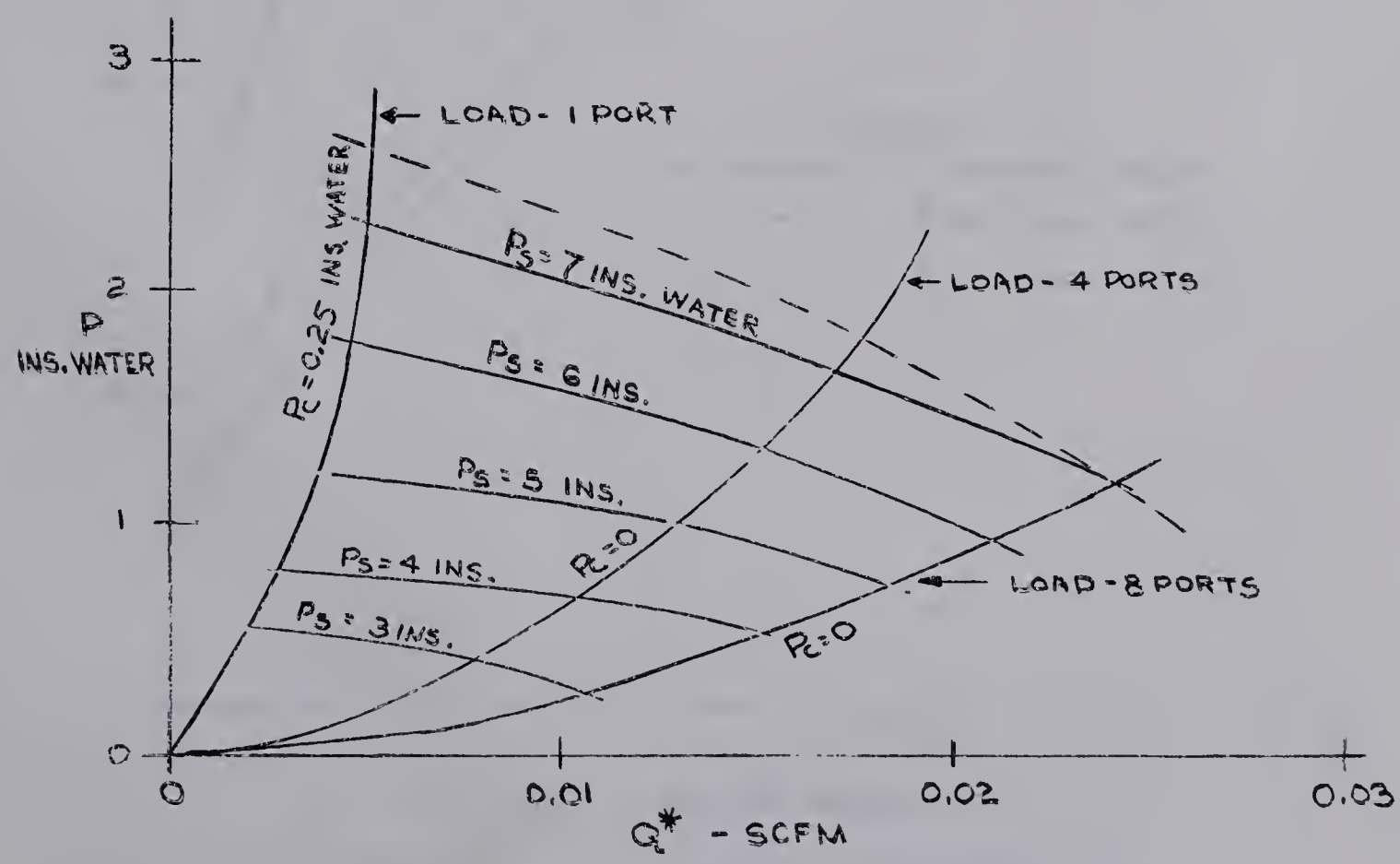

FIGURE 50. T.A. OUTPUT PORT CHARACTERISTICS

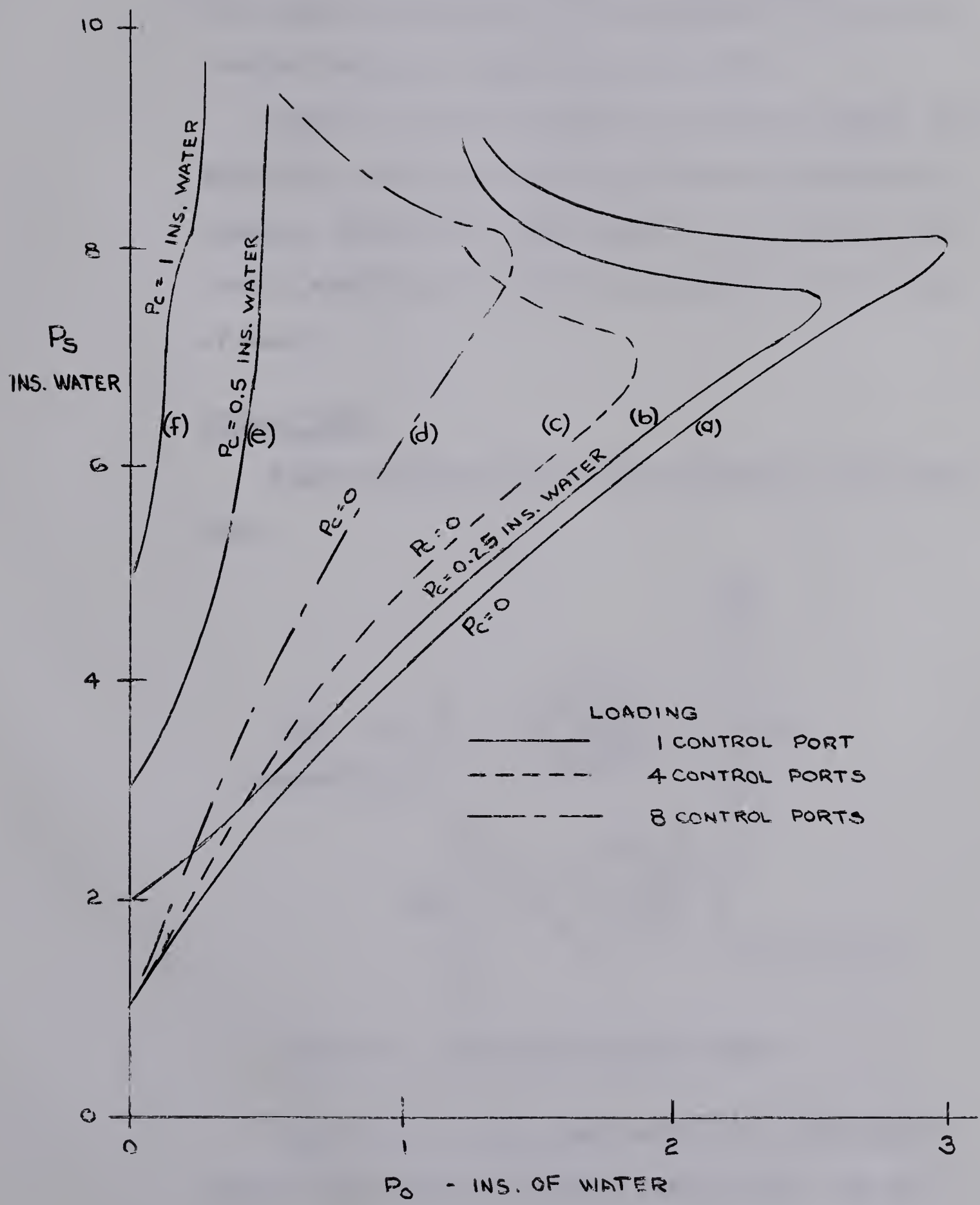

FIGURE 51. T.A. TRANSFER CHARACTERISTICS

Figure 49 shows both the supply port and the control port characteristics.

Figure 50 shows the amplifier output characteristic, with both supply pressure and output load as parameters. The output of the amplifier was loaded with from one up to eight turbulence amplifier input ports.

Figure 51 shows the amplifier pressure transfer characteristic, both as a function of control pressure and loading. Curve (f) of this figure is identical for all loading condtions when the control pressure is one inch of water.

DYNAMIC TEST

Figure 52 shows the turbulence amplifier test schematic.

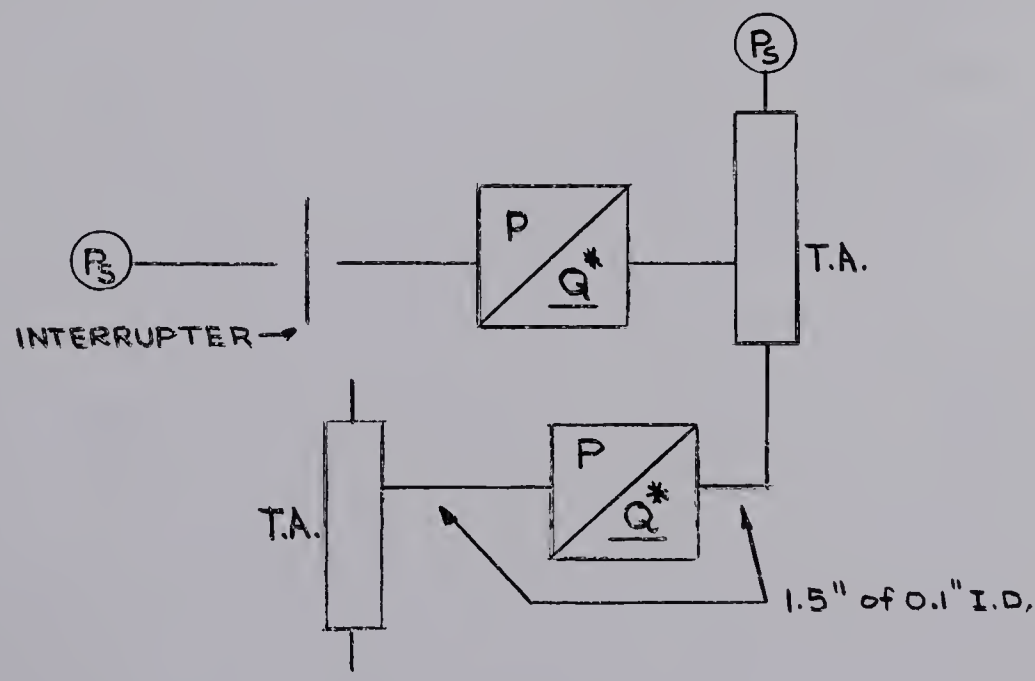

FIGURE 52. TURBULENCE AMPLIFIER TEST

Figure 47 is a photograph showing the interrupted control flow, and the resulting output flow. The out-

put flow rise time was approximately 12 ms., whereas the fall time was approximately 24 ms. The time delay through the amplifier was approximately 4 ms. on output flow increase, but was much less on output flow decrease.

CONCLUSIONS

The instrumentation described in this thesis report was found to be valuable in determining various properties of air operated fluid amplifiers. However, minor improvements to the equipment may be made to increase its usefulness. Some of the suggested improvements are:

(1) The use of a less temperature sensitive piezoelectric ceramic with a higher Curie point would eliminate any measurement drift due to changing air temperature, and would ensure that the ceramic properties remain constant after soldering leads to the electrodes.

(2) Alternately, the use of pressure sensitive paint should be investigated. If this material is found to be satisfactory for the measurement of air pressures, then not only could the frequency response of the pressure measurement extend to d.c., but also, it is conceivable that the paint could be applied to the inner walls of the flow tube.

(3) A shorter hot-wire, with a smaller mounting assembly would allow the construction of a smaller flow tube.

(4) A flow tube with less volume, and preferably with a continuous and constant inner diameter would be an improvement. Preferably the I.D. of the flow tube should be the same as that of the connecting tubing, the order of 0.1 inches. A total length of 0.5 to 1.0 inches would reduce parasitic effects within the flow tube.

(5) The output signal of the closed loop hot-wire circuit is attenuated before it is processed by the linearizing amplifier. It would be preferable to reduce the amount of attenuation required by removing some of the gain from the forward path of the loop, and placing this gain in the feedback path of the loop.

The tests performed on the fluid amplifiers of Chapter Six were by no means exhaustive, but were intended to demonstrate the use of the equipment. The devices tested were found to conform to the latest manufacturer's data available.

REFERENCES

(1) KOMPASS, E.J.: Perspective on Fluid Amplifiers. Control Engineering, September, 1964.

(2) GRAY, W.E. and STERN, H.: Fluid Amplifiers, Capabilities and Applications. Control Engineering, February, 1964.

(3) Piezoelectric Technology Data For Designers. Clevite Corporation, 1965.

(4) EDWARDS, E.M.: Bootstrap Bias. To be published.

(5) KING, L.V.: On the Convection of Heat From Small Cylinders in a Stream of Fluid. Phil. Trans. Roy. Soc., Vol. 214, 1914.

(6) DRYDEN, H.L.: Ind. Eng. Chem., Vol. 31, 1939.

(7) GRANT, H.P. and KRONAUER, R.E.: Fundamentals of Hot Wire Anemometry. Symposium on Measurement in Unsteady Flow. A.S.M.E. Trans., 1962.

(8) SCHUBAUER, G.B. and KLEBANOFF, P.S.: N.A.C.A. Report W 86, 1946.

(9) BELSTERLING, C.A. and TSUI, K.C.: Analyzing Proportional Fluid Amplifier Circuits. Control Engineering, August, 1965.

(10) CALDWELL, W.I., COON, G.A. and ZOSS, L.M., Editors: Frequency Response for Process Control. McGraw-Hill Co., 1959.

(11) ROHMANN, C.P. and GROGAN, E.C.: On the Dynamics of Pneumatic Transmission Lines, Vol. 79, A.S.M.E. Trans., 1957.

BIBLIOGRAPHY

Levine, R.S.: Construction and Use of a Hot Wire Turbulence Measuring Device. Ph.D. Thesis, M.I.T., 1949.

Kuo, B.C.: Automatic Control Systems. Prentice-Hall Co., 1964.

Belsterling, C.A.: Designing Fluidic Systems. Control Engineering, April, 1966.

Proceedings of the Fluid Amplification Symposium. October, 1962. U.S. Dept. of Commerce.

Proceedings of the Fluid Amplification Symposium. May, 1964. U.S. Dept. of Commerce.

APPENDIX A

THE FLOW TUBE ASSEMBLY

FLOW TUBE SUB-ASSEMBLY

The flow tube sub-assembly shown in Figure A-1 was constructed of acrylic plastic. The inlet and outlet tubing was fabricated from brass. The two plastic saddle pieces and the inlet and outlet tubing pieces were fastened to the main body with the Devcon epoxy. Knurled screw caps, with brass housings fastened to them, were made to hold down the transducer assemblies, as well as to protect the transducer assembly connections with the coaxial cable.

HOT-WIRE ASSEMBLY

Figure A-2 shows the hot-wire assembly. The main body of the holder was also fabricated from acrylic plastic. The hot-wire supports were fabricated from 1/16 inch 314 S.S. welding rod. The Wollaston wire was fastened to the flattened ends of the supports by spot welding. Following this, a small amount of epoxy was applied to the welds and allowed to cure. When the epoxy was fully cured, the Wollaston wire was dipped into a 50% nitric acid solution, for ten minutes, to etch away the silver coating of the wire.

CERAMIC ASSEMBLY

The ceramic assembly is shown in Figure A-3. The body of the holder was made of teflon. A flexible single strand of wire was carefully soldered to each electrode of the ceramic. The wires

were then drawn through bore holes in the core of the holder and soldered to terminals which had been screwed into the top of the holder. The ceramic was fastened to the holder with teflon epoxy. When inserted into the flow tube, the ceramic assembly was preceded by a 0.25 inch I.D. O-ring, which acts as a seat for the assembly.

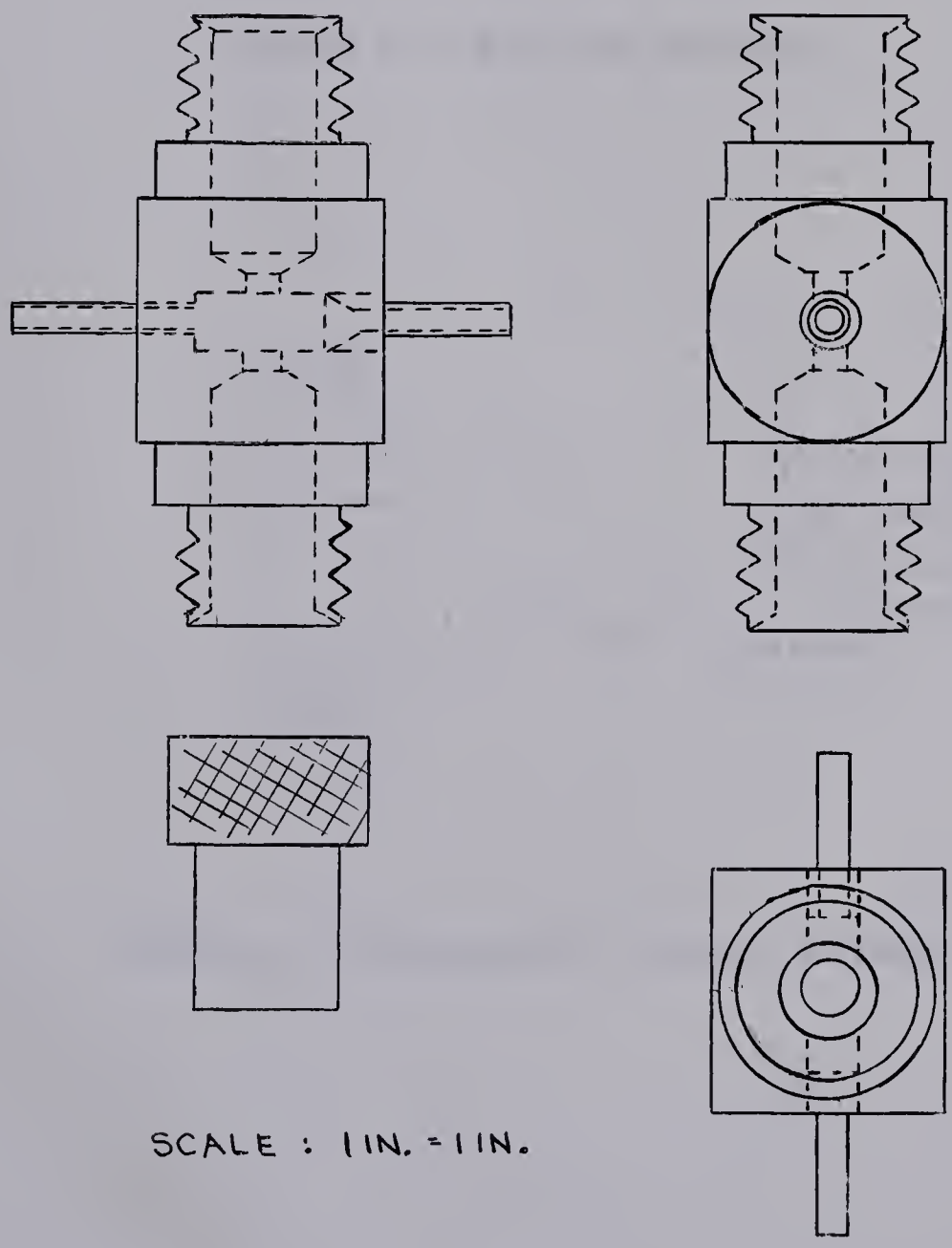

FIGURE A-1 FLOW TUBE SUB-ASSEMBLY

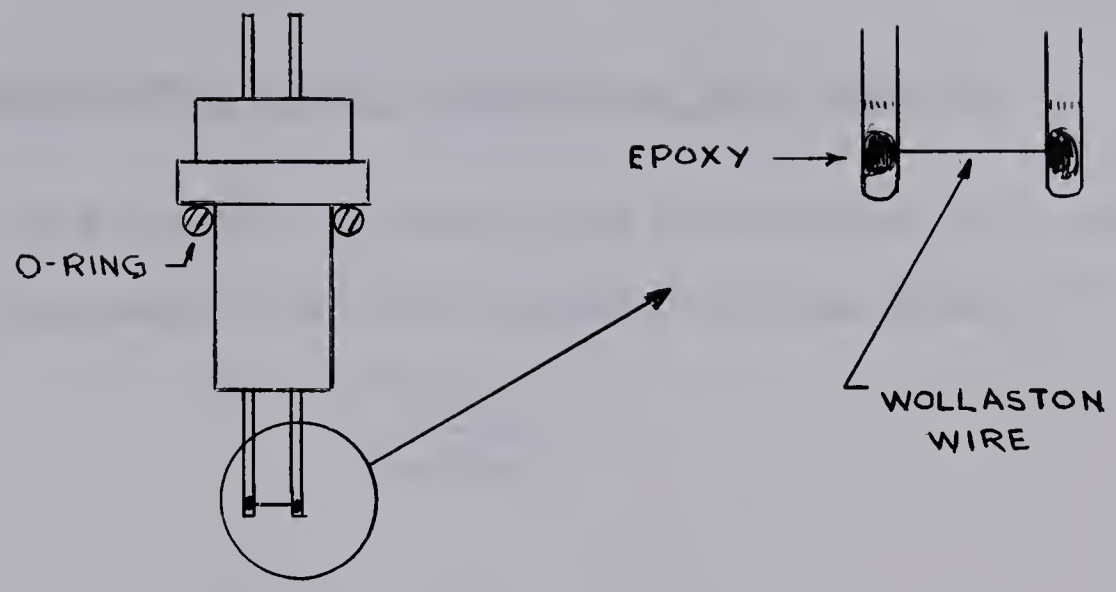

FIGURE A-2 HOT-WIRE ASSEMBLY

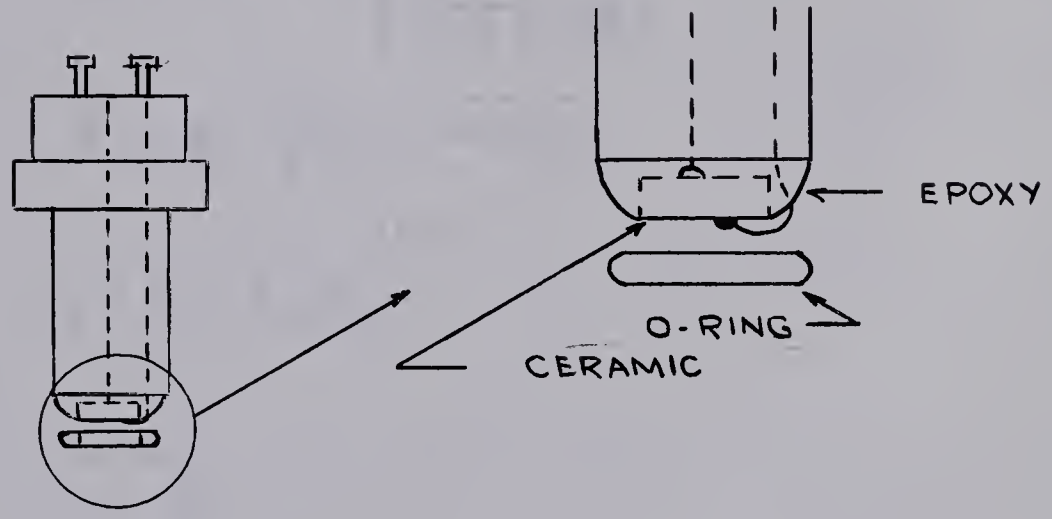

FIGURE A-3 PIEZOELECTRIC CERAMIC ASSEMBLY

APPENDIX B

BOOTSTRAPPING OF THE PIEZOELECTRIC INPUT AMPLIFIER

The bootstrap bias used in the piezoelectric input amplifier is a high pass filter with a transfer function given by [4]

$$H(p) = \frac{P^2+2\zeta_1 P}{P^2+2\zeta P+1}$$

where

$$P = \frac{S}{\omega_o} = S\tau_o$$

Referring to Figure 5 and Reference 4, the following relationships were used:

$$\zeta \doteq \zeta_1 \doteq \tfrac{1}{2}\sqrt{\frac{C_3}{C_4\alpha(1-\alpha)}}$$

$$\tau_o = R_c\sqrt{\alpha(1-\alpha)C_3C_4}$$

where

$$R_c = R_1 + R_2//R_3$$

and

$$\alpha = \frac{R_1}{R_c}$$

Utilizing the above relationships, the following values were found:

$$\zeta \doteq \zeta_1 \doteq 1.04$$

$$\tau_o = 1.6 \text{ sec.}$$

$$R_c = 101.4 \text{ M ohms.}$$

$$\alpha = 0.987$$

The normalized frequency, f_o, based on the normalized

time constant, τ_o, was calculated to be 0.1Hz.

The maximum frequency response boost, H_m, as given by the relationship

$$H_m^2 = \frac{1}{1 - \frac{4\delta\zeta^2}{\left[1+\sqrt{1-8\delta\zeta_1^2}\right]^2}}$$

where

$$\delta = 2\zeta^2 - 2\zeta_1^2 - 1$$

was found to be 1.15 or 1.2 db.

The frequency at which the maximum boost occurs, $f_o U_m$, where U_m is given by

$$U_m^2 = \frac{-1}{2\delta}\left[1+\sqrt{1-8\delta\zeta_1^2}\right]$$

was calculated to be 0.14 Hz.

The lower corner frequency 3 db. down point, $f_o U_{\frac{1}{2}}$ where $U_{\frac{1}{2}}$ is given by

$$U_{\frac{1}{2}}^2 = \sqrt{1+(2\zeta_1^2 - \delta)^2} - (2\zeta_1^2 - \delta)$$

was found to be at 0.0374 Hz.

The effective input time constant, $\tau_{eff.}$, where

$$\tau_{eff.} \doteq \frac{0.16}{f_o U_{\frac{1}{2}}}$$

was found to be 4.3 sec.

APPENDIX C

AUXILIARY TEST EQUIPMENT

AIR PRESSURE OSCILLATOR

The air pressure oscillator, utilized in the tests of Chapter Six, is shown schematically in Figure C-1.

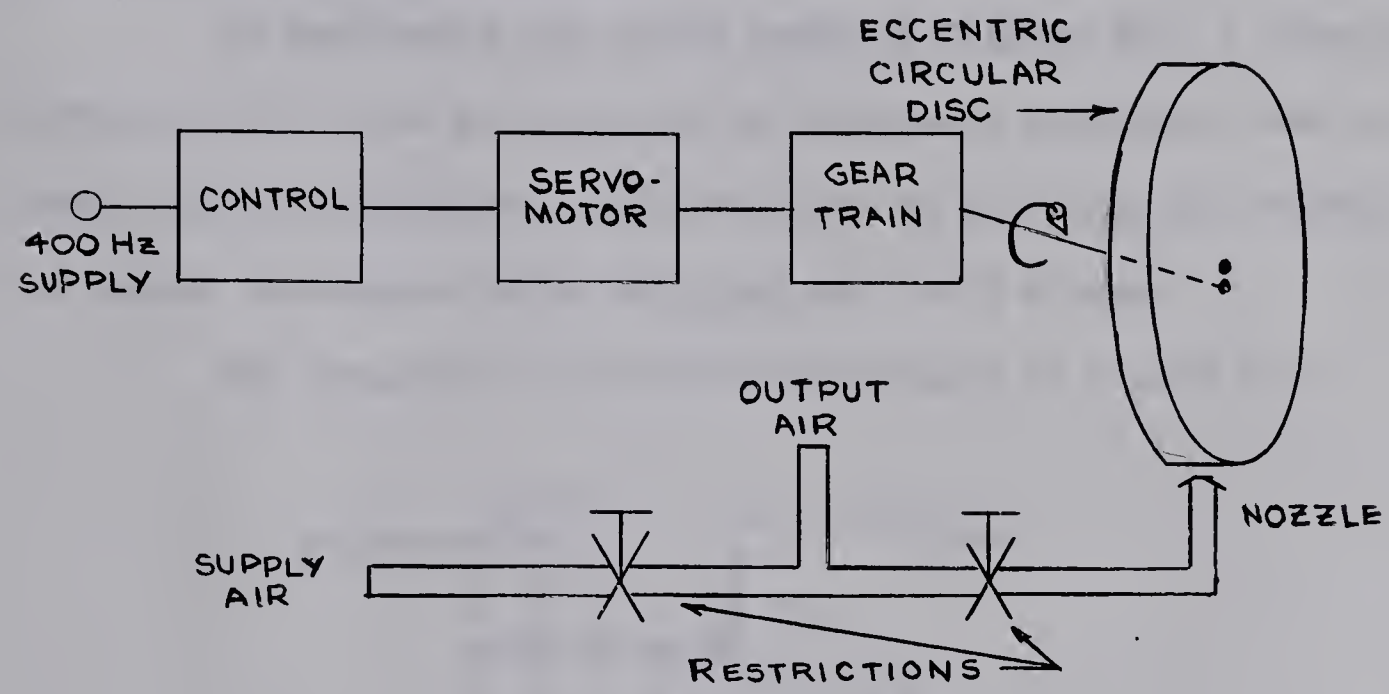

FIGURE C-1. AIR PRESSURE OSCILLATOR

A gearing ratio was employed such that the eccentric circular disc was rotated at a maximum of 200 revolutions per second. The minimum controllable rotation was about 2 revolutions per second. The circular disc, about 0.25 inches wide and 2 inches in diameter was fabricated from aluminum. In operation, the center of the disc was offset from the shaft center by about 10 mils. The air nozzle was mounted as close to the edge of the disc as possible, without touching the disc during any part of its revolution.

When the disc is rotating at a constant r.p.s., air exit-

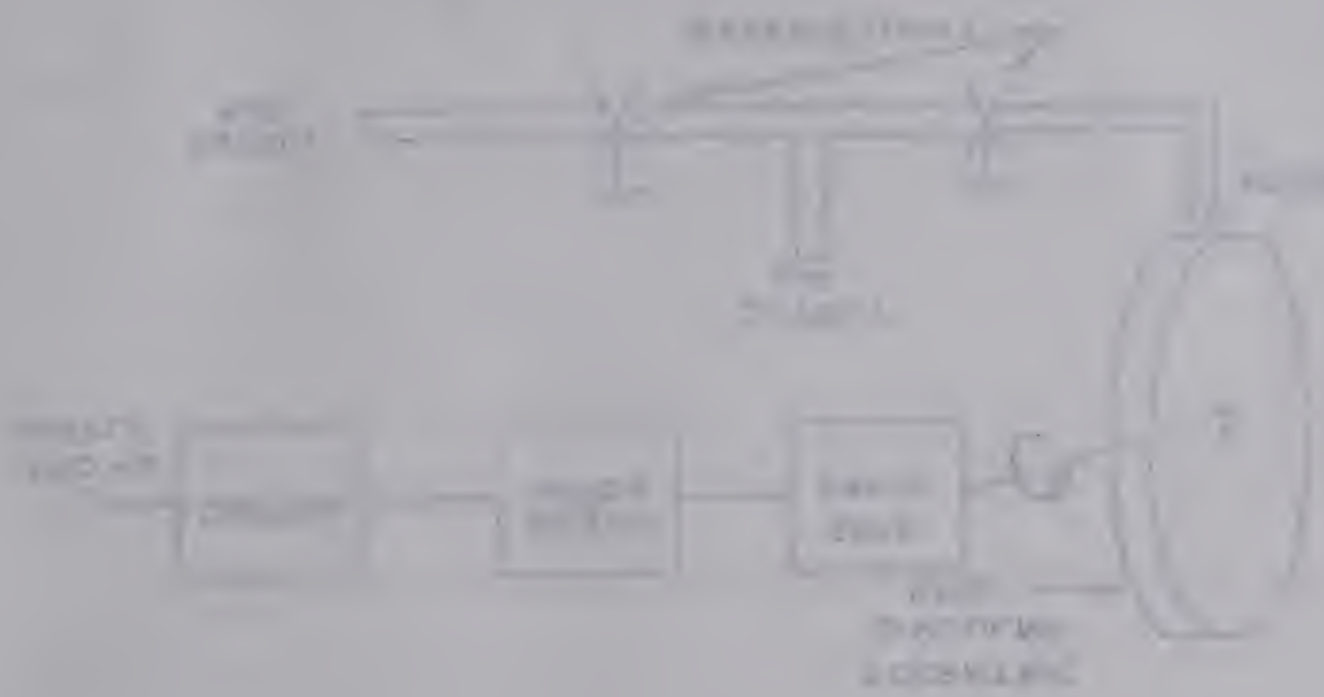

ing from the nozzle is presented with a time dependent variable restriction. When the air supply and the nozzle needle valves are properly adjusted, a very nearly sinusoidal pressure will be present at the output. Since one revolution of the disc represents one air pressure cycle, the frequency range of this oscillator is from 2Hz to 200Hz.

STATIC AIR PRESSURE MEASUREMENT

In performing the static tests of Chapter Six, a Giannini differential bellows air pressure to resistance transducer was utilized. The input pressure range was given as 0 to 5 psid., whereas the output resistance range was given as 0 to 5 K ohms.

The transducer is shown schematically in Figure C-2.

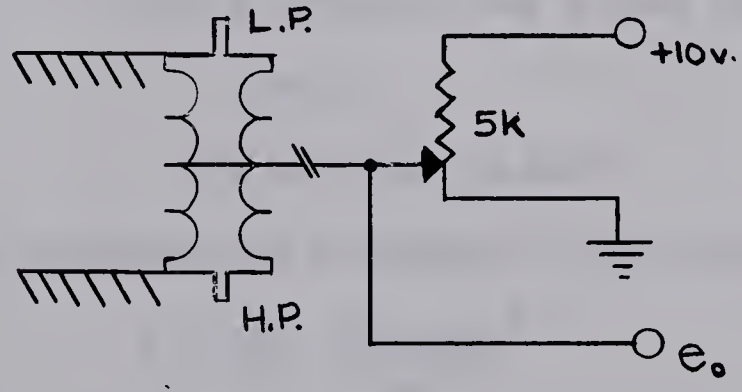

FIGURE C-2. STATIC PRESSURE TRANSDUCER

When ten volts is applied across the resistance, the pressure measured is given by 2 volts/psid.

For lower level pressure tests, water-filled manometers were used, whereas, for higher level pressure tests, a 0.1%, 0 to 30 psig test gage was used.

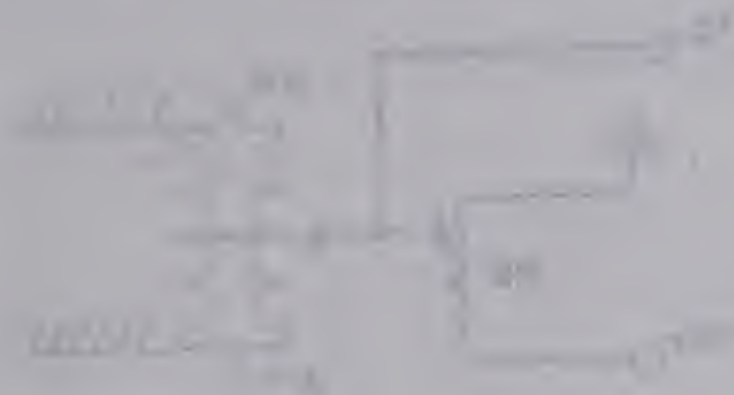

APPENDIX D

PNEUMATIC INDUCTANCE, CAPACITANCE, AND RESISTANCE

According to Caldwell, Coon, and Zoss,[10] the pneumatic capacitance of a tank is given by

$$C = \frac{V}{P^*} \quad \frac{in.^5}{lb.} \tag{D-1}$$

where

V = tank volume in cubic inches

P*= standard air pressure, 14.7 psia.

The pneumatic resistance of a restriction is given by

$$R = \frac{\Delta P}{Q^*} \quad \frac{lb.\text{-}sec.}{in.^5} \tag{D-2}$$

where

ΔP = pressure drop across the restriction in psi.

Q*= air flow in SCIS.

The inductance of a pneumatic line is given by

$$L = \frac{d^* l}{A} \quad \frac{lb.\text{-}sec.^2}{in.^5} \tag{D-3}$$

where

d* = fluid mass density at 14.7 psia.

l = length of line in inches

A = cross-sectional area of line in square inches.

Rohmann and Grogan[11] state that the pneumatic resistance, capacitance, and inductance of an air transmission line may be determined by the following formulae,

$$L' = \frac{1.15 \times 10^{-7}}{\pi r^2} \quad \frac{P}{14.7} \quad \frac{\text{lb.-sec.}^2}{\text{in.}^5}/\text{in.} \qquad \text{(D-4)}$$

$$C' = \frac{\pi r^2}{P} \quad \frac{\text{in.}^5}{\text{lb.}}/\text{in.} \qquad \text{(D-5)}$$

$$R' = \frac{2.5 \times 10^{-8}}{\pi r^4} \quad \frac{\text{lb.-sec.}}{\text{in.}^5}/\text{in.} \qquad \text{(D-6)}$$

where

P = absolute ambient pressure in psia.

r = radius of line in inches.

Equations D-4 and D-5 are the same as equations D-3 and D-1 except for the pressure conversion. Equation D-6 is based on the viscosity of air at 20°C.

In calculating pneumatic time constants, both sets of equations are valid. L and C may be converted from one set to the other by using the appropriate pressure term.

For 0.1 inch I.D. tubing, the second set of equations yields

$$R'_1 = 3.3 \times 10^{-6} \quad \frac{\text{lb.-sec.}}{\text{in.}^5}/\text{in.}$$

$$L'_1 = 1 \times 10^{-6}P \quad \frac{\text{lb.-sec.}^2}{\text{in.}^5}/\text{in.}$$

$$C'_1 = \frac{7.9}{P} \times 10^{-3} \quad \frac{\text{in.}^5}{\text{lb.}}/\text{in.} \qquad \text{(D-7)}$$

For 0.05 inch I.D. tubing, the parameters are

$$R'_2 = 5.3 \times 10^{-5} \quad \frac{\text{lb.-sec.}}{\text{in.}^5}/\text{in.}$$

$$L'_2 = 4P \times 10^{-6} \quad \frac{\text{lb.-sec.}^2}{\text{in.}^5}/\text{in.}$$

$$C'_2 = \frac{2}{P} \times 10^{-3} \quad \frac{\text{in.}^5}{\text{lb.}}/\text{in.} \qquad \text{(D-8)}$$

The flow tube of Appendix A also exhibits properties of resistance, capacitance, and inductance. Figure D-1 shows the flow tube in cross-section with the cross-hatched area displaying the pneumatic passages and chambers.

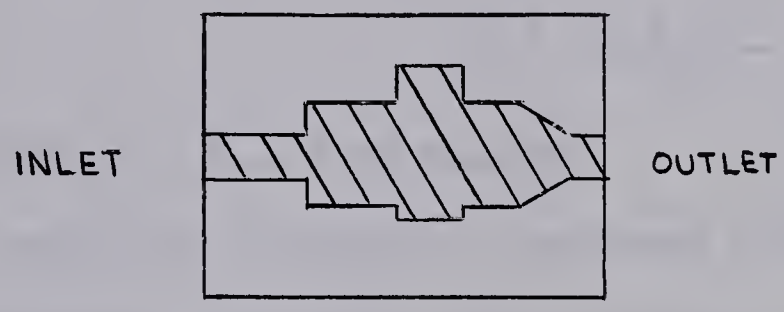

FIGURE D-1 FLOW TUBE CROSS-SECTION

The approximate pneumatic volume within the flow tube was calculated to be 4.3×10^{-2} cubic inches. Thus, the lumped pneumatic capacitance of the flow tube is given by

$$C_F = \frac{4.3 \times 10^{-2}}{14.7} \quad \frac{\text{in.}^5}{\text{lb.}}$$

or

$$C_F' = \frac{4.3 \times 10^{-2}}{P} \quad \frac{\text{in.}^5}{\text{lb.}} \qquad \text{(D-9)}$$

The inlet and outlet passages to the main body of the flow tube are 0.1 inch I.D., whereas the lengths of these passages are 0.3 and 0.2 inches respectively. Figure D-2 shows the flow tube analogue based on these dimensions and equations D-4 through D-6. As may be seen from the figure, the flow tube resistance and inductance may be neglected for relatively low pressure operation at a relatively low frequency.

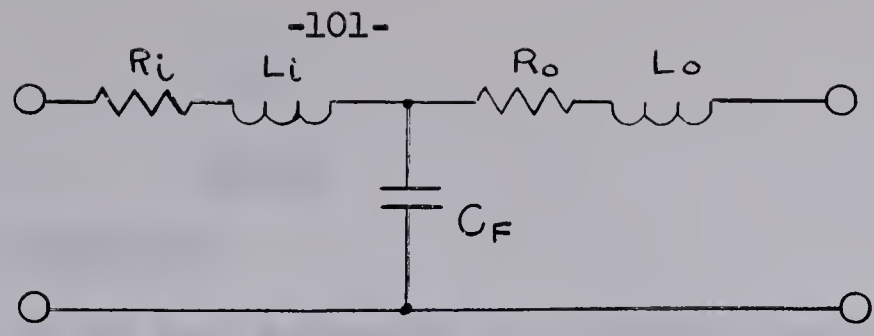

$L_i = 3P \times 10^{-7}$ $\quad R_i = 1.1 \times 10^{-6}$

$L_o = 2P \times 10^{-7}$ $\quad R_o = 7 \times 10^{-7}$

$C_F = \frac{4.3 \times 10^{-2}}{P}$

FIGURE D-2. FLOW TUBE ANALOGUE

Since it was found convenient to represent pneumatic units of capacitance, inductance, and resistance in electrical terms, the following definitions were adopted:

(i) For equatons D-1, D-2, and D-3, where the air is considered under standard conditions,

$\frac{\text{in.}^5}{\text{lb.}}$ = SAC, standard air capacitance unit

$\frac{\text{lb.-sec.}}{\text{in.}^5}$ = SAR, standard air resistance unit

$\frac{\text{lb.-sec.}^2}{\text{in.}^5}$ = SAL, standard air inductance unit (D-10)

(ii) For equations D-4, D-5, and D-6, where the air is considered under absolute conditions,

$\frac{\text{lb.-sec.}^2}{\text{in.}^5}$ = AL, air inductance unit

$\frac{\text{in.}^5}{\text{lb.}}$ = AC, Air capacitance unit

$\frac{\text{lb.-sec.}}{\text{in.}^5}$ = AR, air resistance unit (D-11)

Under the definition of equations D-10, a resistance of 1×10^6 $\frac{\text{lb.-sec.}}{\text{ft.}^5}$, will have a value of 4 SAR.

ERRATA

PAGE	CORRECTION
9	In the last paragraph, zero diodes should read as zener diodes.
12	In the first sentence of the last paragraph, through is misspelled.
35	In the second sentence, numerator is misspelled.
84	In the second sentence of the third paragraph, conditions is misspelled.
101	In subsection (i), equations is misspelled.